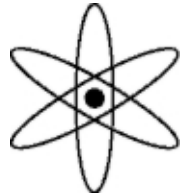


Physik-Department



**Utilisation of Evanescent Fields
for the Characterisation of
Thin Biosensing Layer Systems**

Dissertation

von

Thomas Zacher



Technische Universität
München

Technische Universität München
Physik-Department
Lehrstuhl für Biophysik E22

Utilisation of Evanescent Fields for the Characterisation of Thin Biosensing Layer Systems

Thomas Zacher

Vollständiger Abdruck der von der Fakultät für Physik
der Technischen Universität München
zur Erlangung des akademischen Grades eines
Doktors der Naturwissenschaften
genehmigten Dissertation.

Vorsitzender: Univ.-Prof. Dr. M. Kleber
Prüfer der Dissertation: 1. Univ.-Prof. Dr. E. Sackmann
2. Univ.-Prof. Dr. A. Laschewsky,
Universität Potsdam

Die Dissertation wurde am 10.04.2002 bei der Technischen Universität München eingereicht und durch die Fakultät für Physik am 17.06.2002 angenommen.

Table of Contents

1	SUMMARY	5
2	INTRODUCTION	7
3	FUNDAMENTALS	11
3.1	SURFACE PLASMON RESONANCE.....	11
3.1.1	<i>Surface Plasmon Waves</i>	11
3.1.2	<i>The Kretschmann-Configuration</i>	14
3.1.3	<i>Penetration Depth of SP Waves</i>	17
3.1.4	<i>Reflectivity of a Layer System</i>	18
3.2	BIOMOLECULAR INTERACTION ANALYSIS WITH SPR	21
3.2.1	<i>The Langmuir-Isotherm</i>	22
3.2.2	<i>SPR Biosensor Data Evaluation</i>	24
3.3	BIOSENSING HYDROGELS FOR SPR DETECTION	30
3.3.1	<i>Dextran Hydrogels</i>	32
3.3.2	<i>Synthetic Hydrogels</i>	37
4	AIM OF THE RESEARCH	41
5	THE SPR SETUP	43
5.1	GENERAL DESCRIPTION	43
5.2	ANGLE CALIBRATION	47
5.3	THE AVAILABLE MEASUREMENT MODES	49
5.3.1	<i>Angle Mode</i>	49
5.3.2	<i>Differential Intensity Mode</i>	50
6	THERMO-RESPONSIVE HYDROGELS	53
6.1	SYNTHESIS OF POLYMERS.....	53
6.2	LCST OF AQUEOUS SOLUTIONS	58
6.3	LCST IN SURFACE-ATTACHED STATE.....	59
6.3.1	<i>Concept of the Investigation</i>	59
6.3.2	<i>Experimental Part</i>	62
6.3.2.1	Preparation of Samples	62
6.3.2.2	Temperature Variance of Solvent	63
6.3.2.2.1	Continuous Heating.....	63
6.3.2.2.2	Injection	65

6.3.3	<i>Results</i>	66
6.3.4	<i>Discussion</i>	69
6.3.5	<i>Conclusion</i>	74
6.4	PHOTOCROSSLINKING OF CINNAMOYLATED P-HPMA	75
6.4.1	<i>Experimental Procedure</i>	75
6.4.2	<i>Results and Discussion</i>	77
6.4.3	<i>Conclusion</i>	80
6.5	STUDY OF NON-SPECIFIC ADSORPTION.....	80
6.5.1	<i>Non-Specific Adsorption - A Complex Problem</i>	80
6.5.2	<i>Bovine Serum Albumin</i>	82
6.5.3	<i>Surface Modification and BSA Exposure</i>	83
6.5.3.1	Chemicals.....	83
6.5.3.2	Synthesis of Aminodextran	84
6.5.3.3	Preparation of Samples	84
6.5.3.3.1	Gold Surface.....	84
6.5.3.3.2	Hexadecylmercaptan SAM.....	84
6.5.3.3.3	Undecanoic Acid SAM + Aminodextran.....	84
6.5.3.3.4	P-THMA and Thermo-Responsive Hydrogels.....	84
6.5.3.4	Preparation of HEPES-Buffered Saline.....	85
6.5.3.5	Experimental Procedure	85
6.5.4	<i>Results and Discussion</i>	85
6.5.4.1	150µg/ml BSA in HBS	85
6.5.4.2	2mg/ml BSA in H ₂ O	87
6.5.5	<i>Conclusion</i>	89
6.6	BIO-FUNCTIONALISATION OF ACETYLATED P-THMA.....	90
6.6.1	<i>Immunoglobulin G</i>	90
6.6.2	<i>Protein A</i>	91
6.6.3	<i>Chemicals</i>	91
6.6.3.1	Preparation of Buffers	91
6.6.4	<i>Immobilisation of Protein A</i>	91
6.6.4.1	Activation Chemistry and Protocol	92
6.6.4.2	Immobilisation Kinetics	93
6.6.5	<i>Biomolecular Interaction Protein A – IgG</i>	95
6.6.5.1	Experimental Procedure	95
6.6.5.2	Interaction and Regeneration Kinetics	95
6.6.6	<i>Conclusion</i>	97
7	BINDING PROCESSES IN DEXTRAN HYDROGELS	99
7.1	CONCEPT OF THE INVESTIGATION	99
7.1.1	<i>The Employed Wavelengths</i>	100
7.1.2	<i>Different Binding Regimes - Different Time-Dependence</i>	102
7.1.3	<i>The Three-Zone Model</i>	102
7.2	SURFACE MODIFICATION AND BIORECOGNITION PROCEDURES	105
7.2.1	<i>The Streptavidin - Biotin Complex</i>	105
7.2.2	<i>Chemicals</i>	106
7.2.2.1	Preparation of Buffers.....	106

7.2.2.2	Preparation of Liposome Solution	107
7.2.3	<i>Surface Chemistry</i>	107
7.2.4	<i>Interaction Experiments</i>	107
7.3	RESULTS AND DISCUSSION	109
7.3.1	<i>Determination of the Optical Properties of the Initial Hydrogel Layer System and Employed Solutions</i>	109
7.3.2	<i>Equilibrium SPR Signals During Binding Experiments and Comparative Simulation</i>	113
7.3.3	<i>Time-Dependence of Binding Processes</i>	119
7.3.3.1	Immobilisation of Streptavidin	119
7.3.3.2	Binding of Biotinylated Protein A to Streptavidin.....	122
7.4	CONCLUSION	125
	REFERENCES	127
	ACKNOWLEDGEMENT	139

1 Summary

In this thesis biocompatible hydrogel coatings were investigated with surface plasmon resonance (SPR), specifically utilising the particular properties of evanescent fields: the exponential decay of the electric field with distance from the surface and the wavelength-dependence of the penetration depth.

In addition to conventional modes of operation, (Θ - 2Θ , measurement of the intensity variation on the SPR-minimum flank), the SPR setup developed here enables for the first time simultaneous real-time measurement of two SPR-signals generated by surface plasmon waves being excited by two different wavelengths. $\lambda = 600\text{nm}$ with 150nm penetration depth and $\lambda = 784\text{nm}$ with 324nm penetration depth were employed. Besides being experimentally easily accessible, they are well suited for the particular problem formulation. The setup allows a detailed investigation of thin three-dimensional layers on surfaces with a thickness in the range of the penetration depth of the evanescent fields. The real-time measurement capability allows for the resolution of the dynamics of such systems.

Hydrogels are organic layer systems, which swell to a multitude of their dry state thickness in aqueous solutions. They are employed to render surfaces biocompatible as well as for biosensing purposes. Although these systems are already used for several applications, some important aspects of their behaviour are not resolved yet. For the class of thermo-responsive hydrogels the phase transition in immobilised state had not been evidenced up to now. In the field of biosensing hydrogels, the dynamics of binding processes had not yet been measured with spatial resolution normal to the surface.

SPR-measurements on novel thermo-responsive hydrogels evidenced for the first time a thermo-responsive effect of a surface-attached polymer. Upon heating, the previously solvated polymer chains collapsed onto the surface, analogous to the precipitation from aqueous solution. The collapse induced a shift in SPR-resonance angle. The thermo-responsive effect was quantified by comparison with simulations: the thickness of the swollen hydrogel amounted to 60nm , in collapsed state its thickness was 5.7nm .

Furthermore, the applicability of thermo-responsive hydrogels for biosensing purposes was investigated. Their ability to suppress non-specific adsorption of BSA decreased significantly with the fraction of hydrophobic groups in the polymer.

Moreover, a thermo-responsive hydrogel was successfully functionalised with protein A and biospecific interactions with rabbit anti-mouse IgG could be measured.

Dextran hydrogels were investigated with the two-wavelengths SPR setup. Its ability to provide vertical spatial resolution was tested in interaction experiments employing a dextran hydrogel.

A relatively uncomplicated three-zone model was developed, which can elegantly explain the time behaviour of the two SPR signals and gives suggestions for the mechanisms of binding processes and preferred binding regions in the hydrogel. The measurements suggest that the hydrogel expands during covalent immobilisation of biomolecules and that the binding process starts at the topmost reactive sites and then advances into deeper zones of the hydrogel. In contrast to this result, biospecific interaction does not change the expansion status of the hydrogel and occurs only in an upper hydrogel zone with limited extension, which remains constant in time.

2 Introduction

As early as 1909, Sommerfeld had introduced the concept of electromagnetic surface waves as a solution of Maxwell's equations for an interface between a non-conducting and a conducting medium (air and earth); he dealt with the problem of wave propagation in radio telegraphy (Sommerfeld 1909). Experimental evidence for the existence of electromagnetic surface waves on a metal / dielectric interface -surface plasmon (SP) waves- was found in the 1950's by experiments with fast electrons passing through metal foils. In 1957, Ritchie assigned the observed characteristic energy losses of the electrons to the excitation of SP waves (Ritchie 1957). In 1960, Stern and Farrell had derived the resonance conditions for these modes and called them "surface plasmons" (Stern 1960).

The excitation of SP waves by light was introduced by Otto in 1968 (Otto 1968). The waves were resonantly excited by means of an attenuated total reflection (ATR)-setup. The resonant excitation of SP waves is called surface plasmon resonance (SPR). In the Otto-configuration, the evanescent field of totally reflected light couples via an air gap to the SP waves on a silver substrate. However, it was the work of Kretschmann that paved the way to a practical application and commercial use of SPR. Also in 1968 he discovered that SP waves can also be excited on top of a silver film deposited on a glass substrate by light being totally reflected on the backside of the silver film, i.e. being reflected at the interface glass / silver (Kretschmann 1968). Thus the Kretschmann-configuration allowed the separation of the elements needed for excitation and detection spatially from the sensing region. The metal film serves as the border between these two parts.

In the early 1980's, Nylander *et al.* and Liedberg *et al.* have demonstrated that surface plasmon resonance in the Kretschmann-configuration is well suited for both gas and biomolecular sensing purposes (Nylander 1982; Liedberg 1983). From there, it took to 1990 until a commercial product came into the market, which made use of the distinct properties of surface plasmon waves: Pharmacia Biosensor (Sweden) introduced the BIAcore biosensor based on surface plasmon resonance (Liedberg 1995). Since then biosensors based on surface plasmon resonance have developed from instruments for a few interested scientists into widespread analytical tools (Homola 1999; Rich 2000; Hall 2001). Their success can be attributed to their ability to detect biomolecular interactions in real time without the need for any labelling. Today, SPR biosensors are routinely used for the analysis of protein-protein, antigen-antibody and protein-peptide interactions. Although the instruments currently available are merely able to handle a small number of samples simultaneously, the current post-genomic era of proteomics (Humphery-Smith 1997) can accomplish a further push for this technique if instrument

developers can succeed in merging SPR detection technique with real high-throughput capabilities. In this context, the development of so-called imaging SPR is promising (Steiner 1999; Brockman 2000; Johansen 2000).

The resonant excitation of surface plasmon waves on a metal film -in biosensing applications usually gold- by totally internal reflected light can be observed as a minimum in the intensity of the reflected light at a certain angle of incidence, the resonance angle Θ_{SPR} . This phenomenon is very sensitive to the refractive index on top of the metal film; changes of the refractive index lead to a shift in the resonance angle. Surface plasmon waves are charge density oscillations on a metal surface and therefore an electric field is associated with them. The electric field is exponentially decaying with increasing distance from the surface. Typically, the decay length or penetration depth of the electric field makes up a third to a half of the exciting wavelength, e.g. for $\lambda = 784\text{nm}$ the penetration depth for gold / water amounts to 324nm. Hence, SPR is an evanescent wave technique, with maximum sensitivity at the interface: only changes of the refractive index in close proximity to the gold surface alter the resonance angle (Stenberg 1991; Liedberg 1993). By tracking the shift of the resonance angle, the deposition of molecules on the surface can be followed in real time. Since the change in refractive index is probed, no labelling of the molecules is necessary. Affinity biosensing makes use of these properties for the investigation of biochemical binding processes between immobilised biomolecules on the sensor surface and analyte biomolecules supplied in solution: monitoring of the interaction in real time enables the user to deduce kinetic and affinity constants of the reaction from the experimental data (Fivash 1998).

However, an important prerequisite for the success of the method is a chemically tailored sensor interface which has to fulfil several tasks:

- stable (covalent) immobilisation of biomolecules as receptors
- providing an environment which maintains the unique biological function of the immobilised biomolecules (specific interaction with their biological counterpart)
- prevention of non-specific adsorption

Often, hydrogels are employed to achieve the desired characteristics: hydrogel functionalised surfaces provide a biocompatible 3D matrix for covalent biomolecule immobilisation. Compared to a flat surface the three dimensional structure allows a higher number of receptor molecules per area unit in addition to lower orientational requirements for the receptors. Furthermore, the entropy elasticity of polymers may play an important role in reducing non-specific adsorption (Lee 1995).

Frequently, dextran, a α -1,6-linked polyglucose with 1,2- and 1,3-branchings is employed (Elam 1984; Piehler 1996). For instance, the "standard" sensor surface for the Biacore biosensor employs a dextran hydrogel that is carboxymethylated to the extent of one carboxyl group per glucose residue and is about 100 to 150nm thick (Löfås 1990; Fägerstam 1992; Earp 1998). For immobilisation of biomolecules the carboxy groups are converted into activated esters which are reactive towards primary amino functions. These surfaces are well established for routine analysis comprising the determination of

the active concentration of analyte molecules and the measurements of reaction kinetics and affinity constants (Rich 2000). However, the actual shape and size of carboxymethylated dextran gels can change due to electrostatic repulsive forces between the carboxy groups, depending on the pH and ionic strength of the solutions the hydrogel is in contact with (Karlsson 1997). Furthermore, the dextran matrix provides binding sites in a three-dimensional arrangement. This is raising the question about the dynamics of binding site occupation and the resulting biomolecule density distribution normal to the surface. In spite of its exponential decay, the evanescent SP wave field is probing refractive index changes in the entire dextran hydrogel. Therefore, the SPR response is also affected by the actual density profile in the hydrogel. These issues are addressed in theoretical papers (Schuck 1996; Witz 1999; Wofsy 2002), but there is no direct experimental evidence of how these layer properties influence the SPR signal respectively to what extent these effects actually occur.

Although dextran fulfils the required tasks satisfactorily in many respects, synthetic hydrophilic polymers are attractive alternatives as they offer some potential advantages. First, they may be more resistant to harsh chemical conditions (strong acids, fouling etc.), since in particular those polymers exhibiting exclusively C-C bonds in their backbone. Second, they allow the synthesis of polymers with new physical properties by tailoring their structure. Impressive examples for the potential provided by tailored hydrogels are so-called thermo-responsive or thermo-sensitive hydrogels (Peppas 1994). The behaviour of thermo-responsive polymers in aqueous media often contradicts intuition because they generally exhibit a lower critical solution temperature (LCST). Upon heating, when the temperature increases beyond a certain value commonly referred to as “cloud point”, they precipitate from solution. Thermo-responsive hydrogels should undergo an analogous transition even under the particular conditions existing in confined space at a surface (Zhu 1999). Such a behaviour is of special interest for applications at sensor surfaces because it allows to switch their properties, or to introduce new functionalities. However, there is no experimental proof for the effect at an interface, yet.

3 Fundamentals

3.1 Surface Plasmon Resonance

Electromagnetic waves guided along the boundary of two media with different dielectric constants are called evanescent waves. Their characteristic feature is the propagation along the interface. They do not transport energy into the adjacent media. However, the electric field of an evanescent wave penetrates into the adjacent media, decaying exponentially with distance from the interface. If one of the media is a dielectric and the other is a metal, these evanescent waves are called surface plasmon (SP) waves or surface plasmon oscillations, because collective oscillations of the free electrons of the metal are associated with these waves. Surface plasmon waves can be resonantly excited by internally reflected p-polarised light. The resonant excitation of surface plasmons is observable as a minimum in the intensity of the reflected light at a certain angle of incidence -the resonance angle Θ_{SPR} - and is called surface plasmon resonance (SPR) (Raether 1988).

3.1.1 Surface Plasmon Waves

For a comprehensive derivation of surface plasmon waves as electromagnetic modes of an interface dielectric D / metal M the reader may be referred to (Boardman 1982; Zhizhin 1982; Raether 1988). Here, the fundamental properties of SP waves on an interface between two semi-infinite media D and M are to be mentioned (figure 1).

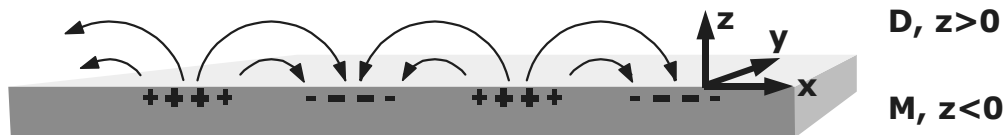


Figure 1. Scheme of a p-polarised surface wave and its electric field on the interface between two semi-infinite media. D: dielectric, M: metal. The oscillating charge density being associated with the electromagnetic wave is indicated.

On an interface as sketched in figure 1, the electric field \mathbf{E}

$$\mathbf{E} = E_0 \cdot e^{i(k_x x - \omega t)} \cdot \left\{ \begin{array}{l} \left(\begin{array}{cc} 1 & 0 \\ 0 & \frac{k_x}{k_{zD}} \end{array} \right) \cdot e^{-ik_{zD} z} \\ \left(\begin{array}{cc} 1 & 0 \\ 0 & \frac{-k_x}{k_{zM}} \end{array} \right) \cdot e^{+ik_{zM} z} \end{array} \right\} \text{ for } \begin{cases} z > 0 \\ z < 0 \end{cases} \quad (1)$$

and the magnetic field \mathbf{H}

$$\mathbf{H} = \frac{\omega}{c} E_0 \cdot e^{i(k_x x - \omega t)} \cdot \left\{ \begin{array}{l} \left(\begin{array}{cc} 0 & \frac{-\epsilon_D}{k_{zD}} \\ 0 & 0 \end{array} \right) \cdot e^{-ik_{zD} z} \\ \left(\begin{array}{cc} 0 & \frac{\epsilon_M}{k_{zM}} \\ 0 & 0 \end{array} \right) \cdot e^{+ik_{zM} z} \end{array} \right\} \text{ for } \begin{cases} z > 0 \\ z < 0 \end{cases} \quad (2)$$

fulfil Maxwell's equations and the continuity relations for the tangential electric and magnetic field components and for the normal components of the electric displacement, when

$$k_x^2 + k_{zj}^2 = \epsilon_j \cdot \left(\frac{\omega}{c} \right)^2, \quad j : D, M \quad (3)$$

$$k_x = \frac{\omega}{c} \cdot \left(\frac{\epsilon_M \cdot \epsilon_D}{\epsilon_M + \epsilon_D} \right)^{1/2} \quad (4)$$

with ω the angular frequency, c the speed of light in vacuum, k_x and k_z the wave vector components, $\epsilon_D = \epsilon_D(\omega)$ the frequency dependent dielectric function of the dielectric and $\epsilon_M(\omega) = \epsilon_{rM}(\omega) - i\epsilon_{iM}(\omega)$ the complex dielectric function of the metal. The dielectric functions are related to the refractive indices by $\epsilon_D(\omega) = n_D(\omega)^2$ and $\epsilon_M(\omega) = (n - ik)^2$.

The case $\epsilon_D \geq 1$ and $\epsilon_{rM} < 0$, $|\epsilon_{rM}| > 1 > \epsilon_{iM} > \epsilon_D$

In this case k_{zj} becomes imaginary or complex, which means the electric fields having their maxima in the surface at $z=0$ with exponential decay into the media. This is characteristic for surface waves.

Furthermore, the expression under the root in equation 4 is larger than ϵ_D , thus $k_x > \epsilon_D^{1/2} \cdot \omega/c = n_D \cdot \omega/c$. Since k_x is always larger than $n_D \cdot \omega/c$, the surface waves cannot directly couple to light in the dielectric ($k_{\text{light}} = n_D \cdot \omega/c$, coupling is forbidden by the law of conservation of momentum). Another distinct characteristic for surface waves.

Although the wave vector k_x is also complex, the dispersion relation of the surface waves can still be calculated from equation 4, simply by substituting ϵ_M by ϵ_{rM} . The

imaginary part of k_x is describing the internal damping Γ_i of the surface waves in x -direction.

The system M: gold, D: water fulfils the conditions $\epsilon_D \geq 1$ and $\epsilon_{rM} < 0$, $|\epsilon_{rM}| > 1 > \epsilon_{iM} > \epsilon_D$ from the wavelength $\lambda = 570\text{nm}$ on (see figure 2). Therefore, in this system SP waves exist. The dielectric functions plotted in figure 2 are taken from (Raether 1988) for gold and from (Lide 1998) for water.

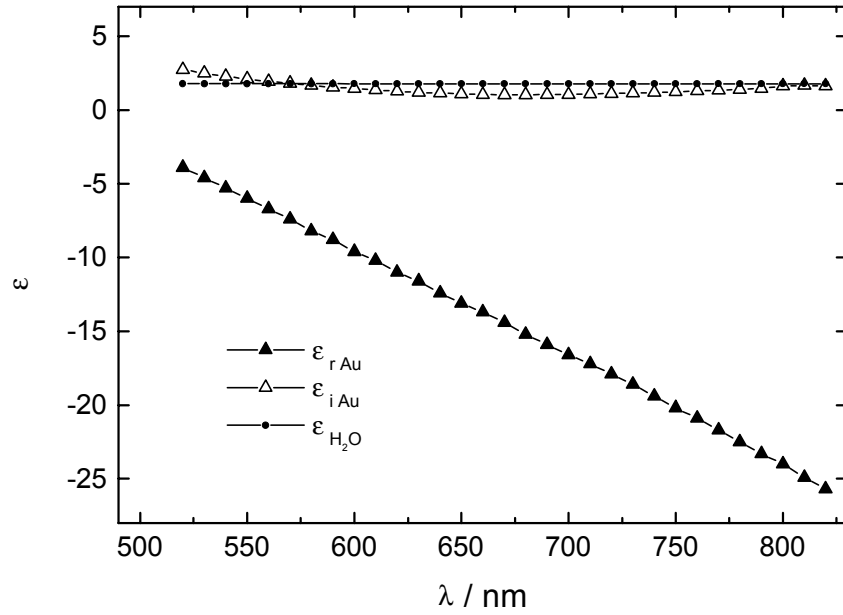


Figure 2. Dielectric functions of gold and water in dependence of the wavelength. From $\lambda = 570\text{nm}$ on the functions fulfil the conditions for the existence of an electromagnetic wave (surface plasmon wave) on the boundary gold / water. The values are taken from (Raether 1988) for gold and from (Lide 1998) for water.

Figure 3 shows the dispersion relation for the interface gold / water and gold / vacuum ($\epsilon_{\text{vac}} = 1$) calculated according to equation 4. The employed dielectric function of gold is calculated according to the model of a free electron gas (Jackson 1982):

$$\epsilon_{Au}(\omega) \approx 1 - \frac{\omega_{p Au}^2}{\omega^2} \quad (5)$$

with the plasma frequency $\omega_{p Au}$

$$\omega_{p Au} = \left(\frac{ne^2}{m\epsilon_0} \right)^{1/2} = 13.7 \cdot 10^{15} \text{ rad / s} \quad (6)$$

(n : electron density, e : elementary charge, m : electron mass, ϵ_0 : permittivity of free space).

For $k \rightarrow \infty$ the dispersion relation approaches an upper bound

$$\lim_{k \rightarrow \infty} \omega_{SP} = \frac{\omega_p}{\sqrt{1 + \epsilon_D}} \quad (7)$$

(equation 4: $k \rightarrow \infty$ means $\epsilon_M \rightarrow -\epsilon_D$, $-\epsilon_D$ inserted in equation 5 yields equation 7).

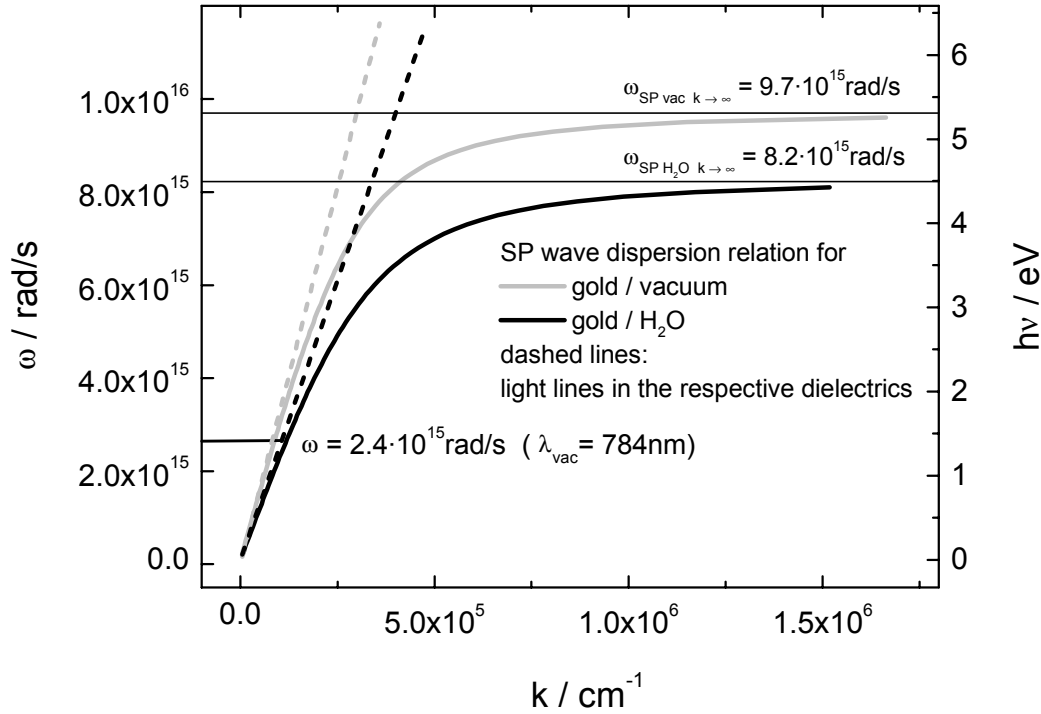


Figure 3. Dispersion relations for SP waves on the interfaces gold / vacuum and gold / water. For water a constant refractive index of 1.330 was assumed. The dielectric function for gold was calculated according to equation 5. The dashed lines are the light lines $\omega = kc/n_D$ in the respective media. The wave vectors of the SP waves are always larger than the respective wave vectors of light. The horizontal lines mark the upper bounds of the angular frequencies of the SP waves. Furthermore, the angular frequency of $\lambda_{vac} = 784\text{nm}$ is drawn in; an often used wavelength in this work.

The dependence of the dispersion relation of SP waves from ϵ_D respectively n_D is the fundamental feature for the application of SPR. A change in the SP wave propagation characteristics means the occurrence of a change in n_D .

3.1.2 The Kretschmann-Configuration

In the Kretschmann-configuration, SP waves on top of a thin metal film deposited on a glass substrate are resonantly excited by totally reflected light (Kretschmann 1968). Their field probes the dielectric properties of the medium on top of the metal film.

At angles larger than the critical angle totally reflected light forms an evanescent wave which penetrates the thin metal film. The evanescent light field can couple to the SP waves, since the wave vector of light in glass is increased by the factor n_{glass} . The x-component of the light wave penetrates the interfaces without alteration and can be adjusted by varying the angle of incidence Θ (see figure 4).

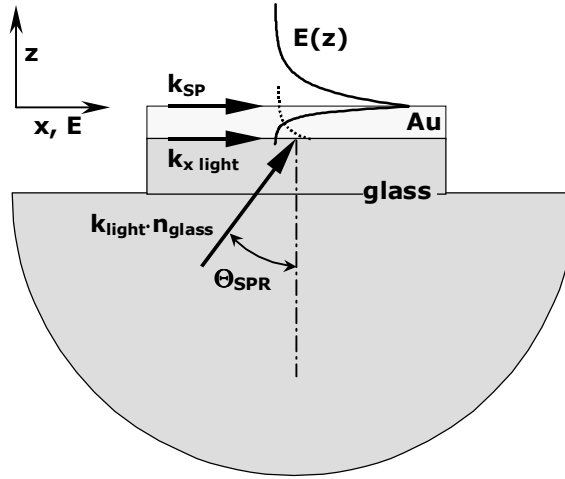


Figure 4. Excitation of surface plasmon waves by internally reflected light in the Kretschmann-configuration. A gold coated glass slide is optically coupled to a glass prism. At the resonance angle Θ_{SPR} the projection of the light wave vector in glass $k_{x \text{ light}}$ is equal to the wave vector of the surface plasmon wave k_{SP} . The dashed line indicates the evanescent light field which is penetrating the gold film and exciting the SP waves. The exponentially decaying electric field $E(z)$ of the SP wave is also sketched. Since the SP waves are excited resonantly their electric field is enhanced (resonance amplification).

At the particular angle of incidence Θ_{SPR} -the resonance angle- the SP waves are resonantly excited by the evanescent light field, because the resonance conditions are fulfilled: $\omega_{\text{light}} = \omega_{\text{SP}}$ and $k_{x \text{ light}}(\Theta_{\text{SPR}}) = k_{\text{SP}}$.

Although equation 4 must be modified for the Kretschmann-configuration (Kretschmann 1971; Chen 1981), it holds as a good approximation, thus

$$\Theta_{\text{SPR}} = \arcsin \left[\frac{1}{n_{\text{glass}}} \cdot \left(\frac{\epsilon_M \cdot \epsilon_D}{\epsilon_M + \epsilon_D} \right)^{1/2} \right] \quad (8).$$

Figure 5 shows the measured dispersion relation for the system BK7 glass / gold / water in comparison to dispersions relations calculated according to equations 4 and 5. The good accordance proves the employed equations to describe the system decently.

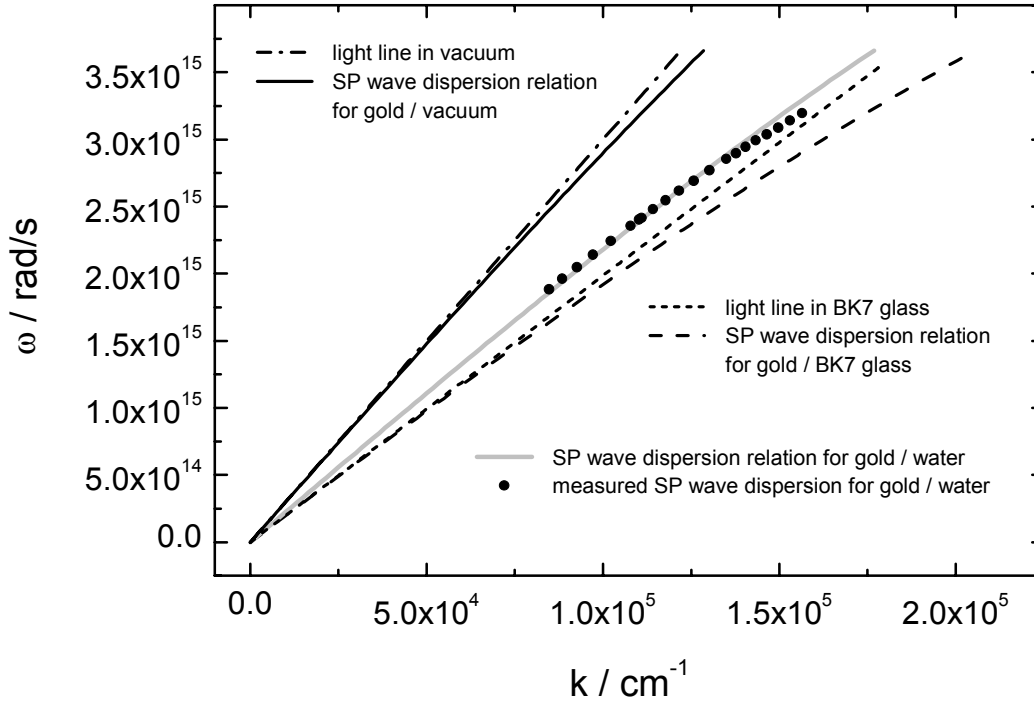


Figure 5. Calculated and measured dispersion relations of SP waves (compare with figure 3). The filled circles represent measurements between $\lambda = 590\text{nm} - 1000\text{nm}$ in a system BK7 glass / 50nm gold / water. The solid lines represent calculated dispersion relations according to equations 4 and 5 for different dielectrics. The broken lines represent the light lines in vacuum and BK7 glass. Since SP waves on a gold / BK7 interface have larger wave vectors than light in BK7, they can not be excited by light in BK7. Consequently there is no SP wave excitation on the interface glass / gold in the Kretschmann-configuration and n_D must be smaller than n_{glass} for SPR measurements.

In case of resonant SP wave excitation the light energy is transferred into the SP waves; the reflected light intensity I_r decreases drastically. This can be observed as a characteristic minimum in $I_r(\Theta)$ -plots (see figure 8). In the literature this minimum is sometimes referred to as “plasmon”, although this term is actually reserved to the quantum of plasma oscillations.

In the Kretschmann-configuration plasmons can decay into photons since a fraction of their electric field still penetrates into the glass prism. The imaginary k_z transforms into a real k_z , and a propagating wave is generated leading to an increased $I_r(\Theta_{\text{SPR}})$ - this effect is known as radiation damping Γ_{rad} . The radiation damping can be decreased by larger gold film thickness, however, then the coupling of the evanescent light field to the SP waves becomes less efficient and $I_r(\Theta_{\text{SPR}})$ increases also. Consequently, in order to minimise $I_r(\Theta_{\text{SPR}})$, the gold film thickness needs to be optimised for each wavelength, since the evanescent light field also possesses a wavelength dependent penetration depth. In case of optimal gold film thickness, $I_r(\Theta_{\text{SPR}}) = 0$ is possible.

In the experiments presented in this work, the surface plasmon waves propagate on top of a 50nm thick gold film. This thickness is a reasonable compromise for SPR experiments which employ different wavelengths.

3.1.3 Penetration Depth of SP Waves

The dispersion relation and thus Θ_{SPR} depend on the refractive index which is perceived by the surface plasmon waves within the penetration depth of their electric field. The perceived refractive index can be constant within the penetration depth of the electric field of the surface plasmon waves or can be an effective, averaged refractive index n_{eff} if the medium is not homogeneous within the penetration depth.

If d_{PD} denotes the penetration depth of the surface plasmon waves defined by $E(z = d_{\text{PD}}) = 1/e \cdot E_0(z = 0)$, the effective refractive index can be calculated according to Jung *et al.* (Jung 1998):

$$n_{\text{eff}} = (2/d_{\text{PD}}) \cdot \int_0^{\infty} n(z) \cdot \exp(-2z/d_{\text{PD}}) dz \quad (9)$$

where $n(z)$ is the index of refraction at height z over the gold surface. The factor 2 in equation 9 considers that the refractive index $n(z)$ is probed by the intensity of the electric field of a surface plasmon wave, meaning squared electric field (Liedberg 1993; Jung 1998).

The penetration depth can be calculated by (Jung 1998):

$$d_{\text{PD}} = (\lambda/2\pi) / \text{Re} \left\{ -n_{\text{eff}}^4 / (n_{\text{eff}}^2 + \epsilon_M(\omega)) \right\}^{1/2} \quad (10)$$

The penetration depth varies only weakly with n_{eff} which justifies to assume a constant penetration depth for a certain wavelength. But, since the penetration depth is linearly dependent on the wavelength, it is possible to probe differently deep into the vicinity of the gold film with surface plasmon waves excited by different wavelengths. Figure 6 shows d_{PD} as a function of the excitation wavelength and the variation of d_{PD} with n_{eff} .

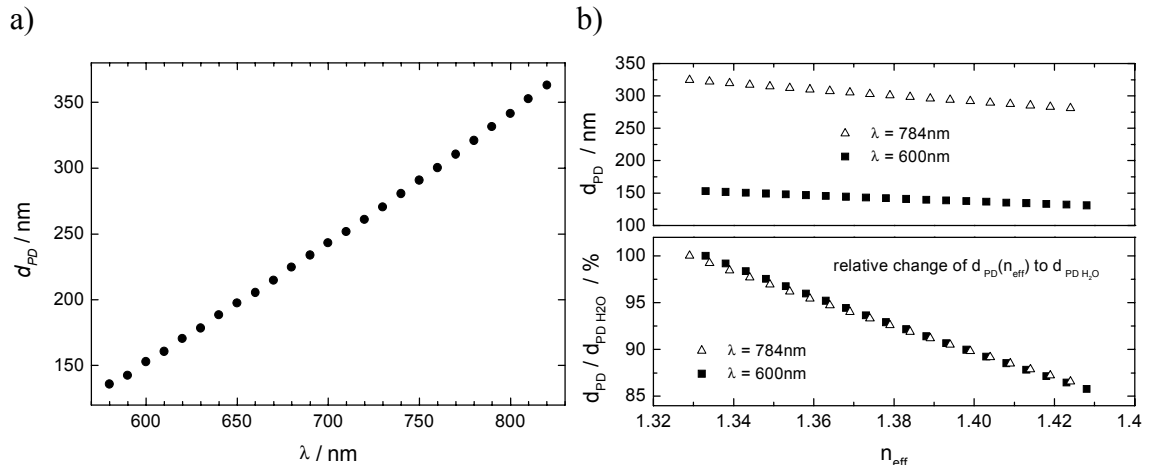


Figure 6. *a)* The penetration depth d_{PD} of surface plasmon waves in dependence of the excitation wavelength according to equation 10. *b)* Upper graph: The variation of d_{PD} with the effective perceived refractive index n_{eff} , calculated for $\lambda = 600\text{nm}$ and $\lambda = 784\text{nm}$. Lower graph: The relative change of d_{PD} to $d_{\text{PD,H}_2\text{O}}$ in water.

3.1.4 Reflectivity of a Layer System

The excitation of SP waves can be observed as a pronounced minimum in $I_r(\Theta)$ -plots, which are showing the reflected intensity as a function of the angle of incidence Θ . The reflectivity of a layer system can be calculated by applying Fresnel's equations. The theory describes the decrease of reflectivity due to occurrence of SPR accurately, if the correct complex indices of refraction are supplied. This enables the comparison of experimental results with calculated SPR curves of a model layer system. An elegant method to calculate the reflectivity of a layer system is the 2×2 - or Jones matrix formulation. This formalism shall be introduced here in short form; a very comprehensive and clear description can be found in (Yeh 1988).

In this work, the reflectivity $R_p(\omega, \Theta)$ of a model layer system is calculated for p-polarised light as a function of frequency ω and angle of incidence Θ by employing the 2×2 matrix formulation in a computer program (Neumaier 1998). As a simplification, the model assumes the layers to be ideally smooth and homogeneous.

Figure 7 shows a layer system consisting of N layers entered by an electromagnetic wave with electric field E (Yeh 1988) (Kajenski 1997).

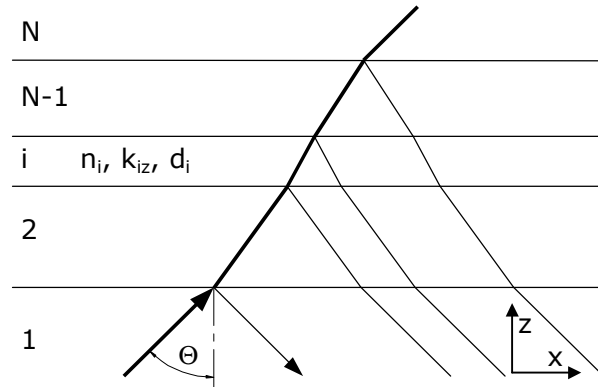


Figure 7. A multilayer system consisting of N layers, each with individual properties, is entered by a light beam with angle of incidence Θ . The reflectivity can be calculated by considering the contribution of each interface and each layer by applying the 2×2 matrix formalism.

Since the whole system is homogenous in the x direction, the electric field can be described by

$$E = E(z) \exp[i(\omega t - k_x x)] \quad (11)$$

The electric field $E_1(z)$ in layer 1 (see figure 7) can be written as

$$E_1(z) = F_1 e^{-ik_z z} + B_1 e^{ik_z z} \equiv F_1(z) + B_1(z) \quad (12)$$

Here $F_1(z)$ represents the amplitude of the wave travelling in positive z direction and $B_1(z)$ the amplitude of the wave travelling in negative z direction. Analogously the amplitudes $F_i(z)$ and $B_i(z)$ for each layer can be written.

The 2×2 matrix formalism assigns a dynamic matrix D_{ij} to each interface:

$$D_{ij} = \frac{1}{t_{ij}} \begin{pmatrix} 1 & r_{ij} \\ r_{ij} & 1 \end{pmatrix} \quad (13)$$

with the Fresnel reflection coefficients for p-polarised light

$$r_{ij} = \frac{n_i^2 k_{jz} - n_j^2 k_{iz}}{n_i^2 k_{jz} + n_j^2 k_{iz}} \quad (14)$$

and the Fresnel transmission coefficients for p-polarised light

$$t_{ij} = \frac{2n_i^2 k_{jz}}{n_i^2 k_{jz} + n_j^2 k_{iz}} \quad (15).$$

D_{ij} describes the effect of the interface of layer i and j on the electric field vectors of the electromagnetic wave. Each layer itself is described by the propagation matrix P_i

$$P_i = \begin{pmatrix} \exp(ik_{zi}d_i) & 0 \\ 0 & \exp(-ik_{zi}d_i) \end{pmatrix} \quad (16)$$

considering the phase relation of the electric field within the concerned layer i at the interfaces with the layers $i - 1$ and $i + 1$.

Ultimately, the relation of amplitudes F_1 , F_N and B_1 , B_N can be calculated by

$$\begin{pmatrix} F_1 \\ B_1 \end{pmatrix} = D_{12} \cdot P_2 \cdot D_{23} \cdot P_3 \cdots D_{N-1N} \cdot \begin{pmatrix} F_N \\ B_N \end{pmatrix} = \begin{pmatrix} M_{11} & M_{12} \\ M_{21} & M_{22} \end{pmatrix} \cdot \begin{pmatrix} F_N \\ B_N \end{pmatrix} \quad (17)$$

and since $B_N = 0$, the reflectance can be calculated by

$$R_p = |r_p|^2 = \left(\frac{B_1}{F_1} \right)^2 = \left| \frac{M_{21}}{M_{11}} \right|^2 \quad (18).$$

Figure 8 shows the calculated plasmon resonance curves for $\lambda = 784\text{nm}$ and $\lambda = 600\text{nm}$. Table 1 contains the employed values for layer thicknesses, the refractive indices and the references for the values.

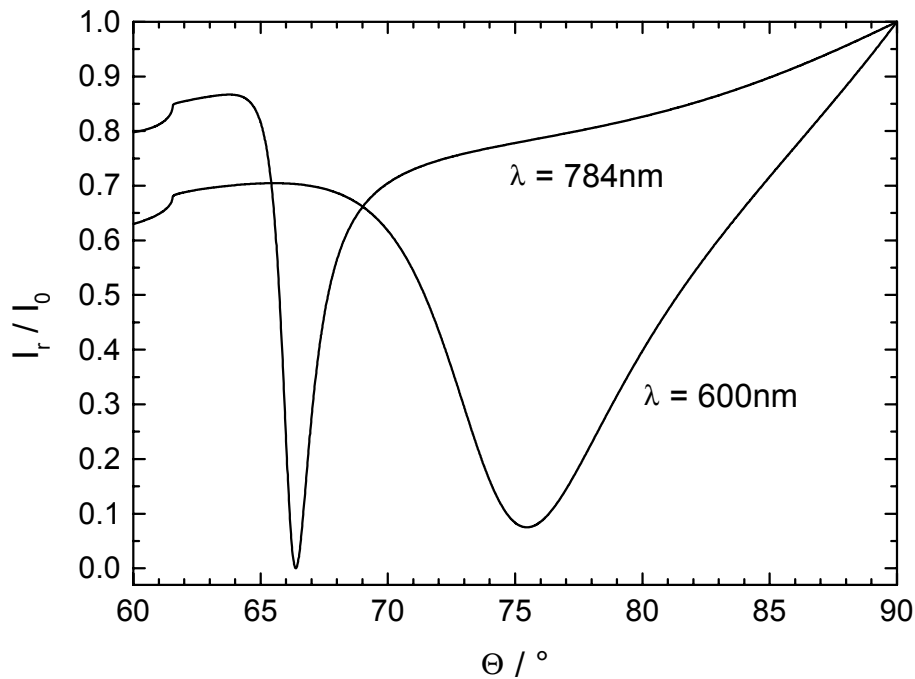


Figure 8. Calculated surface plasmon resonance curves of the layer system given in table 1 for excitation wavelengths of 600nm and 784nm. I_r denotes the reflected intensity, I_0 the entering intensity.

layer no. i	name, reference	d / nm	λ / nm	n
1	BK7 glass, calculated by Sellmeier equation (Schott 2000)	∞	784	1.511
			600	1.516
2	gold, (Raether 1988)	50	784	0.149-i4.779
			600	0.233-i3.107
3	water, second order exp. fit to data (Lide 1998)	∞	784	1.329
			600	1.333

Table 1. The layer system which is employed for the calculation of the surface plasmon resonance curves in figure 8. The given values ensure good accordance between the calculated SPR curves and the real base system used in this work. A 1nm thick NiCr 80/20 adhesion layer between glass and gold is neglected. Based on this layer system, all subsequent simulations in this work were performed.

3.2 Biomolecular Interaction Analysis with SPR

The surface plasmon resonance detection principle allows detection of refractive index changes close to the sensor surface in real time. If these refractive index changes are caused due to binding of a molecule species in solution to a molecule species immobilised onto the sensing surface, real time monitoring of this process allows deduction of chemical rate and affinity constants of the interaction. The investigation of highly specific interaction between a biomolecule and its biological counterpart is called 'biomolecular interaction analysis' (BIA). The method itself is named 'affinity biosensing' and the sensors are 'affinity sensors' or 'SPR biosensors' (Malmqvist 1994).

In typical experiments, one of the interacting species is covalently attached to the sensor surface, giving the biosensor the biospecificity. That member of the specific binding pair is known as the 'ligand', or, often, more intuitively called the 'receptor', although this term is originally used only for acceptor molecules on a cell surface. The 'analyte' is injected on to the surface and the binding is recorded with respect to time. This is known as the association phase. In the dissociation phase, the analyte solution is replaced by buffer solution and the loss of bound analyte from the surface is monitored (Szabo 1995).

The signals versus time plots are evaluated by application of a mathematical model to the curves; Langmuir adsorption isotherms are often suitable for the description of biomolecular interaction measurements. Deviations from the Langmuir model can be caused by the failure of the interacting system to be adequately described by a single unified binding step (e.g., the system exhibiting a conformational changes after forming the complex with altered dissociation constant; two slightly different species of receptors are present with different rate constants, so called surface heterogeneity) (Morton 1995), mass transport phenomena in the flow chamber (Christensen 1997) and probably by employment of a hydrogel matrix used for receptor immobilisation (see chapter 2.3) (O'Shannessy 1996; Schuck 1996; Witz 1999). These effects can be modelled by more complex mathematical models (Morton 1995; Karlsson 1997), but the application needs to be reviewed and should only be taken into consideration if the nature of the participating binding partners or the experimental procedure itself definitely requires the use of a more complex model. Since complex models almost always describe interaction measurements better than a simpler model -in terms of reduced sum of squared residuals between measurement and fit curve- it appears tempting to employ these models. However, the deduced rate and affinity constants are not necessarily closer to the true values. This is determined by application of the right model (Schuck 1997a) and importantly by proper experimental design and execution (Rich 2000) (Karlsson 1997). Ultimately, the prerequisites for Langmuir-like adsorption behaviour are often fulfilled in biomolecular interaction experiments and thus the Langmuir isotherm is often the appropriate model for mathematical description of the measurements.

3.2.1 The Langmuir-Isotherm

The term Langmuir-isotherm was used in 1916 by Irving Langmuir to describe the dependence of the surface coverage of an adsorbed gas on the pressure of the gas above the surface at a fixed temperature (Langmuir 1916).

The main assumptions of the Langmuir model are:

- Adsorption takes place only at specific localised sites on the surface and the saturation coverage corresponds to complete occupancy of these sites.
- Each site can accommodate one and only one molecule or atom (1:1 stoichiometry).
- The surface is energetically homogeneous, and there is no interaction between neighbouring adsorbed molecules or atoms.

The chemical equation 19 describes the formation of a molecular complex AR formed by an analyte molecule A and by a receptor molecule R as it takes place during a biomolecular interaction described by a Langmuir isotherm. The interaction of the two molecules binding to each other is described by two rate constants, the association rate constant k_a and the dissociation rate constant k_d . The association rate describes the collision frequency and the attraction between two molecules, while the dissociation rate describes the stability of the molecular complex AR (O'Shannessy 1996).



The formation of molecule complexes AR with time can be described by

$$dc_{AR} / dt = k_a c_A(t) [c_R - c_{AR}(t)] - k_d c_{AR}(t) \quad (20)$$

where $c_{AR}(t)$ is the concentration of formed complexes, c_R the concentration of immobilised receptor molecules, $c_R - c_{AR}(t) = c_{fR}(t)$ the decreasing number of free receptor molecules c_{fR} with time and $c_A(t)$ the concentration of analyte molecules. The last term describes the dissociation of already formed complexes AR.

For a flow chamber with continuous analyte solution flow during the association phase or for a reaction chamber which is sufficiently large, it can be assumed that $c_A(t) = c_A \approx \text{constant}$.

The SPR response or signal S -usually the shift in resonance angle $\Delta\Theta_{\text{SPR}}$ - is linearly proportional to the amount of bound analyte within a wide range. According to Stenberg *et al.* (Stenberg 1991) the sensitivity $d\Theta_{\text{SPR}}/d\Gamma$ of SPR is constant within a range of mass loading Γ of 2 to 50ng/mm² independent from the species of proteins bound to the sensor surface:

$$d\Theta_{\text{SPR}}/d\Gamma = 0.10^\circ \pm 0.01^\circ (\text{ng/mm}^2)^{-1} \quad (21)$$

Thus equation 20 can be rewritten to

$$dS / dt = k_a c_A [S_{\text{max}} - S(t)] - k_d S(t) \quad (22)$$

S_{\max} is the SPR signal which would be obtained, if all receptors would form a molecule complex with an analyte molecule. An integrated form of equation 22 is

$$S(t) = S_{eq} [1 - \exp(-k_{obs}t)] \quad (23)$$

with the equilibrium signal level S_{eq} which will be reached for $t \rightarrow \infty$ for a certain analyte concentration c_A . S_{eq} is (from equation 22)

$$S_{eq} = \frac{k_a S_{\max} c_A}{k_a c_A + k_d} = \frac{S_{\max} c_A}{K_d + c_A} \quad (24)$$

with

$$K_D = \frac{k_d}{k_a} = \frac{1}{K_A} \quad (25)$$

the dissociation equilibrium constant and K_A the association equilibrium constant.

The right term in equation 24 is the ‘biosensor-analogue’ of the original Langmuir isotherm. (When considering adsorption isotherms the norm is to adopt a definition of surface coverage (θ) which defines the maximum surface coverage of a particular adsorbate on a given surface always to be unity, i.e. $\theta_{\max} = 1$. This way of defining the surface coverage differs from the one usually adopted in affinity biosensing where the more common practice is to equate θ with the ratio of analyte molecule concentration to receptor molecule concentration.)

Equation 23 gives the time behaviour of the SPR signal during a biomolecular interaction measurement with the observed rate constant k_{obs}

$$k_{obs} = k_a c_A + k_d \quad (26)$$

In the dissociation phase the change of the SPR signal in time will be

$$dS / dt = -k_d \cdot S(t) \quad (27)$$

provided, that $c_A = 0$ for all times, implying the removal of analyte molecules originating from dissociated complexes by a continuous buffer flow (see equation 22). Consequently the dissociation phase of the interaction measurement will follow a single exponential decay

$$S(t) = S_0 \exp(-k_d t) \quad (28)$$

Molecular interactions which are described by the equations introduced here, are usually named pseudo-first-order-kinetics analogously to the terminology used in chemistry for chemical reaction kinetics involving one reaction partner having constant concentration (here, in the derivation for biosensing applications denoted by $c_A(t) = c_A \approx \text{constant}$).

Table 2 shows frequently used quantities related to affinity biosensing and their units.

Name	Quantity	Unit	Alternative unit
Association rate constant	k_a	$(\text{mol/l}\cdot\text{s})^{-1} = (\text{Ms})^{-1}$	
Dissociation rate constant	k_d	s^{-1}	
Association equilibrium constant	K_A	$(\text{mol/l})^{-1} = \text{M}^{-1}$	
Dissociation equilibrium constant	K_D	$(\text{mol/l}) = \text{M}$	
Molecular weight (molar mass)	MW (M)	g/mol	Da = g/mol
Concentration	c	mol/l = M	$\mu\text{g/ml} = 1000\cdot\text{Da}\cdot\text{M}$
Mass loading	Γ	ng/mm^2	$\text{ng/cm}^2 = 100\cdot\text{ng/mm}^2$

Table 2. Frequently used quantities related to affinity biosensing and their units.

3.2.2 SPR Biosensor Data Evaluation

The evaluation of kinetic measurements carried out with an SPR biosensor will be concisely outlined here. The measurements were made with the SPR setup used for this PhD thesis, demonstrating its suitability for BIA purposes in spite of the absence of a continuous liquid flow (see chapter 1 for a comprehensive description of the SPR setup and the ‘differential intensity measuring mode’ used for the measurements here).

The interacting system consists of:

- A synthetic peptide (VSV-G peptide) containing 11 amino acids of Vesicular Stomatitis Virus Glycoprotein (VSV-G) as immobilised agent (receptor). $MW_{\text{VSV-G peptide}} = 1565\text{Da}$.
- A monoclonal Immunoglobulin G (IgG) antibody produced by a mouse as analyte (anti-VSV-G). Anti-VSV-G recognises an epitope of VSV-G containing the amino acids of the VSV-G peptide. $MW_{\text{anti-VSV-G}} \approx 150\text{kDa}$.

In infected cells, the antibody localises the immature forms of VSV-G in the rough endoplasmic reticulum and in the cisternae of Golgi complex, as well as mature VSV-G at the cell surface and in the budding virus (Nayak 1985).

Figure 9 shows SPR kinetic measurements of the interaction between VSV-G peptide and anti-VSV-G at two different concentrations of anti-VSV-G. At $t \approx 600\text{s}$ anti-VSV-G is injected; at $t \approx 1800\text{s}$ the analyte solution was replaced by buffer solution. The SPR response is expressed in SPR angle shift $\Delta\Theta_{\text{SPR}}$.

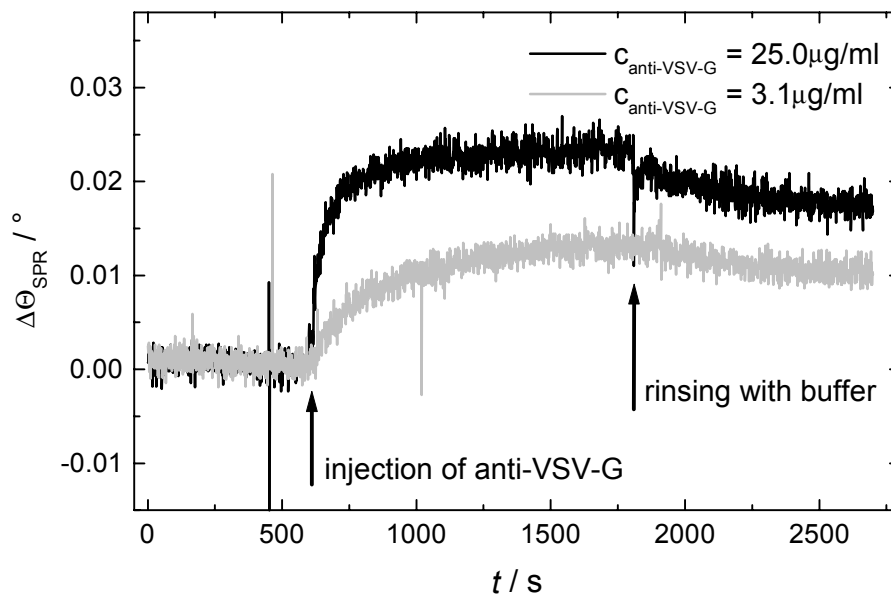


Figure 9. SPR measurements of the interaction between immobilised VSV-G peptide and anti-VSV-G IgG at two different concentrations of anti-VSV-G. The signal decrease due to dissociation of anti-VSV-G – VSV-G peptide complexes starts as soon as the analyte solution is replaced by buffer ($t \approx 1800\text{s}$).

According to equation 23 exponential curves can be fitted to the association part of the kinetics. The fitting parameters are the equilibrium signal level $\Delta\Theta_{\text{SPR eq}}$ (corresponding to S_{eq} in equation 23) and the observed rate constant k_{obs} . Figure 10 shows the fitted curves to five different measurements corresponding to anti-VSV-G concentrations between $1.6\mu\text{g/ml}$ and $25\mu\text{g/ml}$. Furthermore, for $c_{\text{anti-VSV-G}} = 25.0, 12.5$ and $3.1\mu\text{g/ml}$ the dissociation part of the curve is fitted according to equation 28. Table 3 is containing the experimentally determined values.

The number of data points is reduced to facilitate the fitting process.

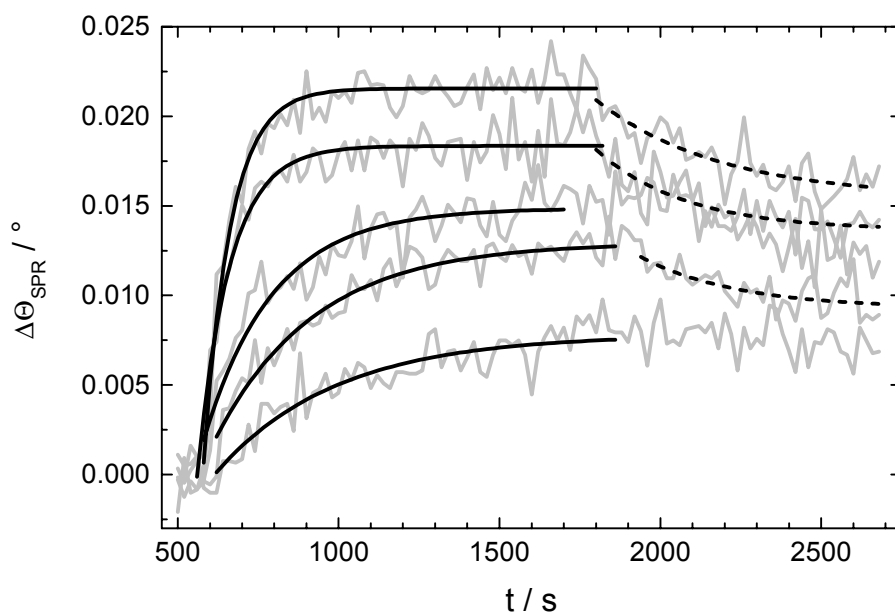


Figure 10. Fitted curves to the association parts (black solid curves, according to equation 23, fitting parameters $\Delta\Theta_{\text{SPR eq}}$ and k_{obs}) and the dissociation parts (black dashed curves, according to equation 28, fitting parameter k_d) of the kinetic measurements between VSV-G peptide and anti-VSV-G. Concentrations of anti-VSV-G (from lower curve to upper curve): 1.6, 3.1, 6.3, 12.5, 25.0 $\mu\text{g/ml}$. The number of data points is reduced in order to facilitate the fitting process. The values generated by the fitting processes are shown in table 3.

$c_{\text{anti-VSV-G}} / \mu\text{g/ml}$	$c_{\text{anti-VSV-G}} / \text{nM}$	$\Delta\Theta_{\text{SPR eq}} / ^\circ$	$k_{\text{obs}} / \text{s}^{-1}$	k_d / s^{-1}
1.6	11	0.0078	0.0026	no data
3.1	21	0.0130	0.0032	0.0033
6.3	42	0.0149	0.0046	no data
12.5	83	0.0181	0.0100	0.0036
25.0	167	0.0216	0.0120	0.0026

Table 3. Results from the fitting processes displayed in figure 10. For $c_{\text{anti-VSV-G}} = 1.6$ and 6.3 $\mu\text{g/ml}$ the fit to the dissociation part of the curve did not give reasonable values.

By plotting k_{obs} against the analyte concentration, the association rate constant k_a and the dissociation rate constant k_d can be determined by means of a linear fit $k_{\text{obs}}'(c)$ to the data (see figure 11). According to equation 26 the slope $d(k_{\text{obs}}')/dc$ of the linear fit yields k_a ; the intersection of the linear fit with the ordinate yields k_d .

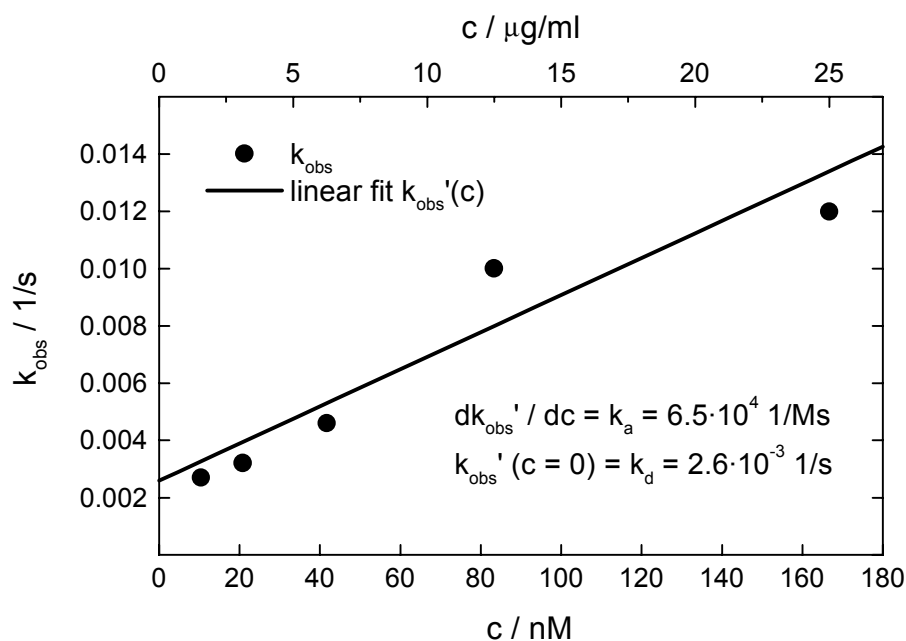


Figure 11. The observed rate constant k_{obs} in dependence of the analyte concentration c as determined by the curve fits displayed in figure 10. The straight line $k_{obs}'(c)$ represents a linear fit to the data. The association rate constant k_a equals the slope of the straight line; the intersection of the straight line with the ordinate gives the dissociation rate constant k_d .

According to equation 24 the equilibrium signal level $\Delta\Theta_{SPR\ eq}$ follows a Langmuir isotherm when plotted against the analyte concentration. Fitting a Langmuir isotherm with the fit parameters $\Delta\Theta_{SPR\ max}$ (corresponding to S_{max} in equation 24) and the dissociation equilibrium constant K_d to such a graph will give the corresponding values (see figure 12).

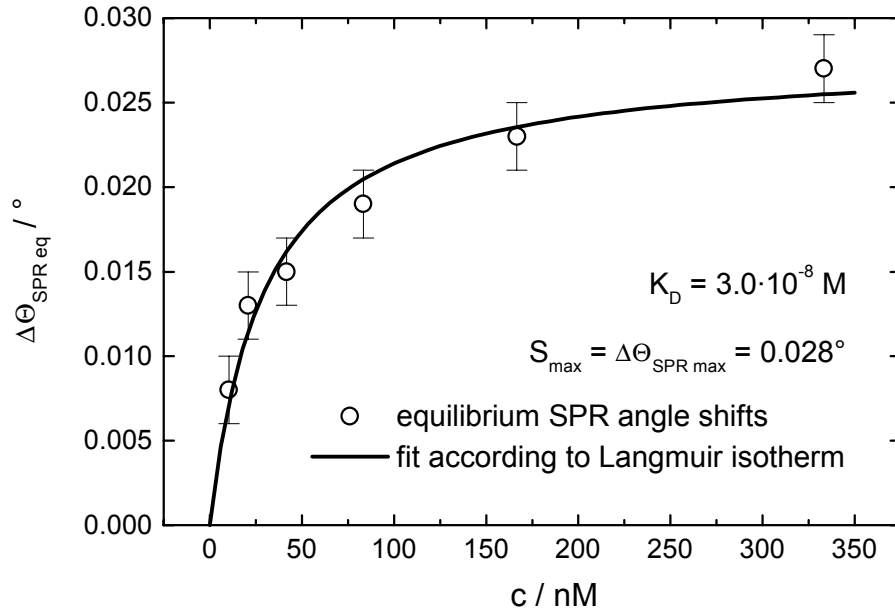


Figure 12. The SPR equilibrium levels as determined by the fits in figure 10 plotted against the analyte concentration c . The evolution of the data follows a Langmuir isotherm. The fit according to equation 24 gives the theoretical maximum SPR angle shift $\Delta\Theta_{SPR max}$, which would be obtained if all receptors are occupied and the dissociation equilibrium constant K_D . The error bars indicate the standard deviation of the measurements caused by instrumental noise.

The determination of the maximum SPR angle shift $\Delta\Theta_{SPR max}$ enables the calculation of the receptor immobilisation density, in case the molecular weight of both the analyte molecule and the receptor molecule is known. According to the Langmuir theory, the value $\Delta\Theta_{SPR max}$ corresponds to the occurrence that every and each single receptor molecule has bound one analyte molecule. Furthermore, $\Delta\Theta_{SPR}$ (and thus also $\Delta\Theta_{SPR max}$) is directly linked to a certain mass loading of the sensor surface by equation 21. Consequently, the mass loading of receptor molecules is simply given by the ratio R_{MW} of the molecular masses of the analyte and the receptor molecules.

According to equation 21 the maximum mass loading $\Gamma_{anti-VSV-G max}$ of the sensor surface with anti-VSV-G antibody is

$$\Gamma_{anti-VSV-G max} = \Delta\Theta_{SPR max} \cdot \left(\frac{d\Theta_{SPR}}{d\Gamma} \right)^{-1} = 0.28 \text{ ng/mm}^2 \quad (29)$$

Since $MW_{anti-VSV-G} \approx 150 \text{ kDa}$ and $MW_{VSV-G peptide} = 1565 \text{ Da}$ the mass ratio is $R_{MW} = MW_{anti-VSV-G} / MW_{VSV-G peptide} \approx 100$ and thus

$$\Gamma_{VSV-G peptide} \approx 1/100 \Gamma_{anti-VSV-G} = 2.8 \text{ pg/mm}^2 \quad (30)$$

This means $1.8 \text{ fmol/mm}^2 = 1.1 \cdot 10^9 / \text{mm}^2$ VSV-G peptide molecules are immobilised on the sensor surface.

Additionally to the outlined approach for kinetic data evaluation, the software “CLAMP” is readily available (<http://www.cores.utah.edu/interaction/clamp.htm>) (Myszka 1998). CLAMP both simulates and analyses biomolecular interaction data; the software program is especially designed to interpret complex interactions (e.g. it also includes terms for mass transport limited binding processes) recorded on biosensors. It combines numerical integration and non linear global curve fitting routines. Morton *et al.* (Morton 1995) have shown that fitting association and dissociation phase data simultaneously often returns better parameter estimates and provides a more stringent test for complex binding mechanisms. Of course, CLAMP can also be applied to simple 1:1 pseudo-first-order kinetics which follow Langmuir isotherms; the strength of the software in that case is, that all curves recorded at different analyte concentrations can be analysed at once. This is not only faster, grouping data sets that share common parameters improves the statistical behaviour of the parameter estimates (Morton 1995) (Myszka 1997). Figure 13 shows the kinetic measurements from figure 10 again, but here fitted by CLAMP with a 1:1 pseudo-first-order model.

The results of the two different evaluation methods introduced here are given in table 4. The association rate constants k_a are in good agreement for both methods; the dissociation rate constants k_d differ from each other. This can be caused by the particular experimental procedure which is applied for the measurement of the dissociation parts of the kinetics. The association is stopped –and thus the dissociation started- by replacing the analyte solution with buffer, but not by supplying a constant buffer flow. Only this would guarantee zero analyte concentration during dissociation; the prerequisite for a dissociation following equation 28 exactly.

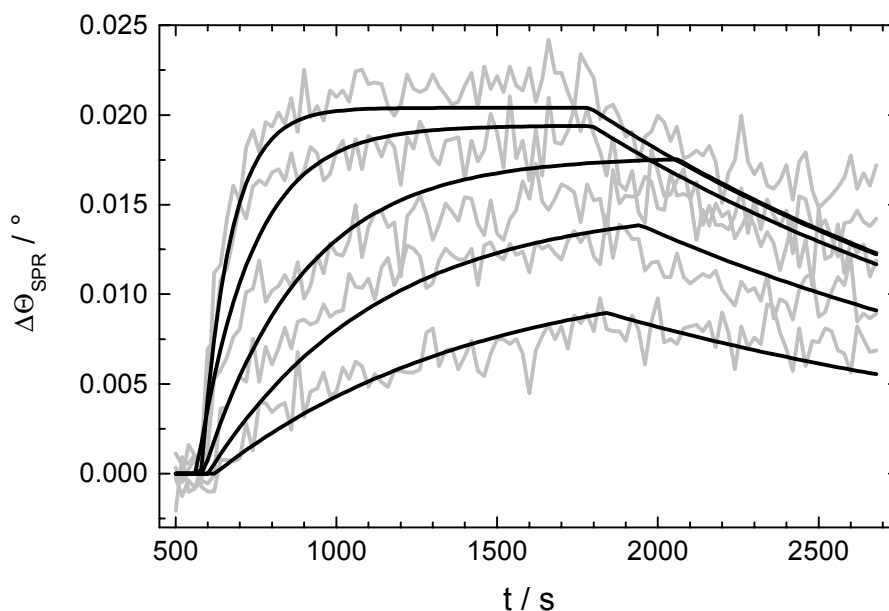


Figure 13. Kinetic measurements from figure 10 fitted by the software CLAMP with a 1:1 pseudo-first-order interaction model (which corresponds to a Langmuir-like adsorption behaviour). The results are given in table 4.

Method of data evaluation	$k_a / (\text{Ms})^{-1}$	k_d / s^{-1}	K_A / M^{-1}	K_D / M	$\Delta\Theta_{\text{SPR eq}} / ^\circ$
fit to each single curve, evaluation according to the Langmuir theory	$6.5 \cdot 10^4$	$2.6 \cdot 10^{-3}$ (from figure 11) $(3.2 \pm 0.5) \cdot 10^{-3}$ (from fit to dissociation parts)	$3.3 \cdot 10^7$ (= $1/K_D$)	$3.0 \cdot 10^{-8}$ (from figure 12)	0.028
CLAMP, 1:1 pseudo-first-order model, all 5 curves at once	$6.4 \cdot 10^4$	$5.7 \cdot 10^{-4}$	$1.1 \cdot 10^8$	$8.9 \cdot 10^{-9}$	0.022

Table 4. The kinetic data for the interacting system VSV-G peptide – anti-VSV-G as determined by two different evaluation methods. The association rate constants k_a are in good agreement; the dissociation rate constant k_d (and thus K_A and K_D) differ. This might be caused by the particular execution of the experiment, which does not really fulfil the condition of zero analyte concentration during dissociation: the analyte solution is only replaced by buffer solution, however, a constant buffer flow removing analyte molecules from dissociated molecule complexes was not applied.

3.3 Biosensing Hydrogels for SPR Detection

SPR is an evanescent wave technique being sensitive for a distance of some hundred nanometers from the surface. Therefore biomolecular interactions which shall be measured by SPR need to occur close to the surface. This is achieved by immobilising one interaction partner on the surface and supplying the other in solution.

In virtually all studies until the late 1980s, the sensing layer of biological recognition molecules was attached directly to the SPR sensor surface by physical adsorption (Garland 1996). Among the biomolecular interactions studied have been those between immunoglobulin G (IgG) and anti-IgG (Liedberg 1983; Geddes 1994), human serum albumin (HSA) and anti-HAS (Kooyman 1988), and those between bovine serum albumin (BSA) and anti-BSA (Mayo 1989).

However, although the method of physical adsorption fulfils the basic need of immobilisation to the sensing surface, it suffers from some severe drawbacks (Löfås 1995; Garland 1996):

- the attachment is not stable; the molecules may be removed from the surface or may diffuse along the surface
- there is a tendency of denaturation and loss of function for sensitive biomolecules
- randomly oriented attachment; recognition sites may be faced downwards
- the surface is prone to promote unspecific adsorption of analyte molecules

Later studies have used organic coupling layers between the sensor metal surface and the biomolecule receptors to aid in receptor immobilisation and alignment. Morgan and Taylor (Morgan 1992) have immobilised streptavidin on a biotinylated gold film (after treatment with chromic acid the surface of a gold film is biotinylated by immersion in a solution of d-biotin nitrophenyl ester). Biotinylated sex hormone binding globulin antibodies (α -SHBG) were bound to the streptavidin and served as a bio-specific sensing layer for SHBG antigens. The sensor worked efficiently, but the biotinylation of one biomolecule species is mandatory. Häussling *et al.* (Häussling 1991) employed self-assembled monolayers (SAM) of alkanethiols on gold. The alkanethiols were functionalised with biotin and the binding of streptavidin to the biotin was studied. It was found that the higher the packing density of the biotin in the SAM was, the less effective was their binding ability, indicating that steric restrictions hamper the binding to a 2D sensing layer. Nevertheless, it was also shown that the coverage of gold with alkanethiol SAMs can passivate the gold surface against unspecific protein adsorption. Self-assembled monolayers consisting of alkanethiols are suited for the immobilisation of almost every protein, thus the application of the system biotin-streptavidin is not obligatory (Wink 1997). The most versatile strategy for covalent immobilisation of proteins employs carboxylate-terminated SAMs. Addition of 1-ethyl-3-(3-dimethylaminopropyl) carbodiimide (EDC) and N-hydroxysuccinimide (NHS) to the SAM results in the formation of NHS esters. Lysines of proteins react with the ester and form an amide bond (Patel 1997). However, this approach still suffers from the random orientation of the immobilised molecules. For instance, Wadu-Mesthrige *et al.* (Wadu-Mesthrige 2000) have proven with atomic force microscopy (AFM) that IgG binds to a SAM in various orientations. Only 30% of the immobilised IgG molecules were able to interact specifically with their biological counterpart.

In view of these shortcomings the application of hydrogels for biosensing purposes is favourable for many reasons. A hydrogel is a polymeric material which swells in water and retains a significant fraction of water within its structure (e.g. a lightly cross-linked derivative of poly(acrylic acid) can absorb approximately a hundred fold water compared to its own mass (Omidian 1999)), but which will not dissolve in water. Hydrogel materials resemble, in their physical properties, living tissue more than any other class of synthetic biomaterial. In particular, their relatively high water contents and their soft, rubbery consistency give them a resemblance to living soft tissue (Hoffman 1977). Often, for biosensing and specifically for SPR applications hydrogels are employed in non-cross-linked form; dissolution is only prevented by the covalent attachment to the substrate. Depending on the structure of the polymer, the single polymer chains can be fixed to the surface either by a certain fraction of reactive groups along the chain or by their terminal group(s). The hydrogel is strongly swollen in aqueous media -often buffers for biosensing purposes- and thus provides binding sites for biomolecule immobilisation in a three-dimensional arrangement. The mixture of loosely packed polymer chains and buffer solution provides a solution-like environment preventing proteins from denaturation. The 3D attachment of biomolecules leads to higher sensitivity and dynamic range of the SPR biosensor because the receptor density per sensor surface area is larger compared to a flat surface (Granzow 1992). Additionally, the extended hydrogel matrix allows more efficient exploitation of the evanescent SPR field. Since analyte molecules can diffuse into the polymer matrix, the

actual orientation of the receptor molecules is less relevant compared to flat sensor surfaces.

However, this issue also highlights a disadvantage of hydrogels: when main interest is in kinetic data, long diffusion pathways in the 3D matrix may lead to an undesirable deceleration of receptor-analyte complexation, especially in case fast kinetics are analysed (Schuck 1997b). Moreover, rebinding effects can affect the apparent dissociation constant in a kinetic measurement (Nieba 1996).

Nevertheless, the outstanding advantages of hydrogels are convincing, therefore that the BIAcore SPR biosensor was already equipped with a dextran hydrogel functionalised sensor surface at its launch in 1990.

3.3.1 Dextran Hydrogels

Hydrogel matrices composed of polysaccharides like dextran as well as the coupling chemistry for covalent immobilisation of proteins to the polymer chains are known from affinity chromatography (Cuatrecasas 1972). In 1990, Löfås and Johnsson (Löfås 1990) introduced a method to modify a noble metal surface with a dextran hydrogel. Noticing the importance of a barrier between the original noble metal surface and the hydrogel itself, they used a self assembled monolayer (SAM) of long-chain ω -functionalised alkyl thiols for primary surface functionalisation, because it forms a layer much less prone to defects than shorter chain variants (Wink 1997). The combination of this dense SAM and the dextran covalently coupled to it is rather efficient and became the "standard" sensor surface for the BIAcore system (figure 14). It still enjoys high popularity among the users of such biosensors today and is well established for routine analysis comprising the determination of the active concentration of analyte molecules and the measurements of reaction kinetics and affinity constants (Rich 2000).

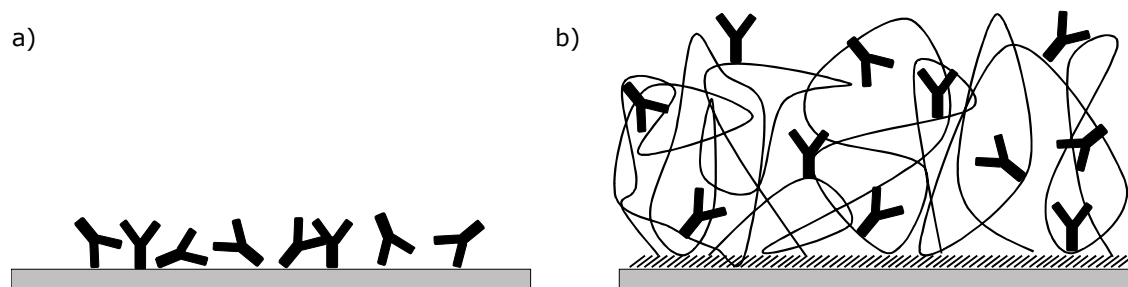


Figure 14. Differences in biomolecule immobilisation strategy between initial experiments successfully proving SPR's capability for detection of biomolecular interactions (a) and the final solution for commercialisation (b). **a)** Antibodies physically adsorbed to a silver surface. The limitations of this strategy are outlined in the text. **b)** Schematic representation of the immobilisation matrix for a gold surface developed by Löfås and Johnsson (Löfås 1990). The self-assembled monolayer serves as a barrier to the gold surface and simultaneously provides the functional groups for the covalent coupling of the dextran. Receptor biomolecules can be immobilised via the carboxymethyl groups on the polysaccharide chains.

Dextran is a α -1,6-linked polyglucose with 1,2- and 1,3-branchings (figure 15) (Elam 1984; Piehler 1996). To immobilise biomolecules dextran is often carboxymethylated. For instance, the Biacore sensor surface employs a dextran hydrogel that is carboxymethylated resulting in a functional group density of one carboxyl group per glucose residue (Löfås 1990). Analogous to the activation chemistry for carboxylate-terminated SAMs which is described in section 3.3, the carboxy groups of the modified dextran are converted into activated esters which are reactive towards primary amino functions of proteins (figure 16) (Löfås 1990). In addition, the immobilisation of proteins is facilitated by carboxy groups which are not converted into esters. Under certain pH conditions during immobilisation (typically around pH 5), a substantial amount of the remaining carboxy groups are negatively charged while the majority of the amino groups of the proteins are protonated and therefore positively charged. The electrostatic attractive forces between these groups lead to protein enrichment in the hydrogel (Earp 1998).

Sensor surfaces employing dextran hydrogels can be reused several (approx. 50) times without loss of binding capacity, since dextran and the covalent dextran-receptor bond resist the chemical conditions which need to be applied for breaking a specific protein-protein (i.e., receptor-analyte) conjunction (Earp 1998). For instance, a common method for regenerating a dextran sensor surface includes the application of 0.05mol/l HCl.

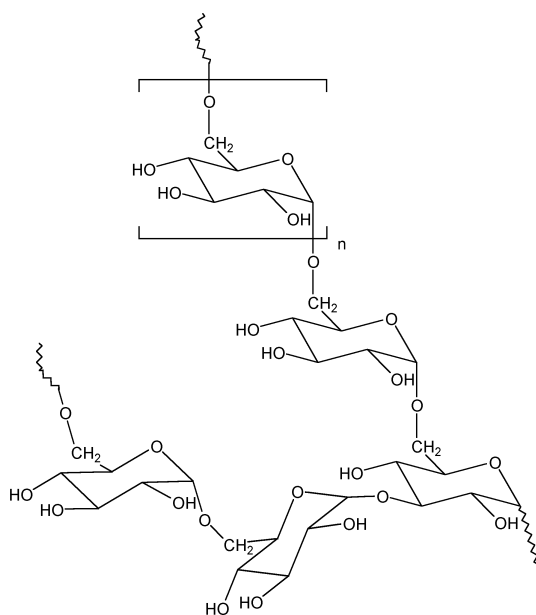


Figure 15. Structure of dextran, a α -1,6-linked polyglucose. Here, shown with a 1,3-branching.

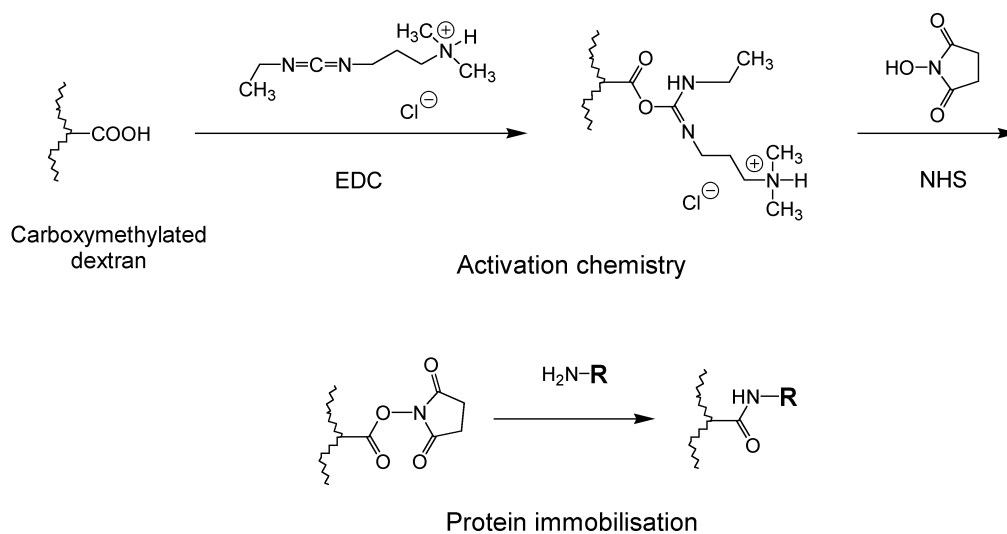


Figure 16. Activation and immobilisation chemistry of carboxymethylated dextran using 1-ethyl-3-(3-dimethylaminopropyl) carbodiimide (EDC) and N-hydroxysuccinimide (NHS) protocol.

Typically, swollen dextran hydrogel layers are about 100 to 150nm thick (Fägerstam 1992). The dextran chains are highly flexible and thus still permit access for big biomolecules like thyroglobulin with a mass of 640 kDa, but not for bacteria or cells (Garland 1996). The flexibility of the polymer chains may also play an important role for the efficient suppression of non-specific protein adsorption provided by dextran hydrogels (see figure 17) (Frazier 2000). Entropy elasticity may generate a repulsive force against approaching molecules, which disturb the equilibrium state of the immersed polymer (Holmberg 1997).

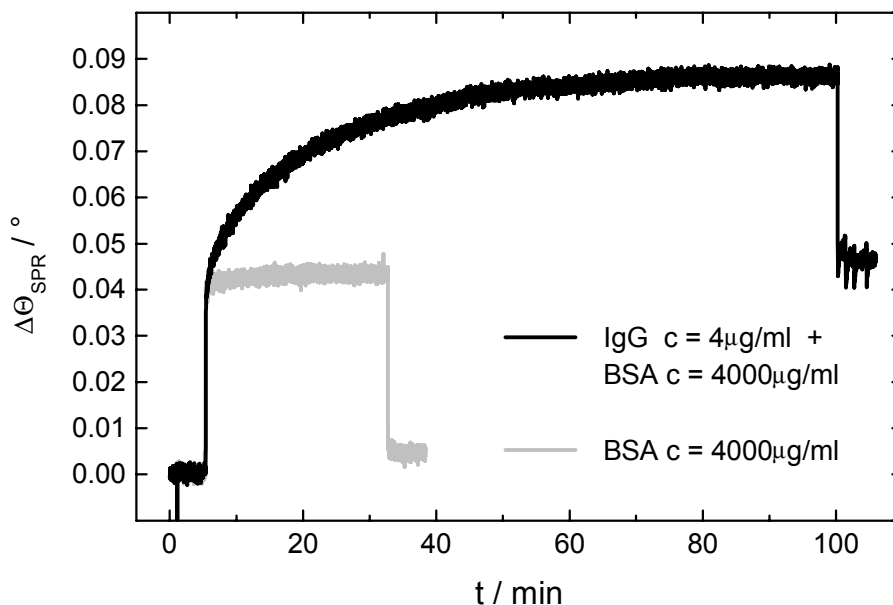


Figure 17. Monitoring of non-specific adsorption of bovine serum albumin (4 mg/ml) to a dextran-modified surface prepared according to a procedure recently developed by Glaucus Proteomics (Wischerhoff 2000) (grey curve). The step-like increase in signal is just caused by the higher refractive index of the BSA solution compared to pure buffer solution. The same surface was also used for a specific interaction experiment: Rabbit-anti-mouse IgG (4 μ g/ml) was mixed with 4 mg/ml bovine serum albumin. The 1000-fold excess of matrix protein did not inhibit the specific binding of the IgG to immobilised protein A (black curve).

However, the flexibility of the dextran chains can also influence SPR measurements. Since the evanescent SP wave field is sensing through the entire dextran hydrogel thickness, changing dextran properties will interfere with actual biomolecular interaction measurements. Depending on the pH and ionic strength of the solutions the hydrogel is subjected to, the actual shape and size of carboxymethylated dextran gels can change due to electrostatic repulsive forces between the carboxy groups (Karlsson 1997). Furthermore, incorporated proteins will also alter the hydrogel conformation due to steric forces and also due to electrostatic forces originating from charged protein amino acid residues (Karlsson 1997; Piehler 1999).

One more parameter potentially inducing artefacts in SPR measurements is the three dimensional arrangement of binding sites in a dextran hydrogel layer. The distribution of biomolecules normal to the sensing surface, the accessibility of binding sites by diffusing biomolecules and possibly preferably occupied regions inside the hydrogel are still questions, which are not satisfactorily answered by experimental evidence. Schuck (Schuck 1996) has performed an extensive computer simulation study about mass transport phenomena concerning transport from the bulk solution into the hydrogel and within the hydrogel. His work clearly indicates the importance of hydrogel effects; in particular he showed that reduced accessibility of neighbouring binding sites by steric hindrance can lead to falsified apparent rate constants measured by SPR. Witz (Witz 1999) considered in another theoretical work the hydrodynamic penetration of analyte flow into the polymer matrix when using a flow cell with steady analyte flow. He noted

that careful choice of the experimental conditions can drastically reduce transport problems. However, finally he also remarked that “a better understanding of the processes that take place in the flow cell of a biosensor obviously requires better knowledge of the organisation of the dextran brush and the distribution of immobilised ligands in its interior”.

Experimental approaches are basically focused on elucidation of hindered diffusion in a hydrogel matrix equipped with receptor molecules (see figure 18). Edwards *et al.* (Edwards 1995) compared the binding kinetics of human serum albumin to an antibody immobilised either in a dextran matrix or on an aminosilane surface. In the presence of the hydrogel matrix, the data were well described by a double exponential, while the binding to the flat functionalised aminosilane surface was described by a single exponential. Concluding that steric hindrance affected binding within the dextran matrix, the investigators interpreted the fast component of the binding progress as representative of binding events similar to those in solution; they interpreted the slow component as produced by artefacts of steric hindrance or restricted access to binding sites. Fischer *et al.* (Fischer 2001) performed an investigation with two surfaces presenting three-dimensional coupling matrices (Biacore chip CM5 with an approx. 100nm thick dextran layer and chip F1 with a thinner dextran layer) and two surfaces presenting binding sites in a two-dimensional arrangement (Biacore chip C1 and a SAM consisting of equal amounts of mercaptoundecanoic acid and mercaptoundecanol). The interaction between calmodulin and an immobilised peptide representing the calmodulin-binding site of nitric oxide synthase I (NOS-I) was measured for different immobilisation densities of NOS-I. The data showed that the apparent rate constant measured with a dextran chip was much more influenced by variation of the immobilisation density than on a flat surface, indicating that dextran coated three-dimensional sensor chips are much more prone to mass transfer limitations than flat surfaces. Fong *et al.* (Fong 2002) also came to the conclusion that a SAM can reduce some of the steric effects and limits on analyte diffusion presented by a dextran hydrogel. They observed these effects in a study where they used a SPR biosensor equipped with a dextran hydrogel (Biacore chip CM5) to measure the binding kinetics of a protein–protein interaction system involving insulin-like growth factor-I (IGF-I) and its binding proteins 1 and 3 (IGFBP-1 and IGFBP-3). Kinetic parameters obtained with either of the binding partners immobilised on the matrix were compared to evaluate the effects of the matrix on the binding kinetics. When the smaller ligand (IGF-I) was immobilised on the hydrogel surface, the association rate was decreased, in comparison to the situation vice versa. The authors conclude that the dextran matrix might pose steric hindrance for the larger IGFBP molecules to bind with the immobilised IGF molecule and that the diffusion of the smaller molecule (IGF-I) is fast, which could enhance the association rate when the larger IGFBP molecules were immobilised. However, substantial deviation from a single exponential was not observed for both immobilisation versions, although such a deviation is expected according to the theories about hindered diffusion in a hydrogel (Schuck 1996). Furthermore, Parsons and Stockley (Parsons 1997) presented a study in which they found no evidence for the dextran matrix affecting the interaction between *Escherichia coli* methionine repressor and operator. They also used two surfaces with different dextran hydrogels (Biacore chip CM5 with a approx. 100nm thick dextran layer and

Biacore SA chip with a approx. 30nm thick dextran layer) and a flat surface (Biacore chip C). The binding curves from the different surfaces overlaid, indicating that the dextran matrix had no significant effect on the values of the apparent rate constants measured.

Summarised, dextran hydrogels are well established for biosensing purposes; rightly as measured by the sum of their properties. However, some uncertainties about the processes occurring in the hydrogel during biomolecule immobilisation and interaction are still not satisfactorily resolved, although some effort concerning different surface architectures and interaction model systems was undertaken. This is may be due to the fact that the opportunity of getting deeper insight into hydrogels by advanced instrumental layout is neglected. This is probably because commercial SPR biosensors are generally employed, making hardware modifications difficult or even impossible.

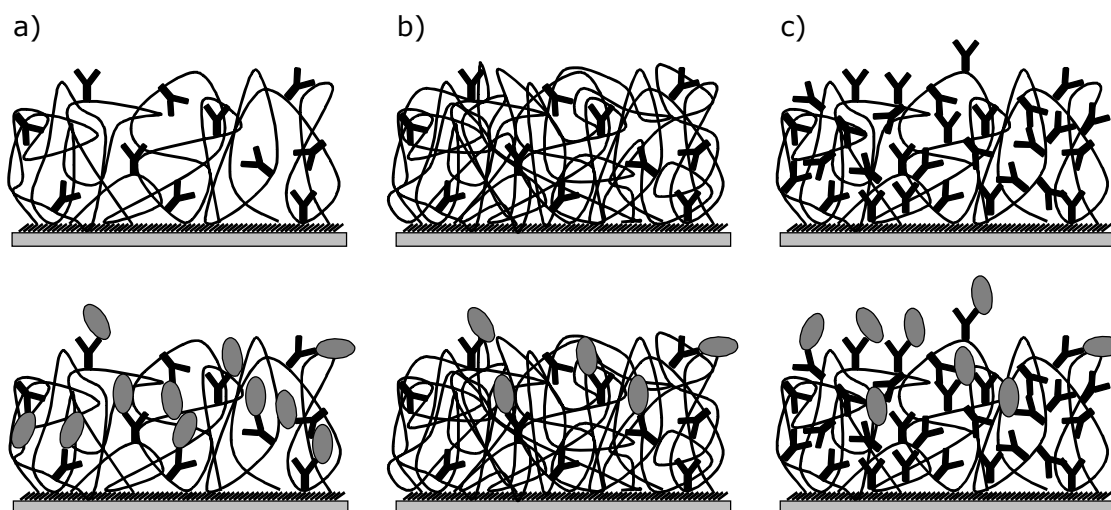


Figure 18. Dextran effects which might influence the binding of analyte molecules (sketched as grey ovals) to immobilised receptor molecules. **a)** Desired ideal binding process in a dextran matrix. The analyte molecules can penetrate the hydrogel and can access the receptors in an unhindered way. **b)** The hydrogel matrix is too dense and is consequently hindering analyte penetration into the hydrogel. Only a fraction of the receptors can be accessed. **c)** The immobilisation density of receptors is too high. The receptors themselves impede the diffusion of analyte molecules into deeper hydrogel regions. With binding of the first analyte molecules to the topmost receptors the situation becomes even worse, preventing analyte molecules for accessing deeper localised receptors.

3.3.2 Synthetic Hydrogels

Although dextran fulfils the requirements for biosensing surfaces in many respects satisfactorily, synthetic hydrophilic polymers are attractive alternatives as they offer some potential advantages. First, they can be more resistant to harsh conditions (strong acids, fouling etc.) compared to polysaccharides, because the polymer backbone of synthetic polymers is formed by C-C-bonds in many cases. Second, they allow to vary

the properties of the compounds in a wider frame, e. g. by copolymerisation of different monomers.

Synthetic hydrogels as coating materials are primarily employed to enhance the biocompatibility of solid surfaces. Applications comprise, for instance, the coating of contact lenses to increase the water content of the surface (Garrett 1998) and the coating of objects which are placed in the blood stream to minimise protein adsorption which generally results in the activation of coagulation and subsequent thrombus formation (Lee 1995). Consequently, most studies concerning synthetic hydrogels have investigated the protein adsorption characteristics (Garrett 1998; Green 2000b). However, biocompatible surfaces suitable for biosensing are complex systems. Many parameters have the potential to influence the final performance of the biocompatible layer: chemical composition and morphology of the substrate, thickness, density and chemical composition of barrier and linker layers, immobilisation density, average molar mass and chemical composition as well as substitution pattern of the biocompatible polymer or oligomer layer. Hence, several studies were performed investigating these different aspects, some of the work also being only related to the prevention of non-specific adsorption, some also extended to actual biosensing applications (Wischerhoff, in press).

Gombotz *et al.* (Gombotz 1991) performed a study on protein adsorption to poly(ethylene glycol) (PEG) layers bound to poly(ethylene terephthalate) (PET) surfaces. The surface coverage with PEG and the adsorption of fibrinogen and albumin were investigated for effects of the average molar mass of the poly(ethylene glycol). Average molar masses reached from 200 to 20,000g/mol. The adsorption studies showed a clear trend: The higher the average molar mass of the PEG, the more effectively non-specific adsorption of both albumin and fibrinogen were suppressed. Piehler *et al.* (Piehler 1996) coated surfaces with various amino- and carboxy-substituted polymers. The polymers used were branched poly(ethyleneimine), α,ω -amino functionalised poly(ethylene glycol), chitosan, poly(acrylamide-co-acrylic acid) and an amino modified dextran (figure 19). When probed with 1mg/ml ovalbumin solution, non-specific adsorption was lowest for the dextran derivative. Notably, non-specific adsorption increased in most cases when a hydrophobic hapten (atrazine) was coupled to the polymer-modified surface.

Although the choice of compounds is limited, this investigation gives some insight into the influence of chemical composition on the non-specific adsorption: it demonstrates that charged as well as hydrophobic groups are undesirable.

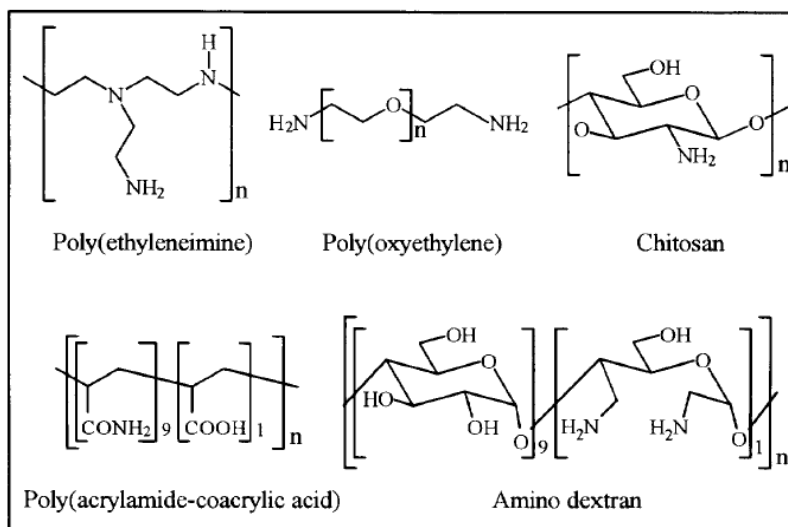


Figure 19. Polymers which were used by Piehler *et al.* to coat glass-type surfaces for biosensing applications (taken from (Piehler 1996)).

However, employing synthetic hydrogels in biosensors just as a substitution of dextran does not exploit all the potential these hydrogels may offer: by tailoring the hydrogel structure, it is possible to create polymers with new physical properties, particularly with controllable dynamics, leading to switchable “intelligent” systems (“stimuli-responsive materials”). Those hydrogels could be utilised to introduce new functionalities to biosensor surfaces, as it will be discussed below.

Stimuli-responsive polymers exhibit reversible phase changes in response to changes in physical and chemical factors such as pH or temperature (Stayton 1995). They are subject of extensive investigations; in the biomedical field main focus is on controlled drug release by pH-sensitive hydrogels (Stayton 2000; Kyriakides 2002). These gels possess ionisable side chains which respond to changes in pH by altering their physical structure or permeability (Peppas 1994). Apart from these systems, which can be considered rather as standard systems, research is mainly focused on chemically closed systems, which respond reversible on physical stimuli like a change in temperature (Peppas 1994). The behaviour of these so-called thermo-responsive or thermo-sensitive polymers in aqueous media often contradicts intuition because they generally exhibit a lower critical solution temperature (LCST). Upon heating, when the temperature increases beyond a certain value commonly referred to as cloud point, they precipitate from solution. This transition is governed by the balance between hydrophilic and hydrophobic forces (HPL/HPB-balance) of polymer-polymer and polymer-solvent interactions. The HPL/HPB-balance has its origin either in the monomeric structure of homopolymers or the polymer composition of copolymers (Kim 2000). Examples of polymers which undergo a phase transition induced by changes in temperature are poly(N-isopropylacrylamide) (PNIPAM) and other N-substituted acrylamides, poly(vinylmethylether) (PVME) and poly(ethylene oxide) (PEO). PNIPAM and PVME have stirred up particular interest because of the abrupt nature of their phase transitions and the fact that their transitions are reversible, which allows repeated thermal switching. Stayton *et al.* (Stayton 1995), for instance, have used temperature induced

conformational changes in PNIPAM to control the binding of biotin to streptavidin. They have covalently bound PNIPAM close to the active centre of streptavidin. At temperatures below 32°C the PNIPAM exists as a hydrated random coil permitting access of biotin to the binding site. When the temperature is exceeding 37°C the polymer collapses and blocks the binding site, so that biotin cannot bind to it. Yamada *et al.* (Yamada 1990) have cultured cells onto PNIPAM at 37°. By lowering the temperature to 4°C the PNIPAM surface became hydrophilic and the cells could be removed from the surface just by applying little physical shock (tapping the dish side with a finger tip). Almost all cells could be recovered from the surface by this procedure and 73% of them adhered again – a measure for the intactness of the cells. In contrast, only 14% of cells were still intact after recovery by the traditional method of treatment with the enzyme trypsin. Tanaka *et al.* (Oya 1999) have created a cross-linked thermo-responsive hydrogel by co-polymerisation of acrylamidopropyltrimethylammonium (MAPTAC) and PNIPAM. MAPTAC worked as an adsorbing agent for pyranine. Fluorescent measurements showed that shrunken gels at 55°C adsorbed all of the pyranine, whereas the swollen gels released pyranine. The adsorption and release were reversible and reproducible.

These examples nicely illustrate the potential provided by thermo-responsive hydrogels. Provided they still undergo a phase transition even under the particular conditions existing in confined space at surfaces (Zhu 1999) they may offer new applications for SPR biosensors. For instance, the thermo-responsive effect may be exploited to regenerate the sensor surface just by raising the temperature above the LCST. This should lead to a collapse of the hydrogel and the steric forces induced by the collapse may be strong enough to break the specific biomolecule-biomolecule interaction between receptor and analyte. Furthermore, the incorporation of photo-reactive moieties into the polymer could be employed to provide the sensor surface with a pattern consisting of hydrophilic / hydrophobic domains just by illuminating the hydrogel through a corresponding mask while the hydrogel is in collapsed state (i.e., the hydrogel is immersed in water with $T > LCST$). The illuminated part of the hydrogel surface will be cross-linked and thus may remain in collapsed, meaning more hydrophobic, state, even if the temperature is lowered below the LCST.

However, up to now, a SPR biosensor surface equipped with a thermo-responsive hydrogel has never been subject to comprehensive characterisation related to biosensing purposes. This comprises the possibility to be functionalised with receptor biomolecules, the ability to suppress non-specific adsorption of proteins and, most of all, the proof of the occurrence of the thermo-responsive effect on the surface.

4 Aim of the Research

The aim of this PhD thesis is to take advantage of the inherent properties of the SPR detection principle to gain new insights into biosensing hydrogels at interfaces. The exponentially decaying sensitivity of surface plasmon waves can be exploited to spatially resolve refractive index changes normal to the sensing surface.

The SPR response depends on the probed effective refractive index n_{eff} representing a convolution of the actual refractive index profile $n(z)$ and the exponentially decaying surface plasmon field (equation 9). Thus, this technique can be potentially employed for verification of changing index profiles $n(z) \neq \text{constant}$ occurring within the evanescent SP wave field. Since the thickness of swollen hydrogels at surfaces is in the same order of magnitude as the penetration depth of the SP field (Salamon 1997), processes which are modifying the hydrogel's structure and density are resolvable in z -direction as a matter of principle.

Development of a multi-purpose SPR setup

Time dependent processes will not be vertically resolvable by measurements with only one wavelength, since there is no unique solution which would allow an unequivocal assignment between an observed SPR angle shift and a certain refractive index profile (convolution of the actual refractive index profile $n(z)$ and the exponentially decaying SP field). This can be overcome by comparison of two SPR signals from two different wavelengths with markedly distinct penetration depths. Comparability of SPR responses generated by time-dependent processes requires true real-time resolution and absolutely simultaneous recording.

A SPR setup needs to be developed which will fulfil these specific demands to enable vertical resolution of dynamic processes in hydrogel layers.

Dextran hydrogels

Dextran hydrogel dynamics, the distribution of receptor molecules in the hydrogel matrix as well as the distribution of bound analyte molecules and respective binding mechanisms are still open questions. Analytical approaches exist (Glaser 1993; Schuck 1996; Witz 1999), but because of the complexity of the problem and the number of parameters influencing real processes in hydrogels an experimental approach seems to be superior (Schuck 1997b). Furthermore, investigations only considering the interaction of biomolecules with their immobilised biological counterpart can merely deliver half the truth about hydrogel effects, because these processes are already

superimposed with probably existing receptor distribution profiles and dextran hydrogel deformations. This implies that the immobilisation process also needs to be monitored and evaluated.

A new experimental approach is to be applied to investigate binding processes in a dextran hydrogel and to study to what extent the apparent dynamics of biomolecular interactions are influenced by the 3D nature of a hydrogel binding matrix.

The binding of biomolecules modifies the refractive index of the dextran hydrogel in space and in time: $n = n(z,t)$: time-resolved SPR measurements performed simultaneously with two different wavelengths should allow to resolve binding events spatially normal to the sensing surface and to gain information about the dynamics in biosensing dextran layers at interfaces.

Thermo-responsive hydrogels

During the hydration of a polymer, water adsorption results in a reduction in the refractive index of the polymer and an increase in polymer layer thickness. Green *et al.* (Green 2000a) showed that the net effect of these two processes results in a reduction in the SPR angle shift upon hydration. The phase transition of a surface-attached thermo-responsive hydrogel should induce a reversed but comparable SPR angle shift, since the refractive index profile on the sensor surface will be modified by a change in temperature: $n = n(z,T)$.

Three novel thermo-responsive hydrogels, synthesised by Laschewsky *et al.* (Laschewsky 2001), will be investigated for their potential application in SPR biosensors. In particular, this comprises the direct proof of the thermo-responsive phase transition while these hydrogels are covalently coupled to the SPR sensor surface. Furthermore, the capability of the hydrogels for bio-functionalisation and suppression of non-specific protein adsorption shall be examined.

5 The SPR Setup

A SPR setup was developed, which allows

- Measurements of the reflected light intensity as a function of the angle of incidence Θ for any wavelength between $\lambda = 580\text{nm}$ and 1100nm
- Measurements of the reflected light intensity as a function of time at a fixed arbitrary angle of incidence Θ_M (in particular in the flank of the minimum of a plasmon resonance curve) for any wavelength between $\lambda = 580\text{nm}$ and 1100nm
- Simultaneous measurements of the reflected light intensities of the wavelength $\lambda = 784\text{nm}$ and a wavelength around $\lambda = 600\text{nm}$ as a function of time

In this chapter the SPR setup will be described.

5.1 General Description

Figure 21 shows a photograph and figure 22 a scheme of the SPR setup.

The layout of the experimental setup is a Θ - 2Θ arrangement: the prism is rotated relative to a spatially fixed light beam in order to vary the angle of incidence; the detector, positioned to measure the reflected light intensity, thus has to move twice the rotation angle of the prism. Motorized goniometer tables (Huber, Rimsting, Germany) manage the Θ - 2Θ movement for both the prism and the detectors. The repeat accuracy of the setup for the determination of Θ_{SPR} for gold / water at $\lambda = 784\text{nm}$ amounts to $\pm 0.005^\circ$ (standard deviation for successive measurements). All constituents of the setup are fixed to an optical table ($(2.0 \times 1.0 \times 0.2)\text{m}^3$, Melles Griot, Cambridge, UK). The legs supporting the tabletop have air suspension mechanisms reducing practically all vibrations by two orders of magnitude.

The SPR setup employs two independent light sources. One is a temperature stabilized GaAlAs diode laser (ThorLabs, Newton, USA, laser diode mount: ThorLabs, TCLDM9-TEC, temperature controller: ThorLabs, TEC 2000) emitting p-polarized light (relative to the coordinate system of the sample) with wavelength $\lambda = 784\text{nm}$ and maximum power of 50mW and a 50W halogen lamp (Owis, Staufen, Germany). By deflecting the laser beam with a glass plate the laser intensity is attenuated by a factor of about 100. The halogen lamp illuminates a monochromator (Acton Research, SpectraPro-150, Acton, USA) which extracts the desired wavelength from the smooth spectrum of the lamp. The bandwidth amounts to about 2.5nm ; much smaller than the width of a plasmon resonance curve (e.g. HWFM $\approx 50\text{nm}$ at $\lambda_{\text{SPR}} = 784\text{nm}$). Since the

light of the halogen lamp is randomly polarised, a polarizer (Owis) is employed to provide only p-polarised light in order to minimise the background signal. A rectangular intensity modulation is accommodated by a chopper wheel (EG&G Instruments, model 651, Wokingham, UK, light chopper controller: EG&G Instruments, model 650), allowing to use a lock-in amplifier (EG&G Instruments, model 7260) for the signal from the halogen lamp. In order to also employ a lock-in amplifier (Femto, Olching, LIA-MV-150, Germany) for the reflected laser light, the intensity of the laser is sinusoidally modulated via the laser diode driver (ThorLabs, LDC 500). Both monochromatic light beams are directed through a cylindrical prism (BK7 glass, Schott, Germany, custom made by Owis) to a gold coated glass slide (BK7 glass, custom made by B&M Optik, Limburg, Germany) coupled via immersion oil (Cargille, Immersion Liquid Code 1160, Cedar Grove, USA) to the glass prism. The intensities of the reflected light beams are measured by Si-photodiodes (Hamamatsu, Hamamatsu City, Japan) as a function of the angle of incidence Θ .

The wavelength dependent intensity from the monochromator as perceived by the Si-photodiode is plotted in figure 20. The intensity distribution is basically a product of

- the spectral intensity distribution of the halogen lamp
- the wavelength dependent diffraction efficiency of the diffraction grating of the monochromator
- the spectral sensitivity of the photodiodes

The power at a certain wavelength is in the nW-range.

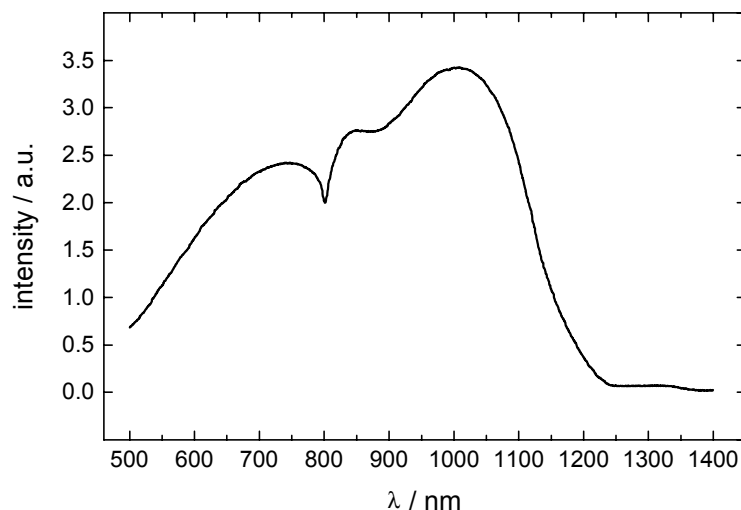


Figure 20. Light intensity from the monochromator in dependence of the wavelength. The measurement is taken using the components of the actual SPR setup, but without the prism.

The focusing effect of the cylindrical prism is compensated by a cylindrical lens. The distance of the photo diode, which is measuring the reflected light intensity, is chosen in a way that the reflected beam is focused onto the photo diode. For the laser beam no compensating lens is necessary because the beam diameter is so small that the resulting angle distribution within the cylindrical prism is smaller than the typical width of a

plasmon resonance curve (e.g. FWHM = 1.2° for $\lambda = 784\text{nm}$). The two monochromatic light beams enclose an angle of 10.7° . Each light beam was adjusted by employment of two aperture plates which were mounted aligned onto the goniometer. The line connecting the apertures was intersecting with the rotation axis of the goniometer. The aperture plates were orientated by means of the goniometer to the desired angle and the corresponding light beam was adjusted afterwards in a manner that the beam passed through both apertures. By construction the rotation axis of the goniometer is located in the gold surface, thus both light beams hit the same spot on the sample. The sample area covered by the light beams amounts to some square millimeters at typical angles of incidence. Since the photodiodes collect all reflected light from any beam the measurements represent an average over this area.

The solutions are supplied to the sample surface by injecting them by hand into a flow chamber made of Teflon. The diameter of the flow chamber is 4mm, the volume amounts to $37\mu\text{l}$.

The setup and the data acquisition are computer controlled.

The presented experimental arrangement with the angle of 10.7° enclosed between the two light beams allows to simultaneously measure intensity changes on the flank of two plasmon resonance curves excited with two distinctly different wavelengths. Although the angle of 10.7° between the light beams is optimised for this kind of measurements, in general a slight readjustment for each individual experiment is necessary in order to find the optimal measuring position within the SPR curve flank for both wavelengths. However, the readjustment is not realised by rearranging the pathways of the light beams; it is accomplished by slightly varying the shorter wavelength by means of the monochromator. Since the SPR curve $I_r(\omega, \Theta)$ depends also on ω , the optimal measuring position for a fixed angle of incidence can be adjusted by varying ω respectively λ . The typical variation of λ lies within the range of about $\pm 2\%$ of the wavelength of 600nm.

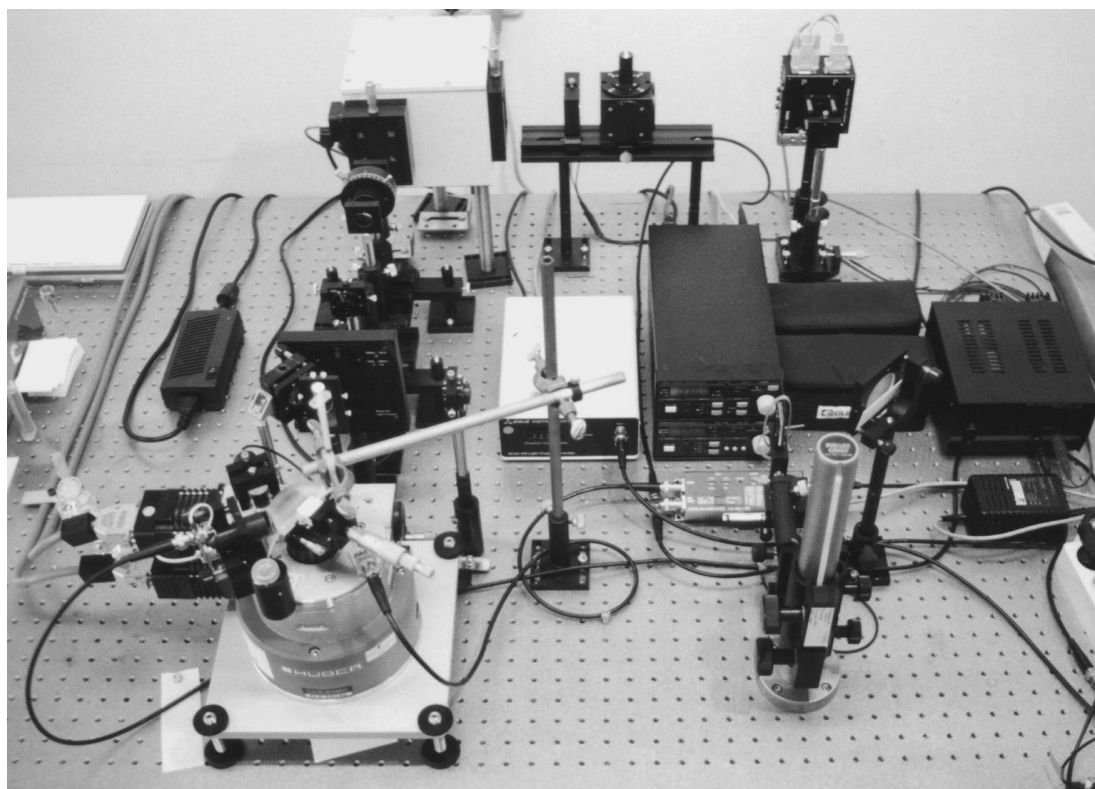


Figure 21. Photograph of the experimental SPR setup. Detailed information about the setup is given in the text and in the caption of figure 22.

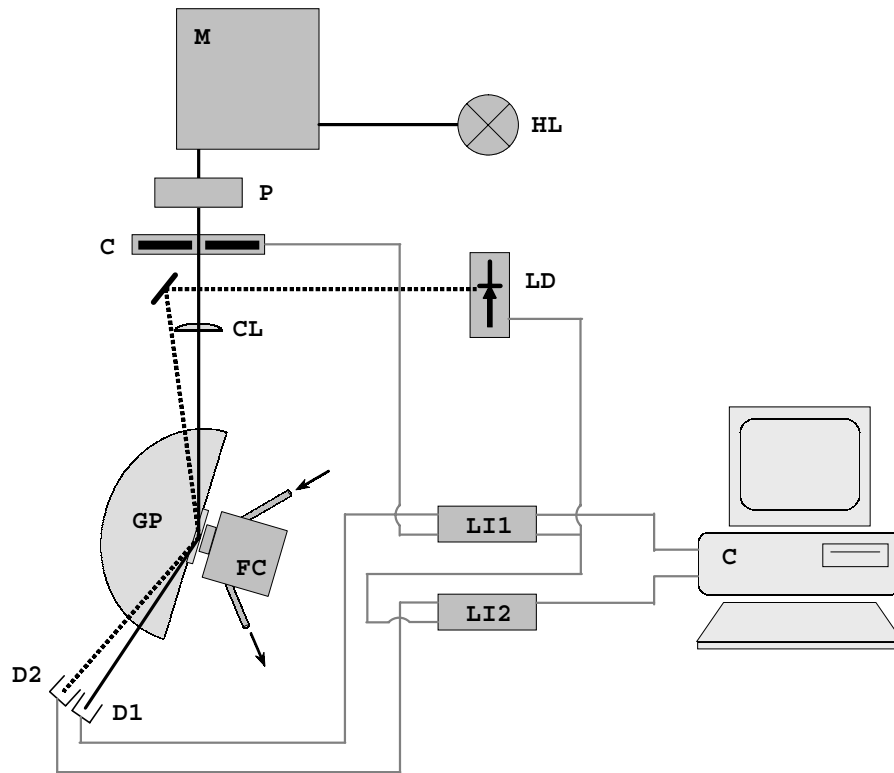


Figure 22. Sketch of the experimental SPR setup. Detailed information about the setup is given in the text. For measurements of the reflected intensity as a function of the angle of incidence Θ the light beam from the monochromator M is used. For simultaneous SPR measurements at two wavelengths in real time the light beam from the laser diode LD is additionally used. For this mode, the light beam with the shorter wavelength comes from the monochromator M and is shown as a thick straight line; the pathway with $\lambda = 784\text{nm}$ from LD as a dotted line. Beam shaping lenses between the halogen lamp HL and the chopper wheel C are not shown for clarity. The angle of incidence Θ is measured between the normal of the gold surface and the respective light beam. Thus Θ is different for each light beam at a fixed position of the prism.

HL : halogen lamp (white light source), M : monochromator, P : polariser, C : chopper wheel, LD : laser diode, CL : cylindrical lens, GP : glass prism, FC : flow chamber, $D1$ and $D2$: photo detector no. 1 and no. 2, $LI1$ and $LI2$: lock-in amplifier no. 1 and no. 2, C : computer used to control the experiment and for the data acquisition. $LI1$ supplies sinusoidal voltage for intensity modulation of LD and as reference for $LI2$.

5.2 Angle Calibration

For reliable comparison of SPR measurements with SPR simulations (calculations of the reflectivity of a layer system) the angle of incidence must be exactly known. For this reason, the SPR setup was calibrated by means of the total reflection occurring at the interface BK7 glass / air.

The angle of total reflection can be calculated by (Jackson 1982)

$$\Theta_{tr\,theo}(\lambda) = \arcsin\left(\frac{n_{BK7}(\lambda)}{n_{air}}\right) \quad (31)$$

with $n_{air} = 1$ for all employed wavelengths and $n_{BK7}(\lambda)$ calculated according to the Sellmeier equation. The Sellmeier equation gives the refractive index of BK7 with accuracy better than $1 \cdot 10^{-5}$ within the used wavelength range (Schott 2000).

The calculated angles of total reflection $\Theta_{tr\,theo}(\lambda)$ were compared with measured values Θ_{gonio} for different wavelengths.

The reflected intensity was measured with an uncoated BK7 glass plate optically coupled to the BK7 glass prism. Figure 23a) shows the measured intensity in dependence of the read angle of incidence from the goniometer Θ_{gonio} . The employed goniometer has a vernier which allows to read the goniometer table position with $<0.005^\circ$ accuracy. The different heights of the curves reflect the wavelength dependent intensities (compare with figure 20).

From the measured curves $\Theta_{tr\,gonio}$ was determined by applying line fits to regions $\Theta < \Theta_{tr\,gonio}$ and $\Theta > \Theta_{tr\,gonio}$ of the measured curves. The calculated intersection points of the line fits were supposed to give $\Theta_{tr\,gonio}$ for each wavelength. Comparison with the theoretical values yield a correction constant of $1.106^\circ \pm 0.003^\circ$ which has to be added to measured angles to get the correct angles of incidence (figure 23b)).

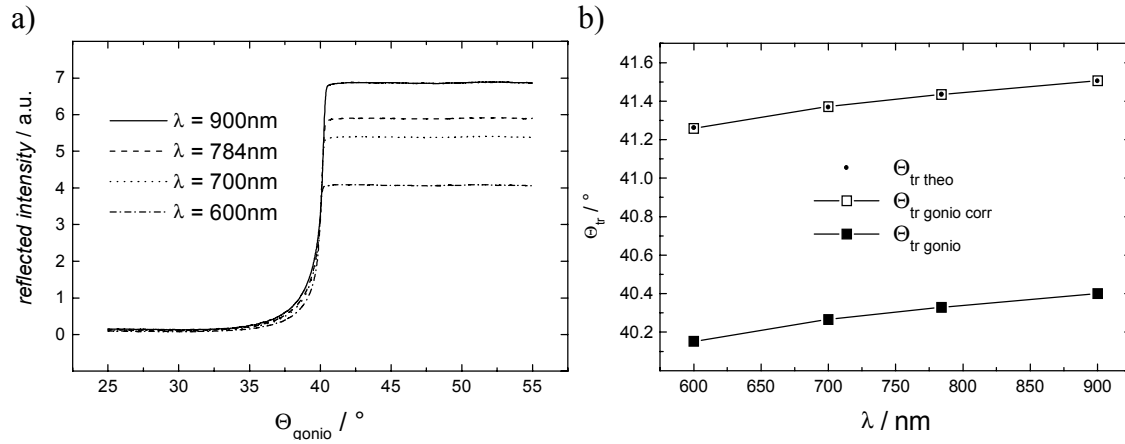


Figure 23. a) Measurement of the reflected intensity at an interface BK7 glass / air for different wavelengths in dependence of the angle of incidence Θ_{gonio} as determined by the goniometer reading. The steep increase in intensity indicates the transition to total reflection. b) Plot of the measured angles of total reflection $\Theta_{tr\,gonio}$ in dependence of the wavelength, the angles $\Theta_{tr\,theo}$ calculated according to equation 31 and the corrected measured angles $\Theta_{tr\,gonio\,corr}$. Applying a correction constant of $+1.106^\circ$ to the measured angles makes them match with the theoretical values.

5.3 The Available Measurement Modes

The SPR setup enables measurements in two modes. They will be described in the following.

Actually the two modes are independent, however, the angle measurement mode (measuring the reflected intensity as a function of Θ) is always used to record the initial SPR curves for each employed wavelength before switching to the differential intensity measuring mode (measuring the reflected intensity as a function of time at a fixed Θ_M).

5.3.1 Angle Mode

The angle of incidence Θ is varied by rotating the goniometer table and the reflected light intensity is measured as a function of the angle of incidence. A large dynamic range is available in this mode, which is necessary, for instance, to follow a surface modification experiment comprehensively from the bare gold surface to final interaction investigations.

Single SPR curves can be measured or a fixed number of curves can be recorded automatically with fixed time increment between each curve. The software which is controlling the goniometer tables as well as acquiring the intensity data is programmed in LabWindows/CVITM (National Instruments, Austin, USA) (see figure 24). The curves are saved in a two column ASCII format; one column is containing the relative angular position RA of the prism (starting from zero) in $1/100^\circ$, the other the respective photodiode signals in Volts (proportional to the light intensity). The data can be processed in batches by a script written for OriginTM (Microcal Software, Northampton, USA). The script calculates the angle of incidence Θ in absolute values by considering the correction value $k = 1.106^\circ$ from the angle calibration and the starting angle $\Theta_{\text{gonio start}}$ which is read from the goniometer (equation 32).

$$\Theta = \Theta_{\text{gonio start}} + k + 0.01 \text{ RA} \quad (32)$$

The Origin script automatically performs a second order polynomial fit to the SPR minimum and calculates Θ_{SPR} . Furthermore, the difference $\Delta\Theta_{\text{SPR}}$ between subsequent curves and the difference to the first measured curve is automatically calculated.

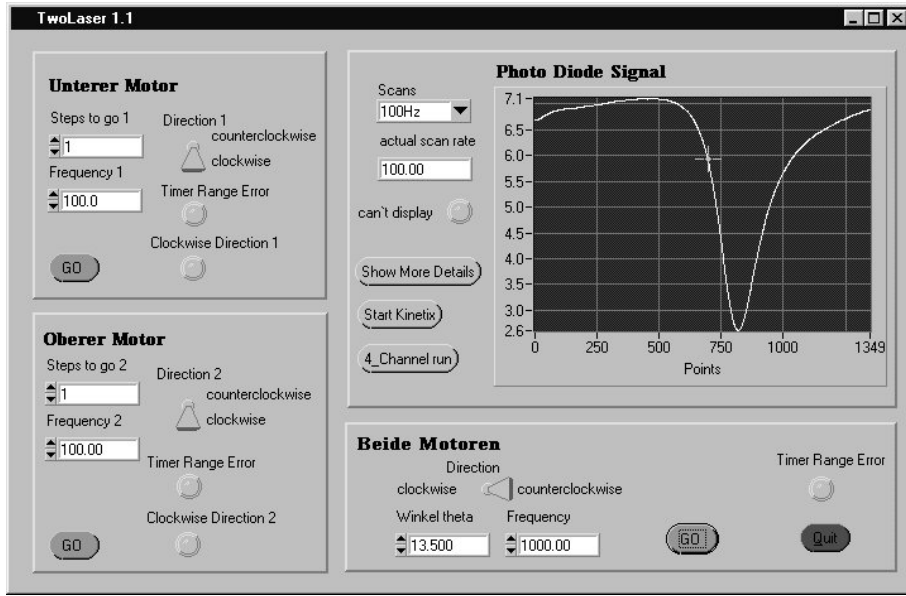


Figure 24. The software interface which is used for computer controlled acquisition of the reflected intensity as a function of the angle of incidence Θ (SPR curves). The two panels on the left are used for the independent control of the prism and the detector goniometer tables.

5.3.2 Differential Intensity Mode

This measuring mode will be described here for the case of simultaneous differential intensity measurements with two wavelengths. The differential intensity measurement with only one but arbitrary monochromator wavelength is also possible.

The reflected intensity $I(\lambda)$ is measured as a function of time at a fixed angle of incidence $\Theta_M(\lambda)$ (different for each beam). If an angle of incidence is chosen, which is situated in the flank of the plasmon resonance curve, events which cause a shift in resonance angle $\Delta\Theta_{\text{SPR}}$ also lead to a change in reflected intensity at this angle (see figure 25).

The advantage of this measuring mode is the almost unlimited time resolution which is explicitly exploited, when using this mode (angle scans take time in the range of some tens of seconds). A shortcoming is the limited dynamic range, caused by the finite width of the SPR curve.

For angle shifts $\Delta\Theta_{\text{SPR}}(\lambda = 784\text{nm}) \leq 1^\circ$, $\Delta\Theta_{\text{SPR}}(\lambda = 600\text{nm}) \leq 1.8^\circ$, the shift of the resonance angle $\Delta\Theta_{\text{SPR}}(\lambda)$ can be very well approximated from the measured intensity changes $\Delta I(\lambda)$ by the simple equation

$$\Delta\Theta_{\text{SPR}}(\lambda) = -1/s(\lambda) \cdot \Delta I(\lambda) \quad (33)$$

with $s(\lambda)$ the slope of the SPR curve at the measuring position $\Theta_M(\lambda)$ (see figure 25). The absolute resonance angle is $\Theta_{\text{SPR}}(\lambda) = \Theta_{\text{SPR}0}(\lambda) + \Delta\Theta_{\text{SPR}}(\lambda)$. $\Theta_{\text{SPR}0}(\lambda)$ are determined from the initial SPR curves which are measured in the angle mode.

The instrumental noise typically allows a SPR angle shift resolution of about $\pm 0.002^\circ$ at $\lambda = 784\text{nm}$.

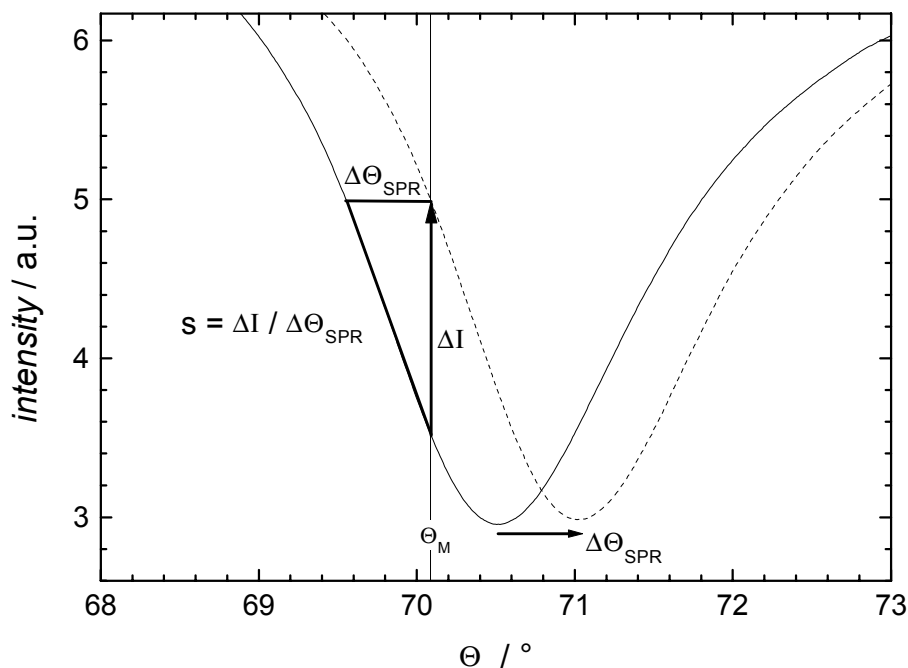


Figure 25. Determination of $\Delta\Theta_{\text{SPR}}$ by measurement of the change of intensity ΔI at a fixed angle of incidence Θ_M . This example shows measured plasmon resonance curves with $\lambda = 784\text{nm}$.

The measurements in differential intensity mode are controlled by a special software module, which is also written in LabWindows/CVITM (figure 26). After positioning the prism at the proper angle of incidence Θ_M , the measurement can be started by the software module and can be stopped after an arbitrary time period. The time resolution can be arbitrarily set.

The data are saved in a three column ASCII format; the first column containing the time in seconds, the second and third column containing the photodiode signals in Volts (reflecting the light intensities) either of the reflected monochromator beam or of the laser beam.

The data can be loaded into a OriginTM template to be processed according to equation 33.

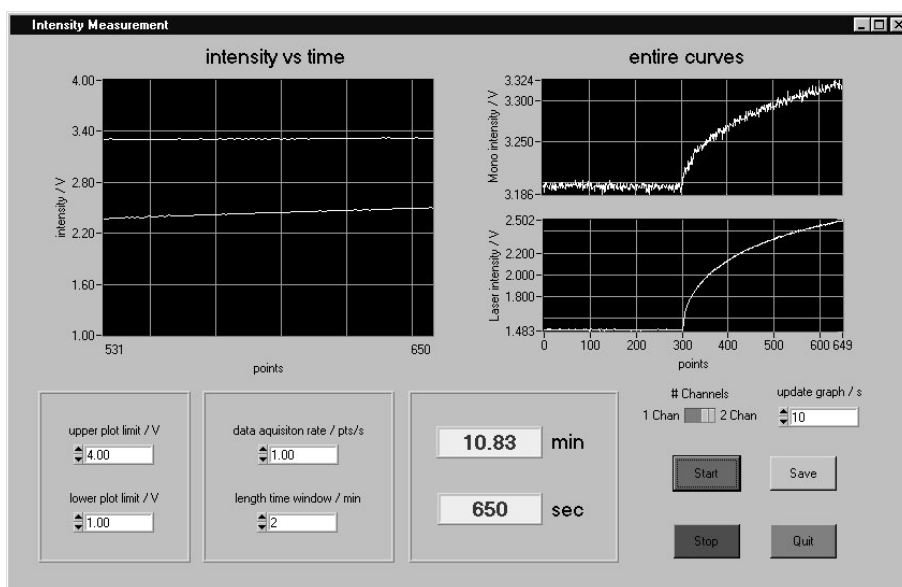


Figure 26. The software interface which is used for computer controlled acquisition of the reflected intensity as a function of time. It can be chosen, if the intensity of one light beam is measured or of two simultaneously. This example shows the acquisition of data during a biomolecular interaction experiment; the upper right graph shows the intensity evolution with time for $\lambda = 600\text{nm}$, the lower right graph for $\lambda = 784\text{nm}$ (laser diode).

6 Thermo-Responsive Hydrogels

The specific balance of hydrophilic and hydrophobic groups is a characteristic feature for many thermo-responsive polymers exhibiting a LCST in aqueous solution (Taylor 1975). Conventionally, the LCST of a polymer is adjusted by choosing an appropriate monomer (Fujishige 1989). The most prominent examples are polyethyleneoxide (PEO) (Kjellander 1981) and N-alkyl substituted polyacrylamides (Taylor 1975). Investigations within the latter class of polymers have been focused mainly on poly-[N-isopropylacrylamide] (P-NIPAM) which exhibits a LCST at about 32°C (Fujishige 1987).

The choice of monomers suited to form LCST polymers is rather limited. Therefore, the adjustment of the LCST by copolymerisation has been studied alternatively (Ringsdorf 1992). However, frequently these copolymers are obtained by non-ideal statistical free radical copolymerisation; and as a consequence, the thermal transition of the materials is broadened and sometimes it is not straightforward to predict the copolymer composition. An elegant way to overcome this problem is by preparing the copolymers by chemical modification of precursor polymers, providing chemically homogeneous, random copolymers with a narrower transition.

In this context, Laschewsky *et al.* (Laschewsky 1999) have explored the use of simple chemical modifications such as the acylation of some non-ionic water-soluble, hydroxy group bearing polymers. They are an example of conceptually simple novel synthesised intelligent materials. In addition, these hydrogels are easily chemically modifiable; a paramount prerequisite for their use in biosensing applications.

The thermo-responsive hydrogels employed for this investigation were synthesised by the Departement de Chimie, Université Catholique der Louvain, Louvain-la-Neuve, Belgium, chair of Prof. André Laschewsky. The aqueous solutions of the hydrogels were characterised by E.D. Rekaï. Here, the hydrogel properties at a sensor surface will be investigated with respect to biosensing purposes in particular.

6.1 Synthesis of Polymers

The investigation comprises four different polymers. One polymer is an unmodified precursor polymer exhibiting no LCST, serving as a standard for comparison. In two of the polymers the thermo-responsive behaviour was induced by polymer analogous modification with hydrophobic groups. The fourth polymer exhibits a LCST as well, but that polymer was made by copolymerisation.

All polymers contain disulfide end-group(s) originating from a disulfide group bearing azo-initiator (as a consequence of recombination and disproportion simultaneously occurring as termination mechanisms in radical polymerisation, the polymer chains have either one or two disulfide groups) (see figure 27) (Laschewsky 2001)) Disulfide-functionalised polymers can attach to gold surfaces by a reductive cleavage of the disulfide group followed by complexation with gold.

Table 5 gives an overview of the employed polymers. The precursor polymers chosen were poly[N-(tris-(hydroxy-methyl)-methyl)acrylamide] (P-THMA) and poly[N-2-hydroxypropylmethacrylamide] (P-HPMA). Although the precursor polymers do not exhibit a LCST under atmospheric pressure themselves, the chemical modification of the hydrophilic -OH groups was expected to induce a LCST. The tailoring of the LCST is achieved by acetylation and cinnamoylation of a certain amount of hydroxy groups of the polymers which means increasing the amount of hydrophobic groups in the polymers. These polymers were obtained by free radical polymerisation. P-HPMA (Konak 1997) and P-THMA (Köberle 1992; Barthélemy 1998) are well known, notably for biomedical applications. The cinnamoyl groups of cinnamoylated P-HPMA do not only modify the hydrophilic-hydrophobic balance of the copolymer, but they are also known to be photoreactive. Irradiation of the polymer with UV light can induce intra- and intermolecular crosslinking by [2 + 2] photocycloaddition (Coqueret 1999; Laschewsky 2000).

Furthermore, a polymer obtained by copolymerisation of N-isopropylacrylamide (95mol%) and N-[tris-(hydroxymethyl)methyl]acrylamide (5mol%) is studied. According to ¹H-NMR integration analysis the copolymer composition was P-NIPAM-co-THMA: 95/5. The consistent compositions of the monomer feed and of the copolymer obtained suggest reactivity ratios of both acrylamides close to 1. The statistical copolymer obtained has a structure similar to a random copolymer (Heinz 2001).

Designation of Polymer	Name of Polymer	Method of modification to induce LCST	Structure	LCST in aqueous solution
P-THMA	poly[N-(tris-(hydroxy-methyl)-methyl)acrylamide]	none	see figure 27	no LCST
acetylated P-THMA	acetylated poly[N-(tris-(hydroxy-methyl)-methyl)acrylamide]	polymer analogous modification with 40mol% acetyl groups	see figure 27	28°C at c = 10g/l see also figure 30
cinna-moylated P-HPMA	cinna-moylated poly[N-2-hydroxypropyl-methacrylamide]	polymer analogous modification with 13mol% cinnamoyl groups	see figure 28	52°C at c = 2.4g/l
P-NIPAM-co-THMA	poly-N-[(sopropyl-acryl-amide-tris-(hydroxymethyl)methyl)acrylamide]	copolymerisation giving a copolymer containing 95mol% of N-isopropylacrylamide and 5% of N-[tris-(hydroxymethyl) - methyl]acrylamide.	see figure 29	30°C

Table 5. The polymers which were employed for characterisation in surface-attached state.

The synthetic pathways for the polymers and the polymer modifications will be described in short. A comprehensive and detailed description concerning all chemical steps and analysis of the polymers can be found in (Laschewsky 1999; Laschewsky 2001).

Synthesis of functionalized poly-N-[tris-(hydroxymethyl)methyl]acrylamide (P-THMA) and acetylated P-THMA

P-THMA was synthesised by free radical polymerisation of N-[tris-(hydroxymethyl)methyl]acrylamide (THMA) in a mixture of ethanol/water: 30/7 (c = 10% v/v) containing 2mol% of the functional azo-initiator dissolved in a minimum of dimethylsulfoxide. The mixture was degassed in vacuum at the temperature of liquid nitrogen, and then reacted at 60°C for 24h. The mixture was dialysed against water for 5 days and lyophilized to give the polymer as white hygroscopic powder.

Acetylated P-THMA was obtained by reacting polymer P-THMA with pyridine and acetic anhydride in DMF (c = 55g/l) at 60°C for 18 h. After cooling, the mixture was diluted with ethanol, and the copolymers were precipitated into diethyl ether.

Figure 27 shows the main participating components for the synthesis of P-THMA and the chemical step of acetylation.

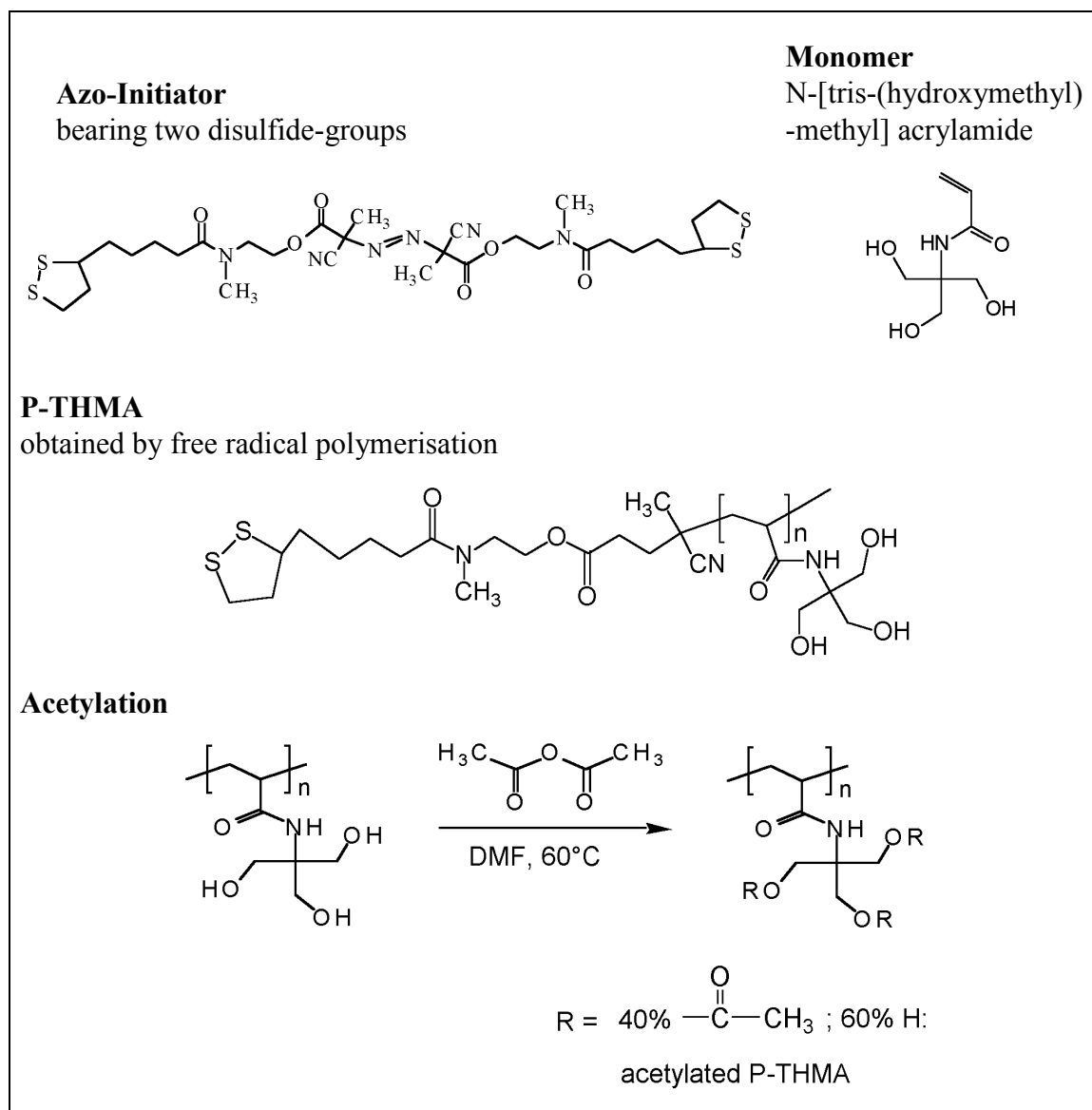


Figure 27. Overview of the components and basic chemical steps involved in the synthesis of acetylated P-THMA. The disulfide moieties of the polymer are used for efficient grafting to the SPR gold surface.

Synthesis of end-group functionalized poly-[N-2-hydroxypropylmethacrylamide] (P-HPMA) and cinnamoylated P-HPMA

P-HPMA was synthesized by free radical polymerization of N-2-hydroxypropylmethacrylamide (HPMA) in absolute ethanol (c = 10% v/v) containing 2mol% of the functional azo-initiator dissolved in a minimum of dimethylsulfoxide. The mixture was degassed in vacuum at the temperature of liquid nitrogen, and then reacted at 60°C for 24h. The polymer was purified by precipitation in acetone (72%) twice.

Partial cinnamoylation of P-HPMA was obtained by cinnamoylchloride / triethylamine / dimethylaminopyridine.

Figure 28 shows the employed monomer for synthesis of P-THMA and the modified polymer.

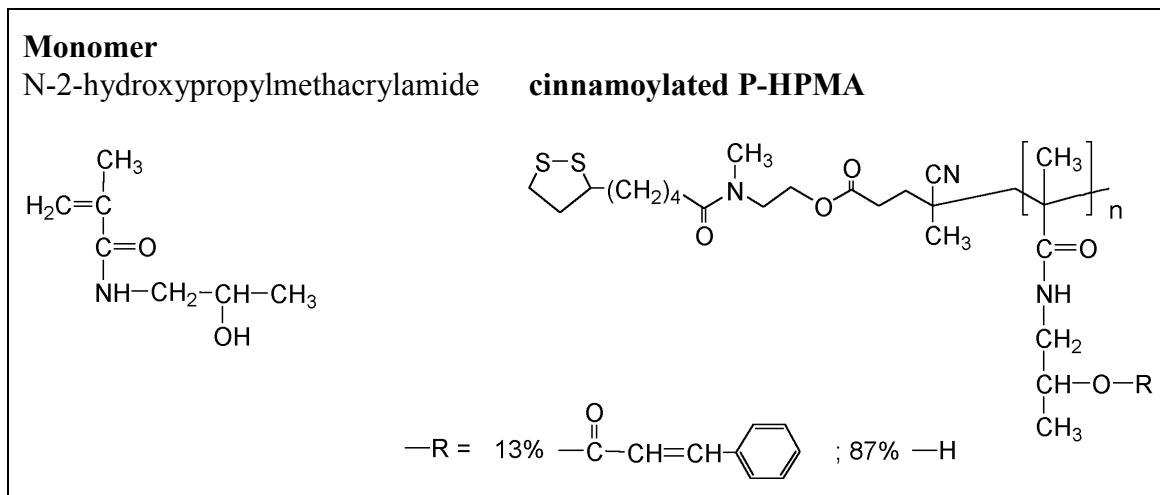


Figure 28. Structures of the employed monomer and the obtained thermo-responsive cinnamoylated P-HPMA containing 13% of cinnamoyl groups.

Synthesis of functionalized poly-N-[isopropylacrylamide-tris-(hydroxymethyl)methyl] acrylamide (P-NIPAM-co-THMA)

P-NIPAM-co-THMA was synthesized by free radical copolymerization of N-isopropylacrylamide (95mol%) and N-[tris-(hydroxymethyl)methyl]acrylamide (5mol%) in absolute ethanol (c = 10% v/v) containing 2mol% of the azo-initiator dissolved in a minimum of dimethylsulfoxide. The mixture was degassed in vacuum at the temperature of liquid nitrogen and reacted at 60°C for 24h. The polymer was purified by two precipitations in diethylether.

Figure 29 shows the obtained thermo-responsive polymer.

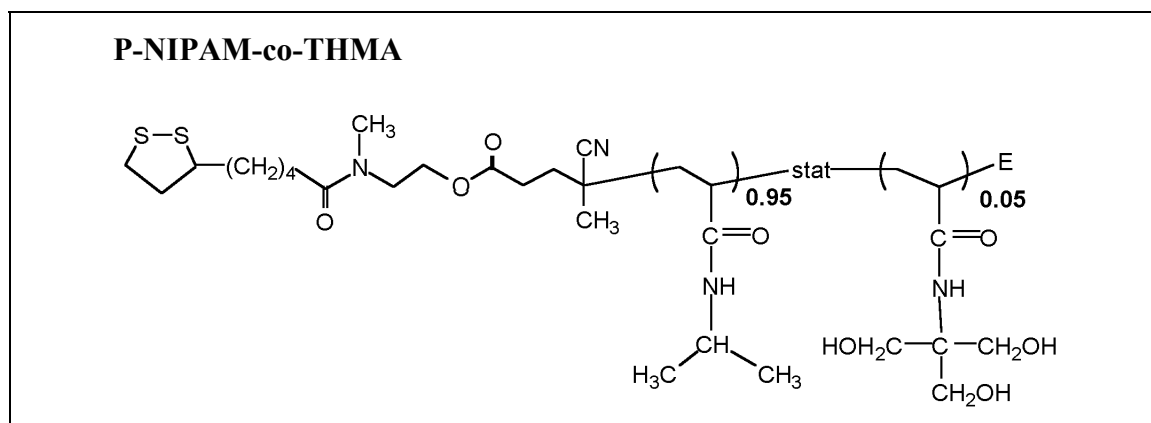


Figure 29. Structure of thermo-responsive P-NIPAM-co-THMA copolymer containing 95% of N-isopropylacrylamide and 5% of N-[tris-(hydroxymethyl)-methyl]acrylamide. E denotes the second end-group depending of the termination mechanism.

6.2 LCST of Aqueous Solutions

Laschewsky *et al.* have synthesised the acylated polymers with varying degree of acylation (Laschewsky 2000):

- acetylated P-THMA with degree of acetylation between 15 and 100mol%
- cinnamoylated P-HPMA with degree of cinnamoylation between 5 and 80mol%

The dependence of the LCST on the degree of acylation and on the concentration was established by E.D. Rekaï. The LCST was determined visually by observing the variation of the turbidity with temperature and concentration. A water bath was heated to a temperature just below the LCST and the sample was immersed into the bath, the temperature was then raised slowly and progressively till the sample became turbid and then the temperature was lowered slowly till the sample became clear again. The LCST determined by cooling is lower than the one determined by heating (Laschewsky 2000). Here, the results of the measurements will be briefly reported.

Regarding the behaviour of the aqueous solutions of the modified polymers, acetylated P-THMA exhibits a LCST in water only between 25% and 50% of acetylation, whereas below 25% of modification, the copolymers dissolve in water at any temperature, and above of 50%, the copolymers are insoluble (figure 30a)). P-THMA bearing 40mol% of acetoxy groups covers the physiologically interesting temperature range of 20°C to 45°C (figure 30b)).

Cinnamoylated P-HPMA is soluble in water at any temperature up to 5% of modification, presents a LCST up to 25% of modification, and is insoluble for 30% of modification and more.

The influence of the concentration on the LCST was studied around a LCST of 30°C. Acetylated P-THMA undergoes a notable and steady decrease of the LCST with increasing concentration; cinnamoylated P-HPMA also undergoes a notable decrease of the LCST with increasing concentration, but it levels off for concentrations higher than 5g/l.

It is important to know the behaviour of the polymers in solution, because analogously to the dependence of the LCST on the concentration in solution, the LCST on a surface will be dependent on the local polymer concentration given by the polymer grafting density. Furthermore, the polymer behaviour will most likely be influenced by the reduced degree of freedom existing in confined space on a surface. Therefore, the characterisation of the aqueous solutions is important information, which must be taken into account for the interpretation of the polymers' behaviour in surface-attached state.

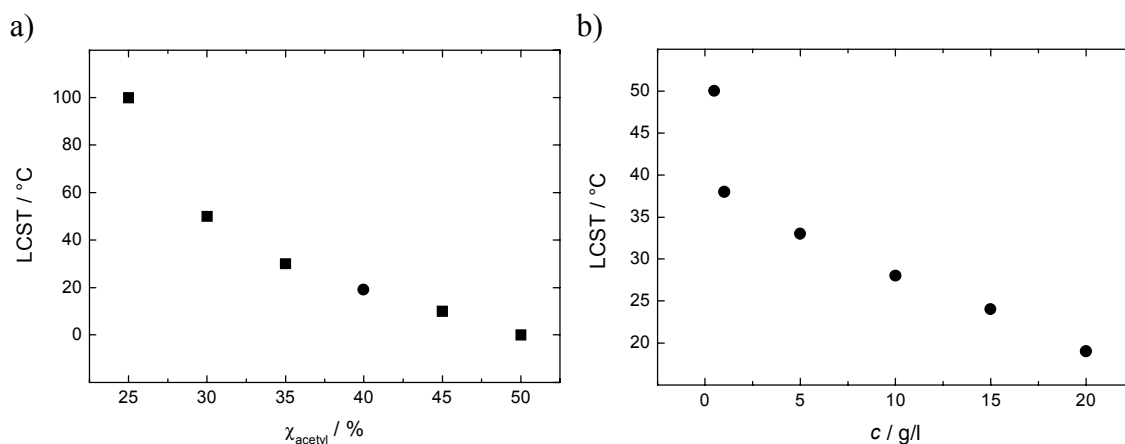


Figure 30. **a)** Dependence of the LCST of aqueous solutions of acetylated P-THMA on the molar fraction of acetylation χ_{acetyl} (concentration 20 g/l). The circular data point at $\chi_{acetyl} = 40\%$ marks the polymer used for the measurements in **b)**. This polymer is also used for the proof of the thermo-responsive effect on the surface. **b)** Dependence of the LCST of aqueous solutions of acetylated P-THMA on the concentration c (degree of acetylation 40%). Measurements performed by E.D. Rekaï, Département de Chimie, Université Catholique de Louvain, Louvain-la-Neuve, Belgium.

6.3 LCST in Surface-Attached State

It is not evident how polymers that are thermo-responsive in solution will behave when grafted to a surface. We have employed the SPR setup operated at a wavelength of 784nm to measure the temperature dependent conformational state of the grafted polymers.

6.3.1 Concept of the Investigation

Thermo-responsive hydrogels precipitate from solution when the temperature exceeds the LCST. The thermal energy is breaking up the hydration structures around the hydrophobic moieties of the hydrogels and hydrophobic forces let the polymer chains crumple up. Analogously, the thermo-responsive effect should lead to a collapse of a hydrogel film onto a surface, if the polymer chains are grafted to it. Since water will be displaced from the hydrogel film during this process, the refractive index of the collapsing hydrogel film must increase. Considering the exponential decay of an evanescent field of a SP wave from the surface, the collapse of the hydrogel when passing the LCST will change the perceived effective refractive index. Consequently, it should be possible to track the collapse following the angle shift in the intensity minimum. Figure 31 summarises these considerations.

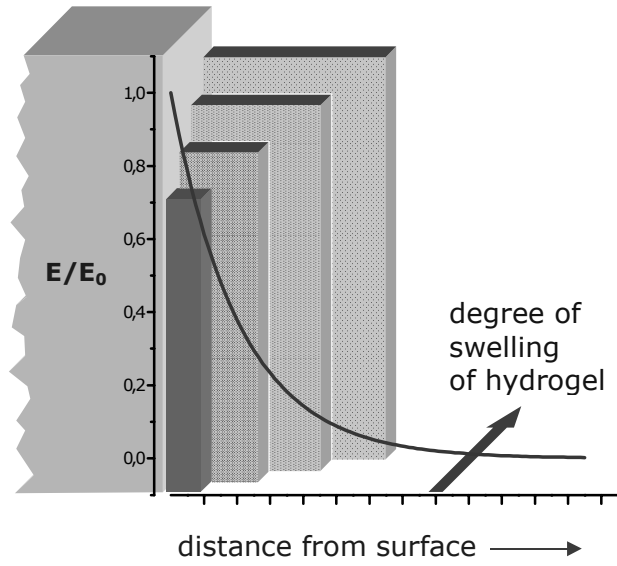


Figure 31. The principle of the investigation of the thermo-responsive effect on a surface. A hydrogel film is sketched with different degrees of swelling. Since the swelling is caused by the incorporation of water within the film, its refractive index will vary correspondingly (indicated with different degrees of shading). The thermo-responsive effect will transform the hydrogel film from swollen state into collapsed state with higher refractive index. The electric field of SP waves is also sketched. The SPR response depends on the convolution of the electric field with the different conformational states of the hydrogel film.

Presuming the hydrated hydrogel film can be considered as a homogeneous polymer solution its refractive index can be calculated according to Garnet's equation (Garnet 1904):

$$\frac{n_F^2 - n_M^2}{n_F^2 + 2n_M^2} = \Phi \frac{n_0^2 - n_M^2}{n_0^2 + 2n_M^2} \quad (34)$$

with n_F the index of refraction of the hydrated hydrogel film, n_M the index of refraction of the medium (here water: $n_M = n_{H_2O} (\lambda = 784\text{nm}) = 1.329$), n_0 the index of refraction of the dry hydrogel and Φ the volume fraction taken up by the polymer. For a swollen hydrogel film the volume fraction is simply given by

$$\Phi = \frac{d_{HG \text{ dry}}}{d_{HG \text{ hyd}}} \quad (35)$$

with $d_{HG \text{ dry}}$ the thickness of the dry hydrogel film and $d_{HG \text{ hyd}}$ the thickness of the hydrated (swollen) hydrogel film. Thus the refractive index of the hydrogel film can be calculated for different thicknesses.

For the layer system depicted in figure 31 (hydrogel film / medium) the effective refractive index n_{eff} perceived by SPR can be calculated according to equation 9 (page 17):

$$n_{eff}(d_{HG\ hyd}) = n_F(1 - \exp(-2 d_{HG\ hyd} / d_{PD})) + n_M \exp(-2 d_{HG\ hyd} / d_{PD}) \quad (36)$$

The change of the resonance angle $\Delta\Theta_{SPR}$ depends linearly on the change of effective refractive index Δn_{eff} in a good approximation. The dependence of $\Delta\Theta_{SPR}$ on the refractive index increment amounts to $\Delta\Theta_{SPR}(\lambda = 784\text{nm}) = 107.2^\circ \cdot \Delta n$ for the experimental setup used for these investigations (within $n_{eff} \approx 1.33 - 1.36$).

Consequently, a resonance angle shift $\Delta\Theta_{SPR\ calc}$ can be calculated for different thicknesses $d_{HG\ hyd}$ of the hydrated hydrogel (meaning different conformational states):

$$\Delta\Theta_{SPR\ calc} = \Delta n_{eff} \cdot 107.2^\circ \quad (37)$$

$$\Delta n_{eff} = n_{eff}(d_{HG\ hyd}) - n_{eff}(d_{HG\ hyd} = d_{HG\ dry}) \quad (38)$$

Figure 32 shows $\Delta\Theta_{SPR\ calc}$ for three different thicknesses of the dry hydrogel. The refractive index n_0 of the polymer in dry state was assumed to be 1.478. This is an estimation, because the thermally responsive copolymers employed in the study are new and no detailed solid state physical data are available to date. Therefore, the solid state refractive index was estimated by using the data of poly(methylacrylate) (PMA), a similar standard polymer which has been investigated in the past. The refractive index of PMA is 1.478 (Krevelen 1990). The refractive index of polyacrylates is only weakly dependent on the chemical nature of side groups, unless aliphatic groups are replaced by aromatic ones. The penetration depth $d_{PD} = 324\text{nm}$ for SP waves excited with 784nm was calculated according to equation 10 with the refractive index values given in table 1.

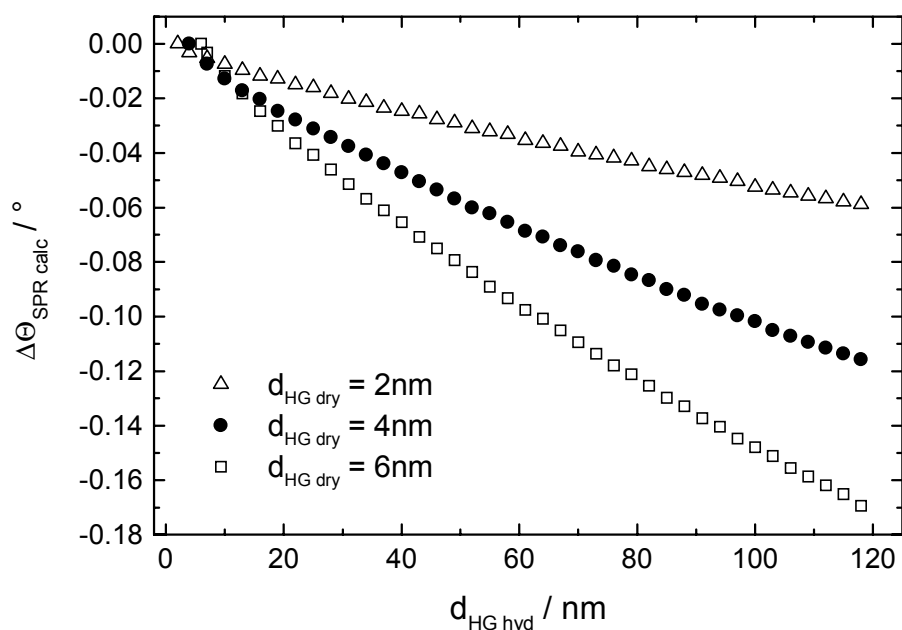


Figure 32. The calculated resonance angle shift $\Delta\Theta_{SPR,calc}$ in dependence of the hydrated hydrogel film thickness $d_{HG,hyd}$, calculated for three different dry hydrogel thicknesses. The plot shows the evolution of $\Delta\Theta_{SPR}$ while the hydrogels hydrate from dry state to swollen state. The thermo-responsive effect should induce a collapse of the hydrogel, thus $d_{HG,hyd}$ decreases and $\Delta\Theta_{SPR}$ increases.

The hydrogel collapse due to the thermo-responsive effect will expel the water from the hydrogel and will lead to a much more densely packed film. If this collapsed hydrogel state is roughly comparable with the dry (or solid) state of the hydrogel, then the thermo-responsive effect on a surface should be detectable by SPR measurements.

6.3.2 Experimental Part

6.3.2.1 Preparation of Samples

Gold coated glass slides were used as substrate for the hydrogel coating. The glass slides ($12 \times 12 \times 0.55 \text{ mm}^3$, BK7, custom made by B&M Optik) were cleaned with piranha solution (1:1 by volume $\text{H}_2\text{SO}_4/30\text{wt}\% \text{H}_2\text{O}_2$ for 20min) and afterwards covered with a 1nm 80/20 NiCr adhesion layer and a 50nm 99.9% gold layer by thermal evaporation (metal film deposition was performed by DTVa, Dresden, Germany). The gold surfaces were cleaned with a 1:1 by volume solution of 0.1M KOH/30wt% H_2O_2 at 70°C for 20min. The hydrophilic gold surfaces were incubated in a 4g/l aqueous polymer solution for 24h. The polymers were chemisorbed on gold via their terminal disulfide group(s) and then the coated substrates were immersed in water which resided in the flow chamber. Figure 33 shows the “grafting to” process of polymer adsorption by diffusion from solution to the surface.

Millipore-filtered water (18 M Ω) was used for the preparation of all aqueous solutions and rinsing.

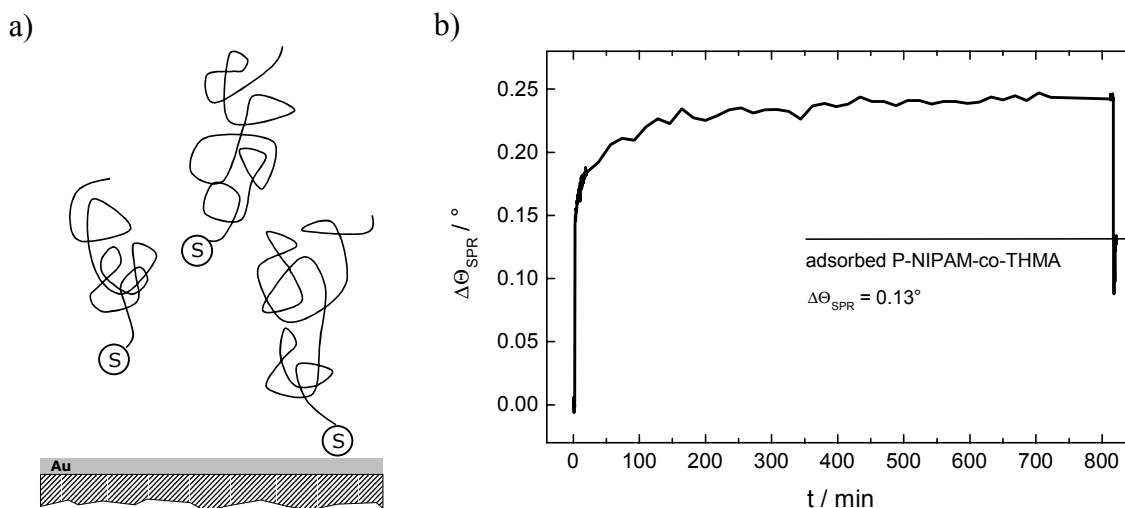


Figure 33. Grafting of disulfide-functionalised P-NIPAM-co-THMA to a gold surface. **a)** The polymer chains have to diffuse against a concentration gradient to the surface. **b)** Adsorption kinetic. After about 8h no more significant signal increase is observable.

6.3.2.2 Temperature Variance of Solvent

In order to trigger the thermo-responsive effect of the polymer, the temperature of the solvent (water) has to be increased. Two different strategies to do this were tested:

- 1) Introduction of water that was gradually heated from room temperature to a pre-determined temperature.
- 2) Injecting water at a specific temperature.

6.3.2.2.1 Continuous Heating

Water from a reservoir was continuously pumped by a peristaltic pump through the flow chamber. The feed rate was 75 $\mu\text{l}/\text{min}$. The water supplying Teflon tube was wrapped with an electrically heatable foil on a stretch of 10cm before entering the flow chamber (see figure 34). The foil was heated with a constant electric current. The water slowly flowing through the Teflon tube in the centre of the foil was continuously warmed. The heat transfer by the warmed water into the flow chamber lead to a steady increase of the water temperature in the flow chamber. The speed of heating up the flow chamber was adjustable by the current through the heating foil (see figure 35).

While the temperature was continuously increased, SPR measurements could be performed in angle mode as well as in differential intensity mode.

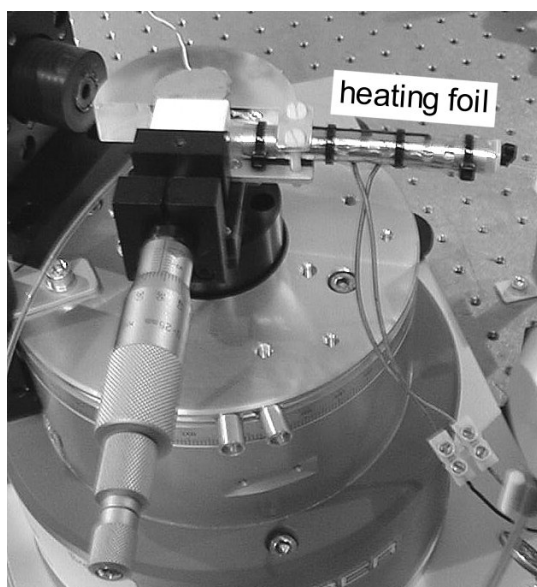


Figure 34. Setup for continuous heating of the water flowing through the flow chamber. More details are given in the text.

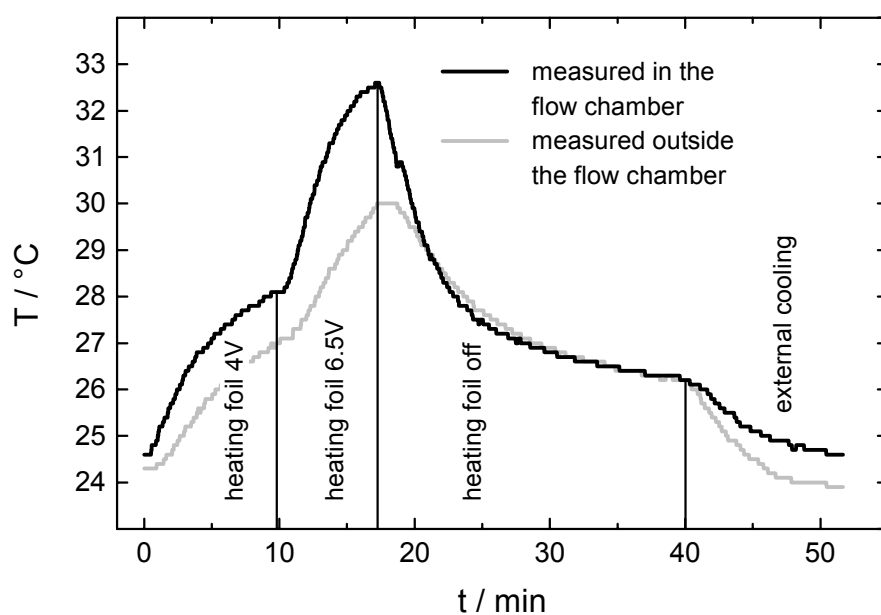


Figure 35. The temperature pattern during heating with the heating foil measured with a thermocouple. The speed of warming up the water in the flow chamber can be varied by the current through the heating foil (respectively by the applied voltage). The black curve indicates the temperature measured directly in the flow chamber; the grey curve was recorded outside but close to the flow chamber.

However, the continuous heat transfer from the flow chamber into the setup seemed to be disadvantageous (see grey curve in figure 35). The SPR signals -both the angle measurements and the differential intensity measurements- reveal tremendous jumps which will make the resolution of the thermo-responsive effect impossible (figure 36). Probably heat induced tensions which slightly deform the setup and abruptly release are

responsible for the observed signal jumps. Furthermore, possibly the optical coupling of the glass slide to the prism by immersion oil is influenced by the transferred heat.

Summarised, the observed noise in the signals made the continuous heating arrangement impracticable.

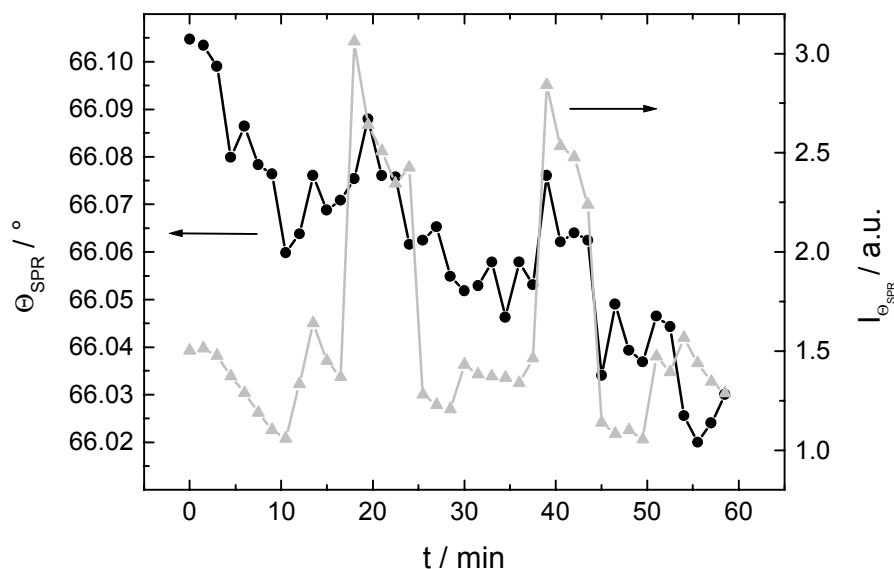


Figure 36. SPR signals of a pure gold film recorded during continuous heating. The heating foil was operated with a voltage of 5V, the temperature in the flow chamber raised from room temperature to about $RT+7K$. The angle measurements are superposed by tremendous noise; the intensity measured in the SPR minimum jumps, too. The intensity at Θ_{SPR} sometimes greatly increases, this may be due to the optical coupling between the glass slide and the prism is influenced. If the coupling is not optimal, light will also be reflected at the interface glass/glass and thus not participate in the excitation of SP waves.

6.3.2.2 Injection

Water heated to certain temperatures was injected into the flow chamber and SPR angle measurements were carried out simultaneously. The measurements are also superposed by noise, but to a much lower extent compared to the continuous heating method. But still, several single measurements need to be averaged to filter the noise below a level which allowed clear identification of effects originating from the hydrogel film.

The differential intensity measurement mode is not appropriate for the injection method, because the signal is drastically influenced by the altered refractive index of water with different temperature. This effect will obscure a possibly occurring collapse of the hydrogel.

Nevertheless, a differential intensity measurement allows tracking the development of the temperature in the flow cell after injection of warmed or cooled water. After injecting water 10K warmer or colder than ambient temperature, it takes ca. 500s for the temperature in the flow chamber to come back to base level (figure 37).

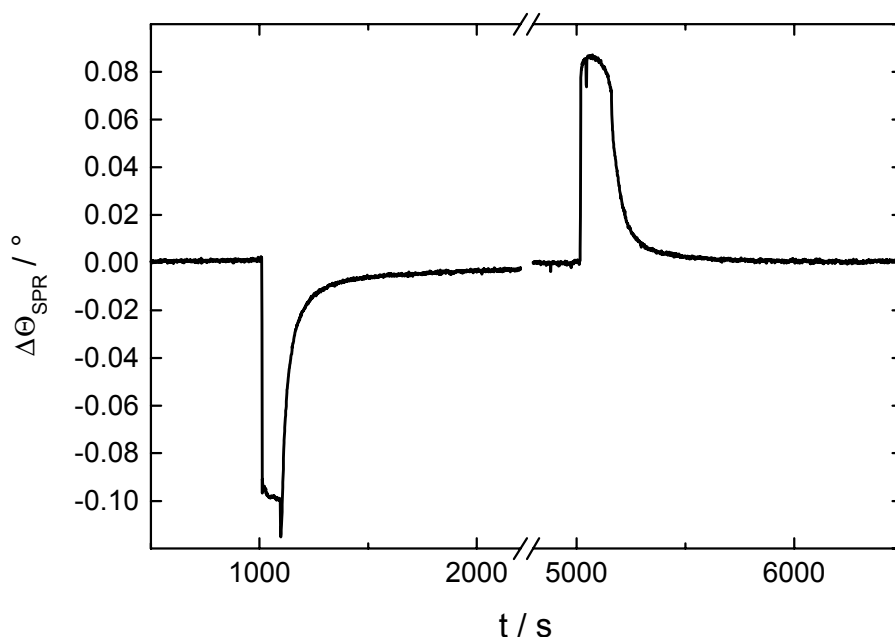


Figure 37. Differential intensity measurement of the injection of water into the flow cell. $T_{H_2O} = RT + 10K$ and $T_{H_2O} = RT - 10K$. The big jump in the signal caused by the different refractive index of the warmed and cooled water will cover a possibly occurring thermo-responsive effect. It takes the signal about 500s to come back to base level.

The moderate levelling speed may be a reason for the noise of the angle measurements carried out during the injection method. Typically, shorter time intervals than 500s went by between successive angle measurements. Therefore, the temperature was most likely not always exactly levelled to base level between single measurements. This means that the actual temperature in the flow cell was probably not that well defined as the heating of water to defined temperatures may suggest. For each measurement the resonance angle was assigned to the temperature the water was heated to: $\Theta_{SPR} = \Theta_{SPR}(T)$. Thus, a deviation of the actual temperature in the flow cell was transformed to a deviation of $\Theta_{SPR}(T)$. The standard deviation of single measurements $\Theta_{SPR}(T)$ to data listed by Schiebener *et al.* (Schiebener 1990) was determined to amount to 0.007° . Consequently, the standard deviation of the mean $\Theta_{SPR\ mean}(T)$ (in the following $\Theta_{SPR}(T)$) from three measurements is 0.004° (standard deviation of a single measurement divided by the square root of the number of measurements). This value is smaller than the systematic error of angle measurements (0.005°) which is used in this work as the limit of accuracy. Averaging at least three measurements reduces the noise to an extent making use of the potential of the employed SPR setup.

6.3.3 Results

The polymers P-THMA, acetylated P-THMA and P-NIPAM-co-THMA were investigated for the thermo-responsive effect while being attached to a surface. Cinnamoylated P-HPMA was not investigated, because the LCST of this polymer is too high, to be measurable in the SPR setup. At temperatures around $50^\circ C$ the signal-to-

noise ratio is too small for meaningful data evaluation. This is probably caused by increased heat flow effects at such high temperatures.

Table 6 shows the number of samples investigated and the number of measurements averaged. The averaging was done in order to reduce the noise inherent to the injection method employed here.

Polymer	Number of samples	Number of measurements averaged
P-THMA	4	4
acetylated P-THMA	4	3
P-NIPAM-co-THMA	2	5

Table 6. Samples used for the proof of the LCST in surface-attached state.

Figure 38 shows the results of the measurements on P-THMA and acetylated P-THMA.

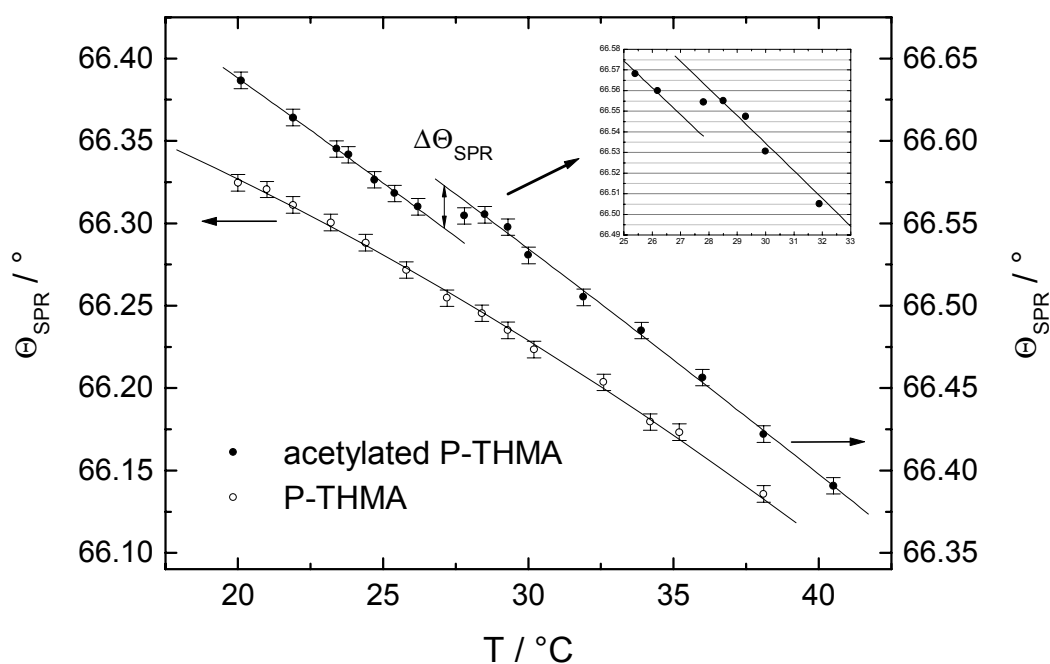


Figure 38. Open circles: $\Theta_{SPR}(T)$ of non-stimuli-responsive P-THMA. The curve reflects the evolution of the refractive index of water with temperature and serves as a reference. Filled circles: $\Theta_{SPR}(T)$ of acetylated P-THMA. The collapse of the hydrogel at $T = LCST$ leads to a significant shift $\Delta\Theta_{SPR}$ indicating the phase transition. The error bars indicate the systematic error of angle measurements. The inset shows an enlargement of the temperature region in which the phase transition of acetylated P-THMA occurs.

Pure P-THMA is a hydrophilic polymer without thermo-responsive properties. Here, a polynomial fit to the data points of simple P-THMA (figure 38, open circles) serves as a reference curve reflecting the temperature dependence of the refractive index of water. The average slope of the curve amounts to $-0.011^{\circ}/\text{K}$ which equals a temperature dependent change of the refractive index of water of $-1.0 \cdot 10^{-4} \text{K}^{-1}$. These values are in good accordance with the data listed by Schiebener *et al.* (Schiebener 1990).

The measurement carried out on acetylated P-THMA shows a different evolution with temperature. In addition to the overall decrease of the resonance angle with temperature, there is a distinct change in the slope between $T \approx 26^{\circ}\text{C}$ and $T \approx 28.5^{\circ}\text{C}$ leading to an offset of $\Delta\Theta_{\text{SPR}} = 0.026^{\circ}$. This indicates the phase transition of the acetylated P-THMA triggered by the increasing temperature. The inset in figure 38 shows an enlargement of the phase transition. The data point at $T = 27.8^{\circ}\text{C}$ shows a substantial deviation from the fit curve traversing the data points at lower temperatures. The next measured resonance angle at $T = 28.5^{\circ}\text{C}$ is even larger, although the temperature difference between these two points demands a decrease in resonance angle of 0.008° . While passing this temperature region the balance between hydrophilic and hydrophobic forces overturns to hydrophobic forces and the polymer is collapsing onto the surface, thus increasing the resonance angle. After the phase transition all data points at higher temperatures show a parallel displacement. This underlines the fact that the hydrogel is in collapsed state and that the deviation of the data points at $T = 27.8^{\circ}\text{C}$ and $T = 28.5^{\circ}\text{C}$ is not merely random. Furthermore, a positive shift in resonance angle was measured, as expected according to the model developed in section 6.3.1 and adducing further evidence against an artefact.

Figure 39 shows the measurements for P-NIPAM-co-THMA and P-THMA (identical curve as in figure 38).

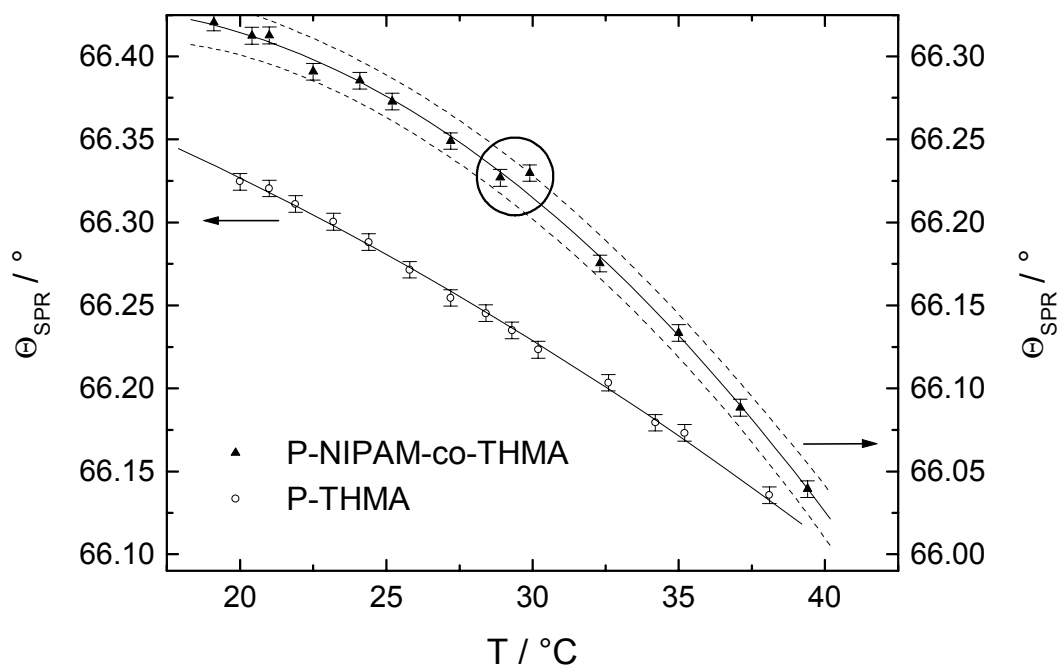


Figure 39. Open circles: $\Theta_{\text{SPR}}(T)$ of non-stimuli-responsive P-THMA (same curve as in figure 38). The curve reflects the evolution of the refractive index of water with temperature and serves as a reference. Filled circles: $\Theta_{\text{SPR}}(T)$ of P-NIPAM-co-THMA. The two encircled data points show similar behaviour as observed during the phase transition of acetylated P-THMA (figure 38). However, no collective shift characteristic for a hydrogel in collapsed state after passing the phase transition can be identified. The strong curvature may be caused by the particular optical properties of P-NIPAM-co-THMA.

The data of P-NIPAM-co-THMA follow a second order polynomial with higher degree of curvature than for P-THMA. This may be caused by the particular optical properties of P-NIPAM-co-THMA. The width of the band drawn around the polynomial fit curve equals the shift $\Delta\Theta_{\text{SPR}} = 0.026^\circ$ as observed for acetylated P-THMA. Around $T = 30^\circ\text{C}$ two data points in figure 39 (encircled) show the characteristic behaviour for a phase transition. The magnitude of the shift against each other as well as the direction (positive shift with increasing temperature) bear resemblance to the behaviour of the data indicating the phase transition of acetylated P-THMA in figure 38. However, the characteristic collective shift of the resonance angles at higher temperatures can not be observed. Consequently, a thermo-responsive effect of surface-attached P-NIPAM-co-THMA cannot be established.

6.3.4 Discussion

Quantitative analysis of the measurements of acetylated P-THMA is done by comparison of the measured data with simulated data. Simulated data were obtained by calculation of surface plasmon resonance curves according to the theory outlined in chapter 3.1.4.

At $T = 35^\circ\text{C}$ acetylated P-THMA is supposed to be in a collapsed state similar to dry state. This justifies assuming the refractive index of the collapsed hydrogel to be equal to the dry state (solid state) refractive index: $n_{\text{ac P-THMA collap}} = n_0 = 1.478$. Dependence of temperature can be neglected. The refractive index of water is $n_{\text{H}_2\text{O}}(T = 35^\circ\text{C}) = 1.327$ according to Schiebener *et al.* (Schiebener 1990). The simulations were carried out for water at room temperature ($n_{\text{H}_2\text{O}}(T = 20^\circ\text{C}) = 1.329$); the difference in refractive index was considered by a constant (0.16°) added to the measured resonance angles.

The layer system employed for simulations is shown in table 7; the simulated SPR curves and the dependence of the simulated resonance angles on the dry hydrogel thickness are shown in figure 40. The thickness of the collapsed hydrogel layer was determined by a linear fit to the simulated data:

$$\Theta_{\text{SPR sim}} = \Theta_{\text{SPR 0}} + 0.08^\circ\text{nm}^{-1} \cdot d_{\text{HG dry}} \quad (39)$$

with $\Theta_{\text{SPR 0}} = 66.15^\circ$. The found value is $d_{\text{HG dry}} = 5.7\text{nm}$.

layer no. i	name	d / nm	n
1	BK7 glass	∞	1.511
2	gold	50	0.149-i4.779
3	acetylated P-THMA	variable	1.478
4	water	∞	1.329

Table 7. Layer system which was employed in SPR simulations to determine the thickness of the collapsed acetylated P-THMA hydrogel.

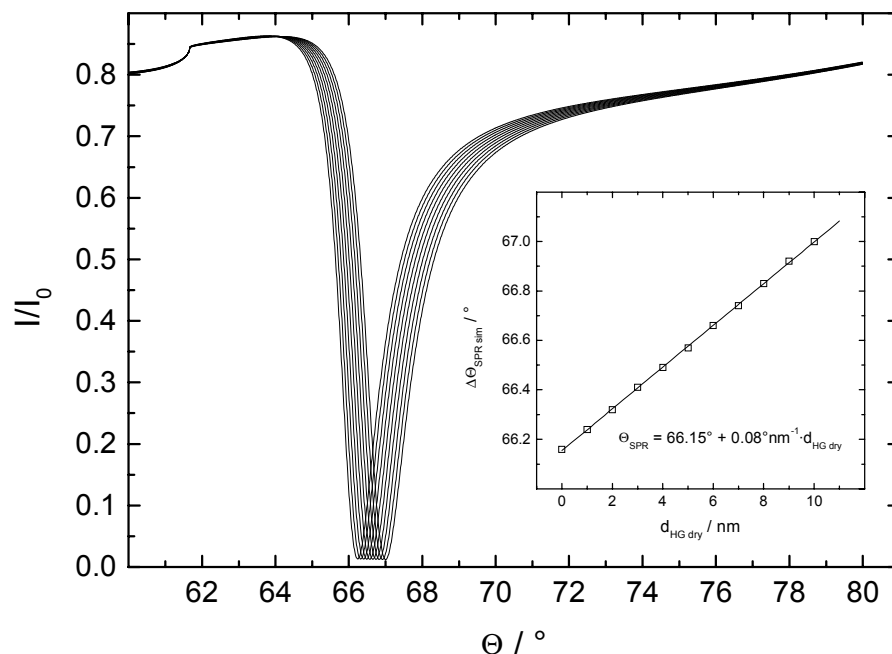


Figure 40. Simulated SPR curves for varying thickness of collapsed acetylated P-THMA. The simulations are based on the layer system shown in table 7. The inset shows the resonance angles extracted from the simulated SPR curves as a function of the thickness of the collapsed hydrogel and a linear fit curve to the data.

The thickness of the hydrated hydrogel film can be calculated assuming that the thermo-responsive effect is the reversed process of hydration. This means the hydrated hydrogel film is supposed to develop from a dry film with the thickness of the collapsed film. By applying equation 34 and 35 with $d_{\text{HG dry}} = 5.7\text{nm}$ the refractive index of the hydrated film can be calculated for different thicknesses. The layer system employing these values and being used to calculate the respective SPR curves is shown in table 8.

layer no. i	name	d / nm	n
1	BK7 glass	∞	1.511
2	gold	50	0.149-i4.779
3	acetylated P-THMA	5.7 - 130	calculated according to equation 34
4	water	∞	1.329

Table 8. Layer system which was employed in SPR simulations to determine the thickness of the swollen acetylated P-THMA hydrogel.

The resonance angles extracted from the calculated SPR curves are plotted in figure 41.

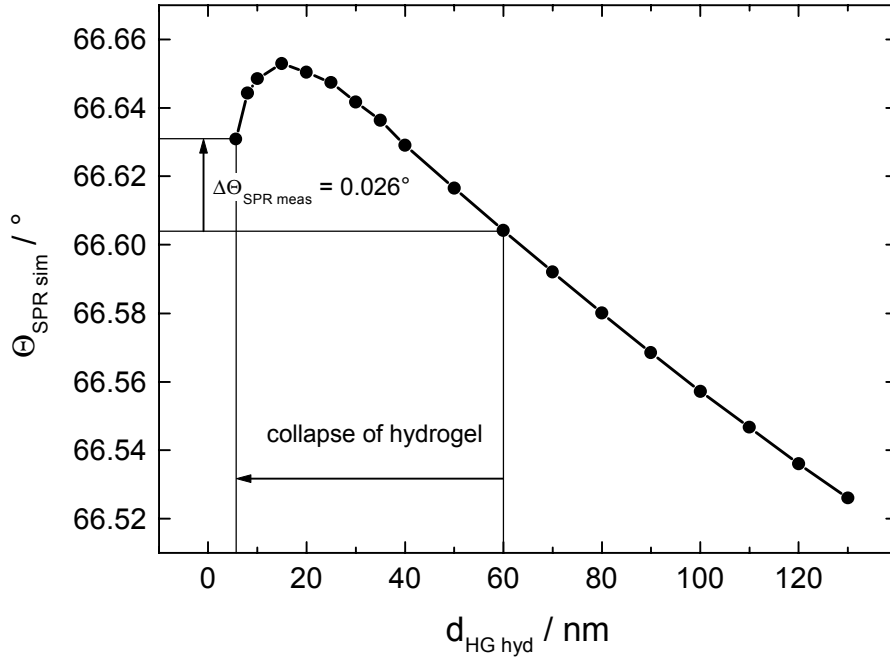


Figure 41. Resonance angles extracted from simulated SPR curves of a layer system resembling a swelling hydrogel (see table 8) (the values are calculated for room temperature). The starting value for the dry hydrogel thickness was $d_{HG\text{ dry}} = 5.7\text{nm}$ as determined previously. The collapse of the hydrogel induced by exceeding the LCST is supposed to be the reverse process (as indicated by the arrow). From the measured resonance angle shift $\Delta\Theta_{\text{SPR meas}}$ a swollen / hydrated hydrogel thickness of $d_{HG\text{ hyd}} = 60\text{nm}$ was determined.

The calculations suggest that the measured values of $\Theta_{\text{SPR}}(T)$ and the observed shift of $\Theta_{\text{SPR}} = 0.026^\circ$ correspond to a swollen hydrogel film which is approximately 60nm thick at $T < \text{LCST}$, and which collapses to a 5.7nm thick film when the temperature exceeds the LCST. For the swollen hydrogel a mixed refractive index equals to 1.344.

The calculated resonance angle $\Theta_{\text{SPR sim}}$ is increasing in the range from 5.7 to 15nm of hydrated hydrogel thickness (see figure 41). This is in contradiction to the calculated expected evolution of the resonance angle $\Delta\Theta_{\text{SPR calc}}(d_{HG\text{ hyd}})$ according to the model developed in section 6.3.1, where it is steadily decreasing (see figure 32).

This can be explained by the different character of the two models the calculations are based on. Calculations applying Fresnel's equations to a model layer system assume homogeneous smooth layers with ideal sharp interfaces. According to electro-magnetic theory the normal component of an electric field E_n changes discontinuously while passing an uncharged interface between two dielectric media with different refractive indices n_3 and n_4 (Jackson 1982):

$$E_{3n} = \frac{n_4^2}{n_3^2} E_{4n} \quad (40)$$

The Fresnel theory is considering such a discontinuity between layers 3 and 4 in table 7 and 8. Furthermore, for the penetration depth d_{PD} of the SP wave different values are considered in the layers. The model developed in section 6.3.1 is neglecting these effects by assuming a continuously decreasing electric field with constant d_{PD} .

The truth will be in between the two models: the hydrogel film -especially in swollen state- certainly cannot be assumed to form a perfectly smooth interface with the medium. Rather the density and thus the refractive index will follow a smoothed step function. Therefore, there will be no discontinuity of the electric field as assumed by the Fresnel formalism. On the other hand, d_{PD} will certainly vary in the different layers, however, only to a small extent (see figure 6).

Nevertheless, both models are in good accordance with respect to the change of Θ_{SPR} with hydrated hydrogel layer thickness:

$$\left. \frac{d\Theta_{SPR\ sim}}{dd_{HG\ hyd}} \right|_{d_{HG\ hyd}=60\ nm} = \left. \frac{d\Theta_{SPR\ calc}(d_{HG\ dry} = 6\ nm)}{dd_{HG\ hyd}} \right|_{d_{HG\ hyd}=60\ nm} \approx 0.001^\circ\text{nm}^{-1} \quad (41)$$

This underlines in particular the validity of the straightforward model developed in section 6.3.1, at least within certain limits. However, for quantitative analysis the Fresnel model is preferred here. The results are depicted in Figure 42.

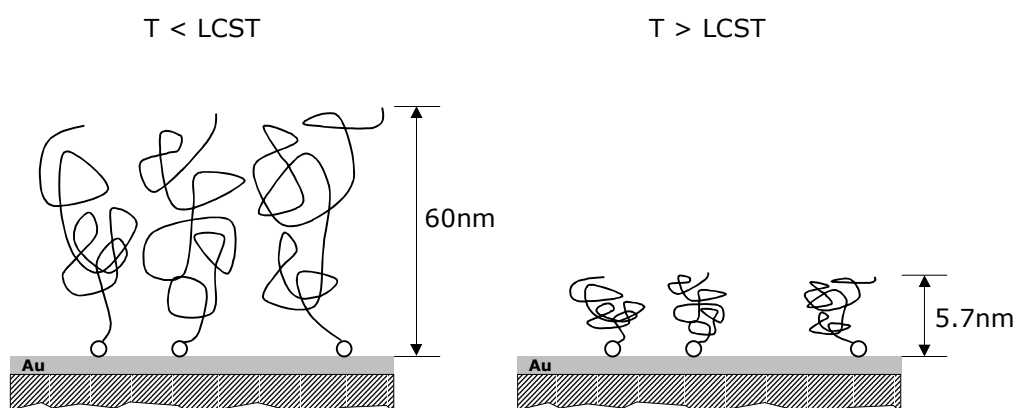


Figure 42. Schematic representation of the thermo-responsive effect of acetylated P-THMA attached to a gold surface as determined and quantified by SPR. The phase transition occurs at $LCST \approx 26^\circ\text{C}$.

The thermal transition on the gold surface occurs at $T \approx 26^\circ\text{C}$ which would correspond to a concentration of about 15g/l in aqueous solutions. However, the dimensions of the collapsed and swollen hydrogel film as determined by the SPR measurements imply a local concentration of the polymer in the chemisorbed swollen hydrogel film of about 120g/l, assuming a density of 1.2g/cm^3 (Krevelen 1990) for the polymer. Two factors may explain this difference: first, the temperatures measured may be systematically slightly too high due to heat flow effects, but, more important, it is very likely the steric restrictions for the polymer chains at the interface have a significant influence on the phase transition (Zhu 1999), shifting the transition temperature to higher values for

polymer chains in confined space. An analogous increase of transition temperatures was reported for example for surface attached brushes of liquid crystalline polymers (Peng 1999).

The width ΔT of the phase transition can be estimated to amount to $\Delta T \approx 2.5^\circ\text{C}$ and is believed to be caused by the polydispersity of the compound. A fully acetylated sample from the same batch was analysed by gel permeation chromatography. The resulting number for the apparent polydispersity was 8 (average number molar mass of 25,000g/mol; average weight molar mass of 200,000g/mol).

For P-NIPAM-co-THMA no LCST could be established. This may be caused either by a lower hydrogel thickness or by the particular conditions characteristic for a surface.

The layer thickness of P-NIPAM-co-THMA amounts to about 2nm. According to figure 32 this is reducing the sensitivity $d\Theta_{\text{SPR calc}}/dd_{\text{HG hyd}}$ of about the factor of two, compared to $d_{\text{HG dry}} = 6\text{nm}$. Furthermore, the P-NIPAM-co-THMA hydrogel layer only has approximately one third of the thickness of the acetylated P-THMA layer. These two features taken together may reduce the SPR response on a collapse of P-NIPAM-co-THMA 6-fold (considering the almost linear dependence of $\Theta_{\text{SPR calc}}(d_{\text{HG hyd}})$ in figure 32). This would mean a reduction of the SPR response below the detection limit of the SPR setup of 0.005° (defined as the standard deviation of repeated measurements (repeat accuracy)).

On the other hand, the results of acetylated P-THMA have shown that the LCST is substantially influenced by the particular conditions existing in confined space on a surface. Two mechanisms are working against each other: the high local concentration actually should shift the LCST to very low temperatures, but the steric hindrance due to the high concentration prevents the hydrogel from collapsing at such low temperatures; indeed higher temperatures are required. The interplay of these effects is rather complex and not easy to predict for all polymers. This may be the reason why it was not possible to experimentally prove a LCST on the surface for P-NIPAM-co-THMA within the investigated temperature range. Probably the LCST of P-NIPAM-co-THMA is shifted by the discussed effects into some other temperature range.

6.3.5 Conclusion

In conclusion, controlled chemical modification allows to induce and to tune the LCST of well-known water-soluble polymers. In the case of acetylated P-THMA, which was chemisorbed to a gold surface, thermal transition was experimentally proven by SPR and the thermo-responsive effect was quantified by comparison of the measurements with calculations.

For P-NIPAM-co-THMA no LCST on a surface could be evidenced within the investigated temperature range.

6.4 Photocrosslinking of Cinnamoylated P-HPMA

The modification of P-HPMA with photoreactive hydrophobic cinnamoyl groups offers an elegant way to prove the thermo-responsive effect on a surface. The cinnamoyl functionalities can undergo intra- and intermolecular crosslinking by [2 + 2] photocycloaddition when irradiated with UV light, turning the soluble polymer into insoluble state. Hence, irradiating cinnamoylated P-HPMA in collapsed state (i.e., the hydrogel is immersed in water with $T > LCST$) could freeze the collapsed conformation. Since the polymer remains permanently collapsed, the thermo-responsive effect could be conveniently proven at room temperature.

Furthermore, the potential possibility of freezing the collapsed state could be employed for new applications. As an example, a sensor surface could be provided with a pattern consisting of hydrophilic / hydrophobic domains just by irradiating the polymer through a corresponding mask while it is in collapsed state. The irradiated part of the hydrogel surface will be crosslinked and thus remain in collapsed, meaning more hydrophobic, state, even if the temperature is lowered below the LCST.

Here, cinnamoylated P-HPMA with 13mol% cinnamoyl groups was investigated for the permanent fixing of the collapsed state by irradiation with UV light.

6.4.1 Experimental Procedure

The preparation of the gold coated glass slides and the grafting of the polymer to the gold surface were done in the same way as for the samples used in the previous part (for preparation details see section 6.3.2.1).

Two samples were investigated, each was measured on two spots. The experimental course for each sample is concisely summarised in table 9.

	Experimental course
Sample 1	<ol style="list-style-type: none"> 1. Hydrogel chemisorption 2. SPR 3. Photocrosslinking: one sample half irradiated, one half shaded 4. SPR 5. 2nd run photocrosslinking: both sample halves irradiated 6. SPR
Sample 2	<ol style="list-style-type: none"> 1. Hydrogel chemisorption 2. SPR 3. Immersion into 65°C water without UV irradiation 4. SPR 5. Photocrosslinking: both sample halves irradiated 6. SPR

Table 9. The experimental course performed on two samples to verify the effect of photocrosslinking of cinnamoylated P-HPMA. The term “SPR” indicates SPR measurements carried out on both halves of a sample.

The setup for crosslinking surface-attached cinnamoylated P-HPMA is depicted in figure 43. The photocrosslinking was attempted by irradiating the samples with a 6W UV lamp with maximum intensity at $\lambda = 254\text{nm}$ for 90min. During UV exposure the samples were immersed in water at 65°C. Most likely the hydrogel on the gold surface will be in collapsed state at that temperature. The water layer covering the surface was only about five millimetres thick, thus avoiding a substantial UV light absorption (absorption coefficient of water at $\lambda = 254\text{nm}$ is about 0.02cm^{-1}). One half of the sample surface was shaded against UV light to allow reference measurements.

After the irradiation process, the samples were mounted onto the SPR setup again and measurements on two spots on each sample were carried out.

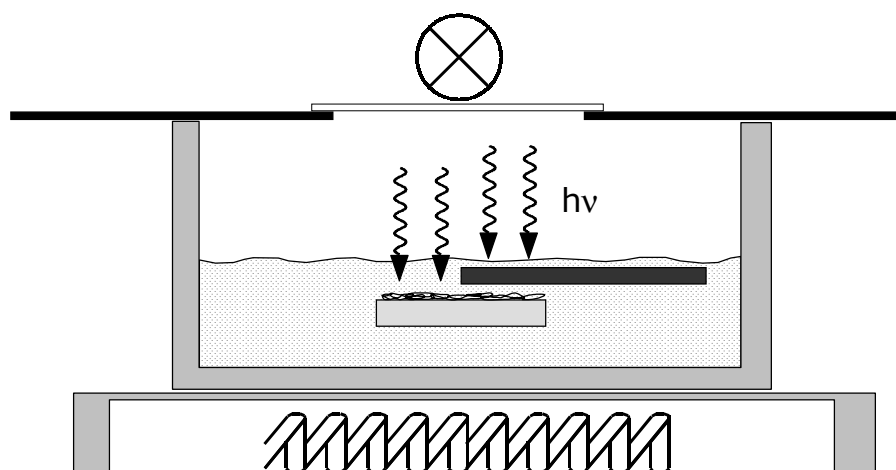


Figure 43. Setup for photocrosslinking of cinnamoylated P-HPMA. The sample is immersed in water at 65°C and is irradiated with $\lambda = 254\text{nm}$. Half of the sample was shaded for reference measurement purposes.

6.4.2 Results and Discussion

According to Laschewsky and Rekaï (Laschewsky 2000), two different reactions can take place when irradiating cinnamoylated P-HPMA. Depending on the molar fraction of cinnamoyl functionalities either *E-Z* (or *trans-cis*) photoisomerisation or [2 + 2] photocycloaddition can occur. The authors have investigated aqueous solutions of cinnamoylated P-HPMA containing 9mol% and 21mol% cinnamoyl groups for modification of the LCST by UV irradiation. In short, the polymer modified with 9mol% cinnamoyl groups gives a rather clean *E-Z*-photoisomerisation. The transformation from *E*- to *Z*-state shifts the thermo-responsive phase transition to higher temperatures, since the *Z*-configuration is more polar. The 21mol% polymer undergoes intramolecular photocrosslinking and precipitates from solution.

The chemisorption of cinnamoylated P-HPMA gave a mean resonance angle of $\Theta_{\text{SPR}} = 66.28^\circ \pm 0.05^\circ$ meaning $d_{\text{HG}} = 1.6\text{nm} \pm 0.6\text{nm}$ according to equation 39. Although the layers are fairly thin, they were investigated for changes possibly detectable.

The results for sample 1 are shown in figure 44. The resonance angles measured for step 3 and 5 of the experimental course (see table 9) are plotted as relative changes towards the values determined in step 2. Measurements carried out on the same sample half are plotted in the same colour.

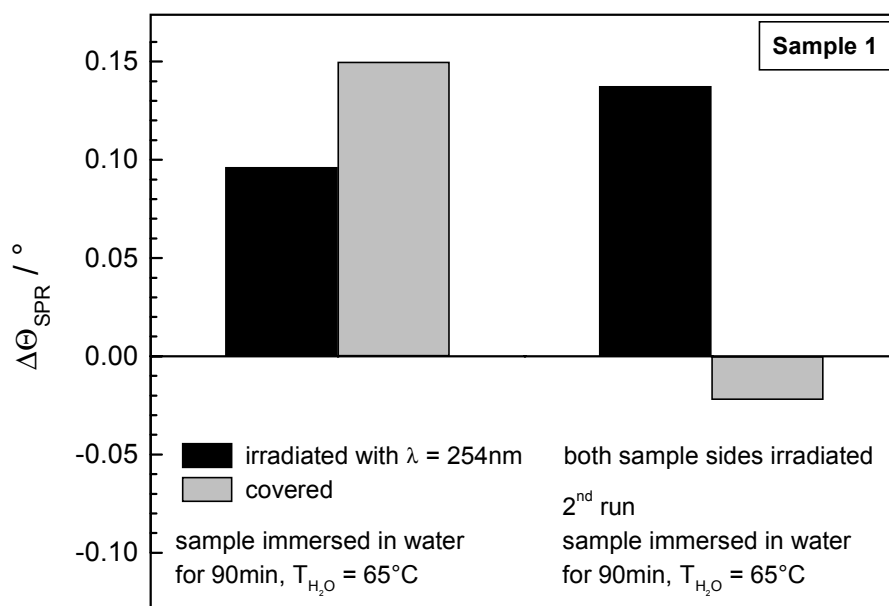


Figure 44. Sample 1: the relative change in resonance angle for experimental steps 3 and 5 (see table 9) of either sample half (each plotted in the same colour). The values are always relative to the values found in step 2.

If the hydrogel is actually crosslinked in collapsed state, the resonance angle should increase. Here, however, the shaded sample half shows an even larger shift than the irradiated half. After repeating the irradiation, the results appear even more confusing. The resonance angle of the sample half irradiated twice increases as expected. However, the resonance angle of the other half is now even smaller than at the beginning. For this occurrence hardly exists any explanation.

Furthermore, the magnitudes of the changes are unrealistically large for such thin films.

The second sample was used to verify the unusual results obtained with the first sample; the outcome is plotted in figure 45.

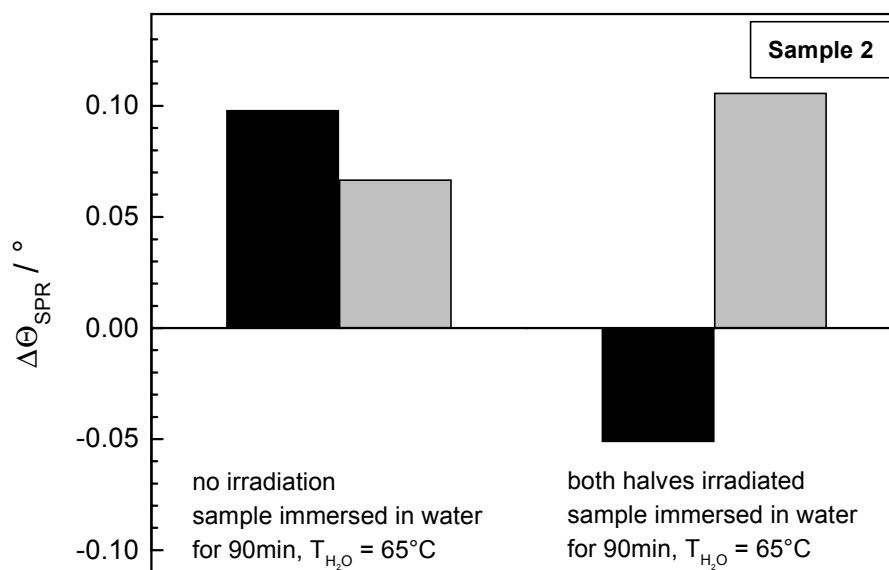


Figure 45. Sample 2: the relative change in resonance angle for experimental steps 3 and 5 (see table 9) of either sample half (each plotted in the same colour). The values are always relative to the values found in step 2.

Obviously, the immersion of the sample in 65°C water without any irradiation is sufficient to induce substantial changes in resonance angle. Then, irradiating the sample leads on one sample half to a drastic decrease in resonance angle, on the other half to a further increase.

The findings for sample 1 and 2 fail to distinguish. Besides the irregular behaviour concerning the direction of the changes (positive / negative) the magnitude of the resonance angle shifts is noteworthy. They are too large to be caused by systematic errors (e.g., variation due to removing and installing the samples is smaller than 0.02°) or to be caused by changes of the hydrogel film dimensions. On the first glance, another explanation could be a change in refractive index of the film. Considering the investigation of Laschewsky and Rekaï (Laschewsky 2000), the irradiation can induce two different photochemical processes in cinnamoylated P-HPMA which certainly also will modify the refractive index of the film. However, at the present degree of cinnamoylation of 13mol% it is hard to tell what will be the dominant process: either *E-Z* photoisomerisation or $[2 + 2]$ photocycloaddition or, may be, a combination out of these two processes. But, anyway, the speculation of varying refractive indices causing the changes in resonance angle does not stand a deeper examination: simulations show that even an unreasonable high refractive index of 1.58 does not generate angle shifts that large like measured.

Furthermore, a change in wettability after each experimental step was not observable by visual inspection. This was supposed to be established by irradiating the samples with UV light.

In general, it is not clear at all if 13mol% cinnamoyl groups are sufficient for permanently fixing the collapsed state of the hydrogel. As observed by Laschewsky and Rekaï (Laschewsky 2000) aqueous solutions of P-HPMA having 21mol% cinnamoyl

groups undergo intramolecular photocrosslinking, but not aqueous solutions of P-HPMA having 9mol% cinnamoyl groups. However, the polymer concentration will also have an important impact on the crosslinking efficiency. As shown in section 6.3.4 the concentration on the surface can be 30 times higher than the concentration in solution. The high grafting density reduces the average distance between neighbouring polymer chains and makes intermolecular photocrosslinking much more likely. From that point of view 13mol% of cinnamoyl groups could be sufficient. On the other hand, despite successful crosslinking the polymer network may be still swellable. The density of crosslinks could be probably too low to fix the hydrogel in collapsed state. Unfortunately, in view of the results presented here, conclusions about the efficiency of photocrosslinking 13mol% cinnamoylated P-HPMA in surface-attached state can not be drawn.

6.4.3 Conclusion

The tremendous shifts observed with sample 1 as well as with sample 2 are not explainable by structural or conformational changes in the cinnamoylated P-HPMA hydrogel film. Evidence for crosslinking the hydrogel and turning the surface from hydrophilic to hydrophobic state could not be supplied.

The reason for the large resonance angle shifts could not be identified. The reproduction of the unusual large variations observed on sample 1 with the second sample is remarkable. However, instrumental errors seem not to be responsible.

6.5 Study of Non-Specific Adsorption

A crucial issue for the application of biosensors is the suppression of non-specific adsorption. Neither SPR and nor any other biosensing technique available today is capable of distinguishing between biomolecules attached to a sensor surface due to specific or non-specific interaction. Consequently, a major task of a biosensor surface is the efficient suppression of non-specific adsorption, especially if proteins are the object of interest.

6.5.1 Non-Specific Adsorption - A Complex Problem

Although a great number of proteins readily dissolve in water, they usually also have a strong tendency to adsorb at interfaces. Knowledge of interaction forces between surfaces and proteins would greatly enhance the prediction of adsorption phenomena. Unfortunately, these interaction forces are still far from being fully understood (Marsh 2001). However, non-specific protein adsorption can be discussed in terms of two dominating mechanisms: adsorption by electrostatic interaction, adsorption by hydrophobic interaction or a combination of these two effects (Ostuni 2001). The adsorbed proteins can undergo conformational changes that especially increase hydrophobic interactions between the proteins and the surfaces. It is believed that the

entropy gains achieved by conformational changes of the protein structure upon adsorption are often the driving force (Marsh 2001).

In practice, surface modifications being able to suppress non-specific adsorption are identified by a kind of trial and error. Some examples for investigations concerning non-specific adsorption to various types of surface modifications are given in section 3.3.2: The study of Piehler *et al.* (Piehler 1996) underlined the remarkable performance of dextran. Among various types of different coatings (poly(ethyleneimine), α,ω -amino functionalised poly(ethylene glycol), chitosan, poly(acrylamide-co-acrylic acid and dextran) non-specific adsorption was lowest for dextran. The study of Gombotz *et al.* (Gombotz 1991) demonstrated the dependence of the efficiency of a coating on the average molar mass of the employed polymer. For PEG on plastics, higher molar masses gave rise to more effective suppression of non-specific adsorption. Likewise, Frazier *et al.* (Frazier 2000) investigated -among other parameters- the influence of the average molar mass of dextrans on the non-specific adsorption. The polymers were directly bound to noble metal surfaces via thiol groups on the glucose repeat units. The molar masses were 5,000, 70,000 and 500,000g/mol. When incubating with a 0.5mg/ml bovine serum albumine solution, the differences observed in non-specific adsorption were relatively small for these systems. Absolute values were in the range of some 0.1ng/mm². However, in contradiction to the work of Gombotz *et al.* (Gombotz 1991), the polymer with smallest molar mass gave rise to lowest non-specific binding. This emphasises that there is obviously no simple rule, making it hard to predict the performance of a certain coating in terms of suppression of non-specific adsorption. For instance, a more recent paper of Piehler *et al.* (Piehler 2000) strongly suggests that the chemical composition of the linker layer and especially the exact experimental conditions of the assembly also have a dramatic influence on the performance. The most comprehensive investigations addressing the influence of the chemical composition of the interface on the non-specific adsorption were performed by the group of Whitesides. Layers systems on noble metals modified with both low molar mass or oligomeric compounds (Chapman 2000; Ostuni 2001) and with polymers (Chapman 2001) were studied. In the last-mentioned study, the authors come up with several conclusions for the chemical structure of surfaces resisting non-specific adsorption: according to them, the surface has to be (1) hydrophilic, (2) overall electrically neutral, (3) a hydrogen bond acceptor, but (4) not a hydrogen bond donor. While statements (1), (2) and (3) are fully consistent with all investigations in the field, (4) is in contradiction to many other results and not even fully justified by the experimental findings of the authors' own studies. Many of the surfaces showing very low non-specific adsorption contain hydrogen bond donors (all dextrans and also many of PEGs). Moreover, even the compound exhibiting the least non-specific binding in the monolayer study of Chapman (Chapman 2000), an oligo(ethylene glycol), has a terminal hydroxy group and therefore does not fit well into the explanation scheme of the authors (Wischerhoff, in press).

After all, despite the complexity and the partly even contradicting results some rules concerning the properties of a protein resistant surface can be deduced:

- surfaces must be rendered hydrophilic and non-charged
- coatings comprising oligomers or polymers seem to be most efficient

- an effective barrier between the original surface and the biocompatible layer seems to be helpful

Here, the thermo-responsive hydrogels will be characterised for their ability to suppress non-specific adsorption. As discussed earlier, this feature is of great importance for biosensing applications. However, the characterisation is also of interest for the verification of the rules as mentioned above. This is due to the thermo-responsive hydrogels only partially fulfilling the above points. First, the polymers are directly chemisorbed to the gold surface via their terminal disulfide group(s). This means a barrier formed by densely packed SAMs and/or polymer(s) is missing between the hydrogels and the gold surface. Second, the thermo-responsiveness is achieved by modifying the hydrophilic precursor polymers with a certain fraction of hydrophobic groups. Since hydrophobic forces play a major role in non-specific adsorption, it needs to be investigated, if and to what extent the hydrophobic groups influence the ability of the polymers to suppress non-specific adsorption.

The performance of the thermo-responsive hydrogels will be compared with a bare gold surface, a hydrophobic SAM, a SAM with covalently linked dextran and P-THMA. As a test substance, the protein bovine serum albumin, which is known for its strong tendency to adsorb to all kinds of interfaces, was employed.

6.5.2 Bovine Serum Albumin

Bovine Serum Albumin (BSA) is the “standard” protein for the investigation of non-specific adsorption. BSA sticks to almost all surfaces. Thus the exposure of a surface to BSA is a rather hard test and a surface resisting BSA adsorption can be supposed to be resistant against adsorption of the vast majority of biomolecules. Furthermore, BSA is one of the cheapest proteins.

BSA is produced from raw bovine serum or plasma collected from cattle. It is the most abundant protein in plasma with a typical concentration of 35-45g/l (Lodish 1996). BSA is the principal carrier of fatty acids that are otherwise insoluble in circulating plasma and it is the key carrier or reservoir of nitric oxide, which has been implicated in a number of important physiological processes, including neurotransmission (Stamler 1992). Furthermore, it performs other functions such as sequestering oxygen free radicals and inactivating various toxic lipophilic metabolites. BSA is one of the most widely studied and employed proteins (Putnam 1975). Typical applications comprise its use as blocking agent to reduce non-specific binding in enzyme-linked immunosorbent assay (ELISA) systems, as stabiliser for other proteins and enzymes and as protein base for controls and calibrators.

Based largely on hydrodynamic experiments and low-angle X-ray scattering serum albumin is presumed to be an oblate ellipsoid with dimensions of about $(14 \times 4 \times 4)\text{nm}^3$. The molecular weight of BSA is 66kDa, the density is 1.36g/cm^3 (Lodish 1996). The isoelectric point of BSA is 4.9 (Putnam 1975).

6.5.3 Surface Modification and BSA Exposure

The different layer systems which were exposed to BSA solutions to test for non-specific adsorption are listed in table 10.

Designation	Layer system	Number of samples
Gold	bare gold, similar to substrates of following samples	1
HDM	Hexadecylmercaptan (HS-(CH ₂) ₁₅ -CH ₃) SAM	1
SAM + AMD	Undecanoic acid (HS-(CH ₂) ₁₀ -COOH) SAM+ covalently bound Aminodextran	1
P-THMA	see table 5 page 55	3
acetylated P-THMA		3
cinnamoylated P-HPMA		2
P-NIPAM-co-THMA		2

Table 10. Samples used for the study of non-specific BSA adsorption.

6.5.3.1 Chemicals

The chemicals 0,965mol/l hydrochloric acid (HCl) (Aldrich, Steinheim, Germany), 1-ethyl-3-(3-diethylaminopropyl) carbodiimide (EDC) (Sigma, St. Louis, MO, USA), 30wt% hydrogen peroxide (H₂O₂) (Fluka, Buchs, Switzerland), 4-(2-Hydroxyethyl)piperazine-1-ethanesulfonic acid (HEPES) (Fluka), 40wt% poly(acrylic acid, sodium salt) MW~30,000 (PAA) (Aldrich), 95wt% sulphuric acid (H₂SO₄) (Prolabo, Fontenay, France), ammonium chloride (Fluka), bovine serum albumin (BSA) (Sigma), cysteamine hydrochloride (Riedel-de Haën, Seelze, Germany), dextran T500 (Pharmacia, Uppsala, Sweden), (Merck), ethylenediaminetetraacetic acid (EDTA) (Fluka), hexadecylmercaptan (Aldrich, Steinheim, Germany), iso-propanol (Merck, Darmstadt, Germany), N-hydroxysulfosuccinimide sodium salt (Fluka), potassium hydroxide (KOH) (Merck), sodium (meta)periodate (Fluka), sodium chloride (NaCl) (Fluka), sodium cyanoborohydride (Fluka), sodium hydroxide (NaOH) (Sigma), were all used as received. Millipore-filtered water (18 MΩ) was used for the preparation of all aqueous solutions and rinsing.

6.5.3.2 Synthesis of Aminodextran

Aminodextran (AMD) (see figure 19) with an average molar mass of 500kg/mol was synthesised according to Piehler *et al.* (Piehler 1996). Briefly, dextran was oxidised by sodium periodate and after dialysing, ammonium chloride was added and reductive amination was carried out by adding sodium cyanoborohydride. Finally the aminodextran was purified by dialysis.

6.5.3.3 Preparation of Samples

For all samples described here gold coated glass slides were the substrates. The preparation of gold coated glass slides is described in detail in section 6.3.2.1.

6.5.3.3.1 Gold Surface

The gold surface was cleaned with a 1:1 by volume solution of 0.1M KOH/30wt% H₂O₂ at 70°C for 20min. During mounting the gold sample into the SPR setup the hydrophilic gold surface was covered by a water film to avoid adsorption and/or chemisorption of impurities from air.

6.5.3.3.2 Hexadecylmercaptan SAM

The gold surface was cleaned with a 1:1 by volume solution of 0.1M KOH/30wt% H₂O₂ at 70°C for 20min. The hydrophilic gold surface was rinsed with iso-propanol and incubated in a solution of 0.02mol/l hexadecylmercaptan in iso-propanol for 24h. After the incubation the sample was thoroughly rinsed with iso-propanol and after that with water. The surface was markedly hydrophobic, indicating the successful chemisorption of hexadecylmercaptan (HDM). The sample was mounted onto the SPR setup in dry state.

6.5.3.3.3 Undecanoic Acid SAM + Aminodextran

The gold surface was cleaned with a 1:1 by volume solution of 0.1M KOH/30wt% H₂O₂ at 70°C for 20min. The hydrophilic gold surface was rinsed with iso-propanol and incubated in a solution of 0.02mol/l undecanoic acid in iso-propanol for 24h. After the incubation the sample was thoroughly rinsed with iso-propanol and after that with water. Then the sample was mounted onto the SPR setup in dry state. After installation the surface was incubated with a solution of 0.1mol/l EDC / 0.1mol/l sulfo-NHS in water for 20min, resulting in a SAM presenting activated NHS esters. After rinsing with water the activated ester groups were used for the following coupling of AMD supplied in a 10wt% aqueous solution via amid bonds. After these preparation steps, the layer system was thoroughly rinsed with water.

6.5.3.3.4 P-THMA and Thermo-Responsive Hydrogels

The preparation of gold coated glass slides equipped with P-THMA and the thermo-responsive hydrogels is described in section 6.3.2.1 in detail. The samples were mounted onto the SPR setup in dry state and then thoroughly rinsed with water.

6.5.3.4 Preparation of HEPES-Buffered Saline

HEPES-buffered saline (HBS) was made by dissolving 0.01mol/l HEPES, 0.15mol/l NaCl and 0.0034mol/l EDTA in water. The pH was adjusted to pH 7.4 by adding 2mol/l NaOH.

6.5.3.5 Experimental Procedure

Two different BSA solutions were employed to test the layer systems listed in table 10 for their ability to suppress non-specific adsorption. First, a BSA solution was supplied with rather moderate concentration of $c = 150\mu\text{g/ml}$ in HBS. The second solution was BSA of $c = 2\text{mg/ml}$ in H_2O .

The application of BSA $c = 2\text{mg/ml}$ in H_2O is much more demanding than the application of BSA $c = 150\mu\text{g/ml}$ in HBS. Apart from the more than 13-fold higher BSA concentration, water as solvent will not shield electrostatic forces, unlike buffers containing relatively high salt concentrations.

After mounting the samples onto the SPR and rinsing them thoroughly with water they were incubated with HBS. The angle measurement mode of the SPR setup was started which records a fixed number of SPR curves with fixed time increment between each curve. After recording 10 curves (thus defining a base line $\Theta_{\text{SPR } 0}$) the BSA solution $c = 150\mu\text{g/ml}$ in HBS was supplied. The samples were exposed to the BSA solution for 30min; the BSA incubation was stopped by rinsing with HBS. During the whole process SPR curves were continuously recorded. The amount of non-specifically adsorbed BSA was determined by the shift $\Delta\Theta_{\text{SPR}}$ of the base line measured before and after BSA incubation. Then HBS was replaced by water and the procedure was repeated with BSA $c = 2\text{mg/ml}$ in H_2O .

6.5.4 Results and Discussion

6.5.4.1 150 $\mu\text{g/ml}$ BSA in HBS

In figure 46 the results for BSA $c = 150\mu\text{g/ml}$ in HBS are plotted. The mass loading Γ is calculated from $\Delta\Theta_{\text{SPR}}$ according to equation 21.

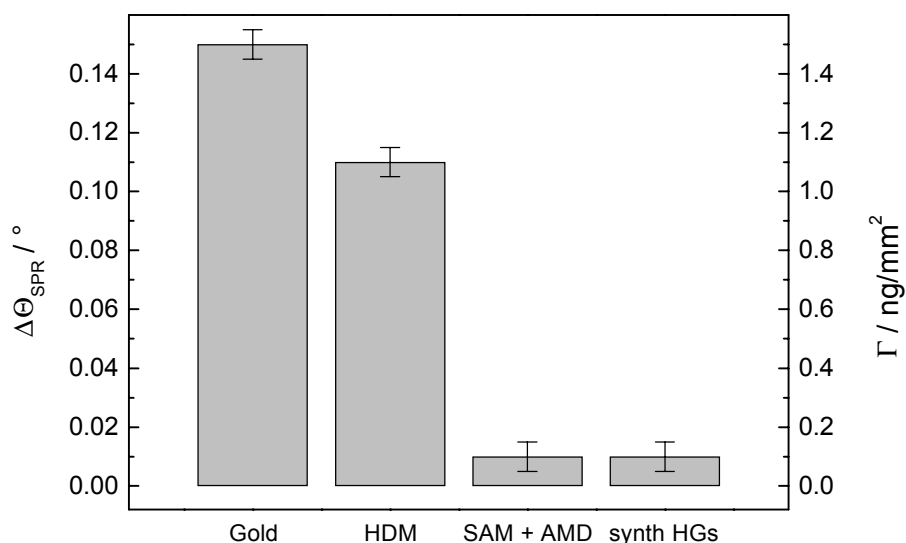


Figure 46. Non-specific adsorption of BSA $c = 150\mu\text{g/ml}$ in HBS onto a bare gold surface, a hexadecylmercaptan SAM, an undecanoic acid SAM equipped with aminodextran and the synthetic hydrogels (P-THMA and the thermo-responsive polymers). For the synthetic hydrogels the mean non-specific adsorption of all hydrogels is plotted. The error bars indicate the systematic error of angle measurements.

Onto a clean gold surface 1.50ng/mm^2 BSA adsorbs. Presuming a BSA monolayer as a layer consisting of densely packed cylinders of dimension $(14 \times 4 \times 4)\text{nm}^3$ and density 1.36g/cm^3 (Lodish 1996) results in a mass loading of about 4.18ng/mm^2 . Hence, BSA adsorbing on a pure gold surface forms less than a monolayer of intact molecules. This may indicate that the interaction forces between the surface and BSA lead to a denaturation of BSA and compel it into a thinner conformation. Most likely, cysteines on the surface of BSA will bind with their SH groups to gold by complexation, forming a stable bond between the protein and the gold surface. This may be also confirmed by the fact, that no material was removed from the surface, while rinsing with 0.05mol/l HCl.

Coating the gold surface with a hydrophobic SAM of hexadecylmercaptan (HDM) decreases the non-specific adsorption of BSA to 1.10ng/mm^2 ; a reduction of 27%. Here, hydrophobic forces between the surface and BSA will be the driving force for the adsorption.

A layer system made of an undecanoic acid SAM, to which a layer consisting of 500kg/mol aminodextran was coupled, reduces the non-specific adsorption of BSA more than 90% (compared to the hexadecylmercaptan SAM) to 0.10ng/mm^2 . Although biomolecules can penetrate into dextran hydrogels, the polymeric properties ensure a drastic reduction of the non-specific adsorption.

Apparently, at BSA concentration of $150\mu\text{g/ml}$ in HBS the polymeric character is the crucial feature. The mean non-specific adsorption of all synthetic hydrogels (P-THMA and the thermo-responsive polymers) also amounts to 0.10ng/mm^2 , independently from the fraction of hydrophobic groups χ in the polymers (the standard deviation of the measurements is smaller than the repeat accuracy given for the SPR setup in angle measurement mode). Furthermore, the presence of a SAM as a blocking barrier between

the gold surface and the hydrogel seems not to be decisive at this BSA concentration. As outlined earlier the synthetic hydrogels are directly bound to the gold surface, in contrast to the aminodextran layer bound to a SAM. This finding is consistent with the work of Frazier *et al.* (Frazier 2000). The authors investigated thiolated dextran directly coupled to gold and they also observed non-specific adsorption of BSA in the range of $0.1\text{ng}/\text{mm}^2$.

6.5.4.2 2mg/ml BSA in H₂O

Differences in the ability to suppress non-specific adsorption became perceptible when exposing the hydrogels to harsher conditions. In this context, the resistance of the hydrogels against BSA $c = 2\text{mg}/\text{ml}$ in H₂O was tested.

In figure 47 the non-specific adsorption onto P-THMA and undecanoic acid SAM plus aminodextran is plotted.

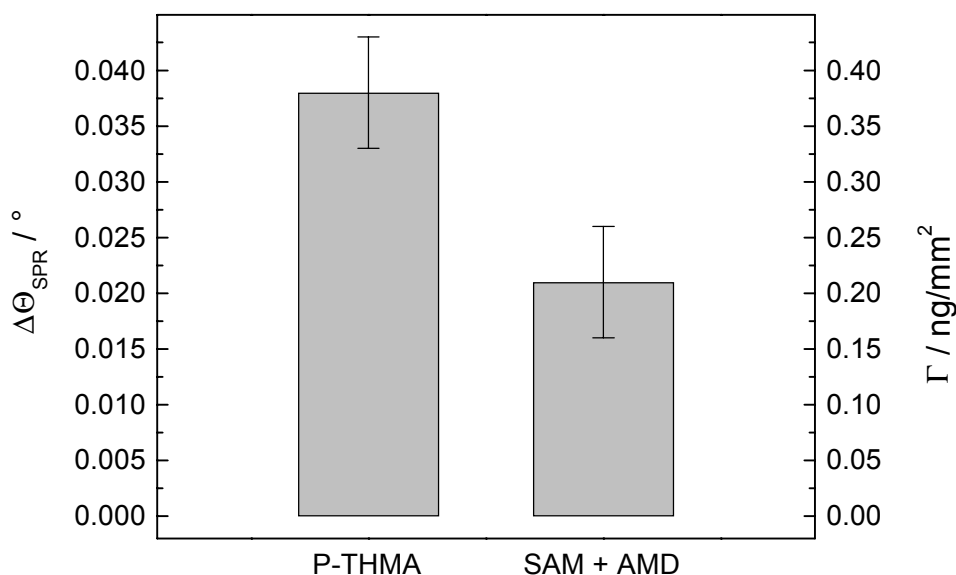


Figure 47. Non-specific adsorption of BSA $c = 2\text{mg}/\text{ml}$ in H₂O onto P-THMA and an undecanoic acid SAM equipped with aminodextran. The error bars indicate the systematic error of angle measurements.

The harsher conditions proof the dextran layer system being more efficient in suppression of non-specific adsorption than unmodified P-THMA. Onto P-THMA, $0.38\text{ng}/\text{mm}^2$ of BSA adsorbed; onto SAM + AMD $0.21\text{ng}/\text{mm}^2$, 45% less.

Both hydrogels are hydrophilic and have no net charge. Therefore, the most influential property making the difference in the amount of non-specific adsorption is hard to identify. As discussed in the concise literature review in section 6.5.1, it is rather the sum and interplay of all properties which can make up the difference. For instance, the average molar mass of the employed polymer plays a role: in general, non-specific adsorption does decrease with the molar mass (Frazier 2000). The average molar mass of the P-THMA polymer is $200\text{kg}/\text{mol}$; of the aminodextran $500\text{kg}/\text{mol}$. Therefore, this can be one of the important differences. Furthermore, the amount of hydrogen bond

donor groups is larger in P-THMA (P-THMA has three OH groups per repeat unit, aminodextran has 1–3 OH groups per repeat unit, depending on the degree of functionalisation); according to Chapman *et al.* (Chapman 2000) an important factor determining the protein resistance of a coating. And finally, there is a SAM barrier layer between the dextran layer hydrogel and the substrate, while the P-THMA layer is attached directly to the substrate.

In figure 48 the non-specific adsorption on P-THMA and on the thermo-responsive hydrogels is compared. The data are plotted as function of the fraction χ of hydrophobic groups in the respective polymer.

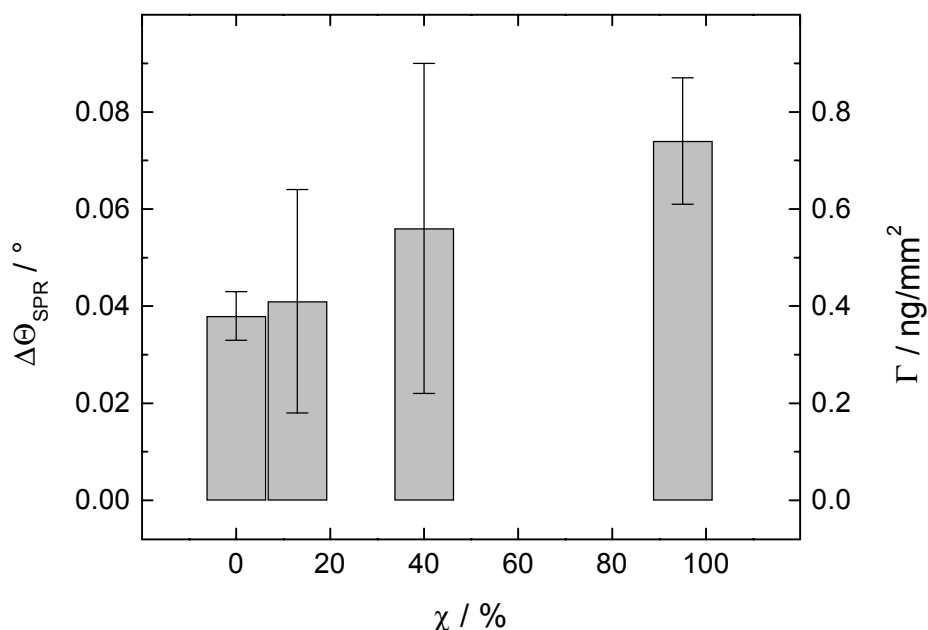


Figure 48. Non-specific adsorption of BSA $c = 2\text{mg/ml}$ in H_2O onto the synthetic hydrogels in dependence on the fraction χ of hydrophobic groups: $\chi = 0\%$: P-THMA, $\chi = 13\%$: cinnamoylated P-HPMA, $\chi = 40\%$: acetylated P-THMA, $\chi = 95\%$: P-NIPAM-co-THMA. The error bars shown for the thermo-responsive hydrogels reflect the standard deviations of the measurements (for the number of investigated samples see table 10).

The amount of non-specific adsorption shows a steady increase with the portion of hydrophobic groups in the hydrogel. Obviously, the dominant interaction mechanism causing non-specific adsorption on the thermo-responsive hydrogels originates from hydrophobic forces. The size of the hydrophobic group does not seem to have very much influence. Otherwise, the polymer with distinctly larger hydrophobic groups -cinnamoylated P-HPMA with 13% hydrophobic cinnamoyl groups- should deviate from the almost ideal linear increase in figure 48.

Chapman *et al.* (Chapman 2000) claim in their work that "elimination of hydrogen bond donor groups appears to be a key structural element in protein-resistant surfaces". Furthermore, the authors state that hydrogen accepting groups are favourable for suppression of non-specific adsorption. While synthesising acetylated P-THMA, 40% of the hydroxy groups are replaced by acetyl groups, exactly meaning the replacement of

40% hydrogen donor groups with hydrogen acceptor groups. In spite of that, the amount of non-specific adsorption to acetylated P-THMA is clearly following the overall trend of the data. This indicates that hydrophobic forces are dominantly driving the non-specific adsorption, otherwise a deviation from the overall trend should be observable. Hydrophobic forces clearly compensate a potentially beneficial effect of the replacement of hydrogen bond donors by hydrogen bond acceptors.

Remarkable are the enormous standard deviations. They could be caused by slight variations during sample preparation. For instance, the polymer concentration is difficult to maintain exactly constant, if several hydrophilic samples covered with a water film are immersed into the solution. Piehler *et al.* (Piehler 2000) pointed out that the exact experimental conditions have a dramatic influence on the performance of a protein resistant layer. However, when looking closely at the data, one more reason for the big standard deviations could be conceivable. There is a tendency in the standard deviations: they are larger for polymers with mixed composition (content of hydrophilic groups / hydrophobic groups), as for polymers with homogeneous (or nearly homogeneous) composition. Probably the process of non-specific adsorption, known to be a very undefined phenomenon anyway, is even more undefined or unpredictable on surface with mixed composition. However, it needs to be mentioned that due to the limited amount of available polymer only few samples were measured (see table 10), making respectable statistics impossible. But still, the tendency in the standard deviations is at least noteworthy and the presented basic idea for its explanation can stimulate future investigations.

6.5.5 Conclusion

Introducing thermo-responsiveness into hydrophilic polymers by modification with hydrophobic groups decreases their ability to suppress non-specific adsorption. Hydrophobic interaction seems to be the dominating driving force. According to the findings presented here, the size and the chemical structure of the hydrophobic group seem to have minor influences on the non-specific adsorption. The amount of adsorbed BSA is mainly determined by the molar fraction of hydrophobic groups. For future design of thermo-responsive biosensing hydrogels, this means employing less but larger hydrophobic groups is more advisable than employing many small hydrophobic groups. Nevertheless, there is always a trade-off between the introduction of thermo-responsive properties and accepting a reduction of the hydrogel's capability to suppress non-specific adsorption.

The performance of the precursor polymer P-THMA is quite remarkable. For instance, its efficiency is better than all the materials (except dextran) investigated by Piehler *et al.* (Piehler 1996). Additionally, it may have the potential for even better performance, when taking into consideration that the molar mass of the used P-THMA was 2.5-fold lower than the one of the used aminodextran (synthesised according to Piehler *et al.* (Piehler 1996)) and bearing in mind that the P-THMA was directly bound to the gold surface without any intermediate layer.

6.6 Bio-Functionalisation of Acetylated P-THMA

The biospecificity of a biosensor surface is accomplished by immobilisation of a receptor biomolecule to the surface. Here, the covalent attachment of *staphylococcus aureus* protein A (protein A) to acetylated P-THMA was investigated. Biospecific interaction is tested with rabbit anti-mouse immunoglobulin G (IgG) which binds specifically to protein A with its F_c part. This interacting pair is well established and often used as model system for biospecific interactions (Andersson 1999). The association equilibrium constant K_A was determined in experiments employing a dextran hydrogel to be in the range of $10^8 M^{-1}$.

6.6.1 Immunoglobulin G

Immunoglobulins are antibody proteins circulating in blood plasma of mammals. Five different classes of immunoglobulins exist. The most important and most abundant immunoglobulin is the immunoglobulin G (IgG); about 80% of all immunoglobulins are IgGs. Figure 49 shows a schematic drawing of an IgG antibody molecule. As indicated, the protein is Y-shaped and has two identical binding sites for its antigen, one on either arm of the Y. The protein is composed of four polypeptide chains (two identical heavy chains and two identical and smaller light chains) held together by disulfide bonds. The antigen-binding site is formed where a heavy chain variable domain (V_H domain) and a light chain variable domain (V_L domain) come close together. These are the domains that differ most in their sequence and structure in different antibodies. F_{ab} denotes the antigen-binding fragment; F_c the constant (or crystallisable) fragment. IgG specifically binds to protein A with the F_c part. The molar weight of IgG amounts to about 150kDa (Lodish 1996).

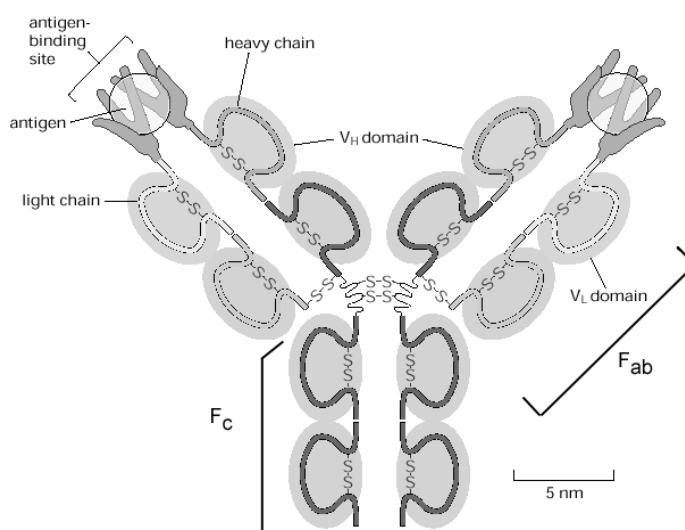


Figure 49. Schematic drawing of an immunoglobulin G (IgG) antibody molecule (Alberts 1998).

6.6.2 Protein A

Protein A is a monomeric protein lacking cysteine residues. Protein A is a highly stable (stability range: pH 1.0-12.0) surface receptor produced by *Staphylococcus aureus*, which is capable of binding the F_c part of immunoglobulins specifically, especially IgGs, from a large number of mammals. The binding does not interfere with the antigen binding site of the IgG. Each protein A molecule can bind 2 molecules of IgG. Often, protein A is immobilised onto a solid support to facilitate the purification and recovery of either polyclonal or monoclonal immunoglobulins (affinity purification). The molecular weight of protein A is 42kDa and the isoelectric point is 4.85-5.10 (Langone 1982).

6.6.3 Chemicals

The chemicals 0.965mol/l hydrochloric acid (HCl) (Aldrich, Steinheim, Germany), 4-(2-Hydroxyethyl)piperazine-1-ethanesulfonic acid (HEPES) (Fluka, Buchs, Switzerland), ethanolamine hydrochloride (Sigma, St. Louis, MO, USA), ethylenediaminetetraacetic acid (EDTA) (Fluka), *N,N*-diisopropylethylamine (Fluka), *N,N*-dimethylformamide (DMF) (Fluka), *N,N'*-disuccinimidyl carbonate (DSC) (Fluka), potassium chloride (KCl) (Merck, Darmstadt, Germany), protein A from *Staphylococcus aureus* (Protein A) (Sigma), rabbit anti-mouse immunoglobulin G (IgG) (Jackson ImmunoResearch, West Grove, PA, USA), sodium acetate (NaAc) (Sigma), sodium chloride (NaCl) (Fluka) were all used as received. Millipore-filtered water (18 M Ω) was used for the preparation of all aqueous solutions.

6.6.3.1 Preparation of Buffers

NaAc-buffer was prepared by dissolving 0.01mol/l sodium acetate in water and subsequent adjustment to pH 4.7 by adding 0.965mol/l HCl.

HEPES-buffered saline (HBS) was prepared as described in section 6.5.3.4.

6.6.4 Immobilisation of Protein A

Acetylated P-THMA bears 60% of the hydroxy groups of unmodified P-THMA. Consequently, acetylated P-THMA still displays enough reactive groups for activation and following covalent attachment of biomolecules.

The immobilisation was accomplished utilising disuccinimidyl carbonate (DSC) using a protocol analogous to the one described by MacBeath and Schreiber (MacBeath 2000) to activate lysine residues of a BSA layer attached to a glass surface. MacBeath and Schreiber immobilised proteins to the activated BSA layer. Here, the protocol is applied in a slightly varied version comply with the demands of this specific system.

6.6.4.1 Activation Chemistry and Protocol

The preparation of the gold coated glass slide and the grafting of acetylated P-THMA to the gold surface were done in the same way as described in section 6.3.2.1.

The sample was mounted onto the SPR setup and was thoroughly rinsed with water. Then it was incubated with 0.1 mol/l DSC / 0.1 mol/l *N,N*-diisopropylethylamine in DMF for 2.75h, followed by rinsing with NaAc-buffer and incubation of 500 μg/ml protein A in NaAc-buffer for 30min. Residual activated ester groups were deactivated by incubating with 1 mol/l ethanolamine hydrochloride pH 8.5. The assembly was rinsed with NaAc-buffer and finally this buffer was replaced by HBS.

The chemical pathway of the activation of acetylated P-THMA and the subsequent immobilisation of protein A is depicted in figure 50. After hydrogel activation primary amino groups of protein A lysines react with the active esters.

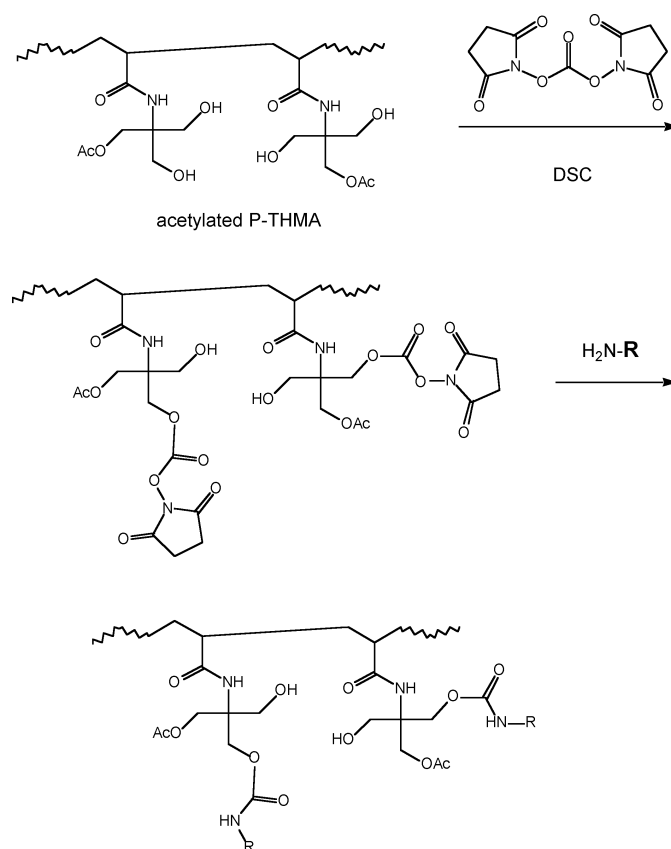


Figure 50. Chemical pathway of the activation of acetylated P-THMA with DSC and the covalent coupling of a protein via a primary amino group.

Figure 51 shows the evolution of the SPR resonance angle (measured in differential intensity mode) during the activation of acetylated P-THMA. About 30min after the incubation with 0.1 mol/l DSC / 0.1 mol/l *N,N*-diisopropylethylamine in DMF the signal starts to increase, indicating the coupling of DSC to the hydrogel. The initial decrease after incubation is difficult to explain. Most likely it is caused by a changing refractive

index of the medium; a decrease of that magnitude is hardly to explain by some other effect. Prior to the injection of the activation solution, water was present in the flow chamber. Although the water should be completely removed while flushing the activation solution through the flow chamber, probably some remains are trapped (e.g., in the slit between o-ring groove and o-ring). A slow mixing of activation solution with remained water by diffusion would lower the refractive index. The refractive index of the activation solution is 1.422. The addition of only 4% of water by volume would reduce the refractive index to 1.417 (calculated according to equation 34), giving rise to a decrease in resonance angle of 1° (at such high refractive indices $\Delta\theta_{\text{SPR}}/\Delta n$ is almost twice the value given in section 6.3.1).

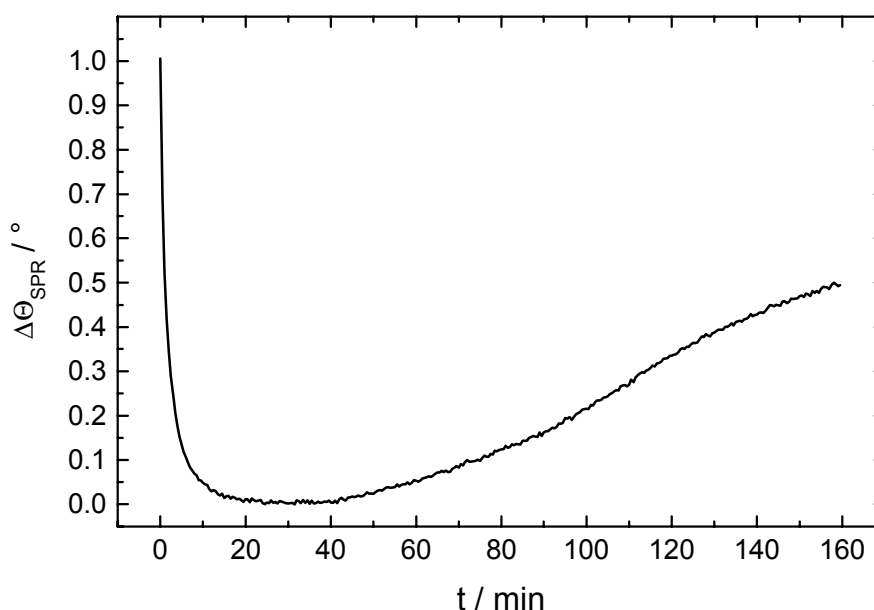


Figure 51. The evolution of the resonance angle during activation of acetylated P-THMA. The initial drop of the signal is probably caused by water remains in the flow chamber. The increase of the signal is indicating the coupling of DSC to the hydrogel. The observed evolution of the resonance angle will be a superposition of these two effects. The signal is arbitrarily set to zero in the minimum.

6.6.4.2 Immobilisation Kinetics

The immobilisation of protein A was also monitored by SPR. The measurement is shown in figure 52.

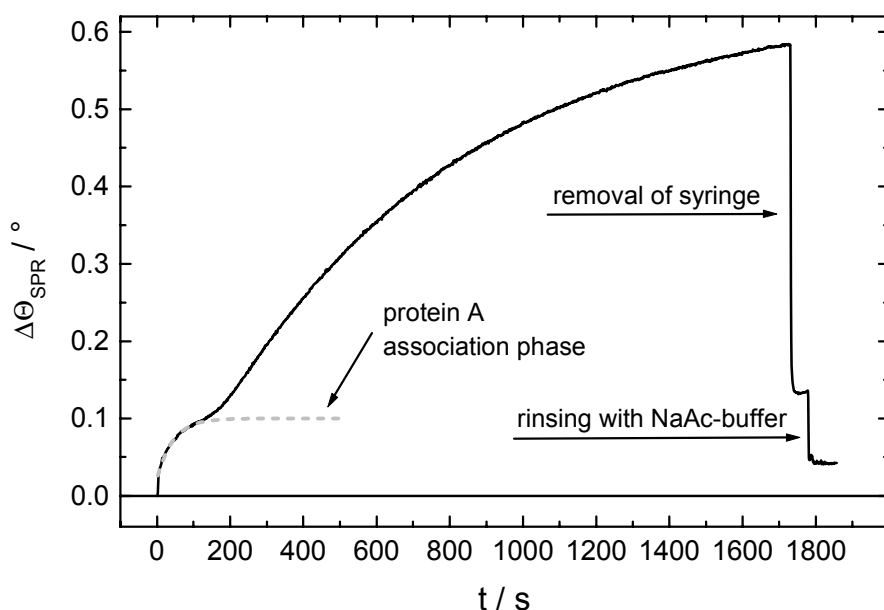


Figure 52. The evolution of the resonance angle during immobilisation of protein A. The loosely adsorption of material superimposes the signal of the immobilisation. When removing the injection syringe the adsorbate vanishes from the surface.

The association part of the curve is divided into two phases. The first phase up to about $t = 200\text{s}$ is believed to represent mainly the binding of protein A to the hydrogel. The second phase, becoming dominant and clearly visible from about $t = 200\text{s}$ seems to represent an undefined adsorption process superimposed to the protein A association. If this explanation is correct, material is adsorbed very loosely. Just by removing the injection syringe the signal drops dramatically, indicating that potentially adsorbed material is removed from the surface. Removing the syringe from the injection tubing system will cause pressure fluctuations inducing a gentle movement of the liquid in the flow chamber. This seems to be sufficient to degrade the adsorbed material on the surface.

SPR angle measurements before and after the immobilisation of protein A reveal a shift in resonance angle of $\Delta\Theta_{\text{SPR Prot A}} = 0.10^\circ$. This value was employed to define an upper bound for the grey dashed curve in figure 52 (an association curve according to equation 23) visualising the protein A association phase. However, this curve will only approximate the binding of protein A. The difference between the measured angle shift of 0.10° and the angle shift deduced from the differential intensity measurement (end level of the black curve after rinsing with NaAc-buffer = 0.04°) is a phenomenon which was repeatedly observed on several samples. A satisfactory explanation can not be given.

According to equation 21 $\Delta\Theta_{\text{SPR Prot A}} = 0.10^\circ$ means $\Gamma_{\text{protein A}} = 1.0\text{ng/mm}^2$, meaning an immobilisation density of 24fmol/mm^2 .

In contrast to the immobilisation to a dextran hydrogel (see section 3.3.1), no electrostatic forces facilitate the immobilisation. The hydroxy groups of acetylated P-THMA are uncharged and hence, there will be no electrostatic attractive force between

the hydrogel and protein A. However, protein A is positively charged at pH 4.7 (pH of NaAc-buffer used for immobilisation) and consequently there will be even an electrostatic repulsive force between protein A molecules already immobilised and approaching protein A. In order to counteract the repulsive forces the concentration of protein A was increased. A concentration of 500 μ g/ml -as applied in this experiment- is apparently appropriate.

6.6.5 Biomolecular Interaction Protein A – IgG

The protein A-functionalised P-THMA was tested for bio-specific interaction with rabbit anti-mouse IgG. Furthermore, the possibility of regeneration of the hydrogel by the thermo-responsive effect was investigated. The steric forces induced by the collapse of the hydrogel may be strong enough to break the specific interaction between protein A and IgG.

6.6.5.1 Experimental Procedure

After immobilisation of protein A the sample was incubated with HBS, defining a base line for the following interaction of IgG $c = 24\mu$ g/ml in HBS (start at $t = 0$ s) monitored in differential intensity mode. Then HBS was injected and the dissociation of the protein A – IgG complex was observed. After a stable state was reached (equilibrium between dissociating IgG and rebinding IgG) 5ml of water at $T = 55^{\circ}\text{C}$ was injected. Subsequently the sample was incubated with HBS and with 0.05mol/l HCl for 5.5min followed by HBS again. Thus, HBS signal levels were established after each single regeneration step allowing comparison with the initial HBS base line. Finally one more kinetic of IgG $c = 24\mu$ g/ml in HBS was measured.

6.6.5.2 Interaction and Regeneration Kinetics

The SPR signal recorded during the experimental course outlined in the previous paragraph is plotted in figure 53.

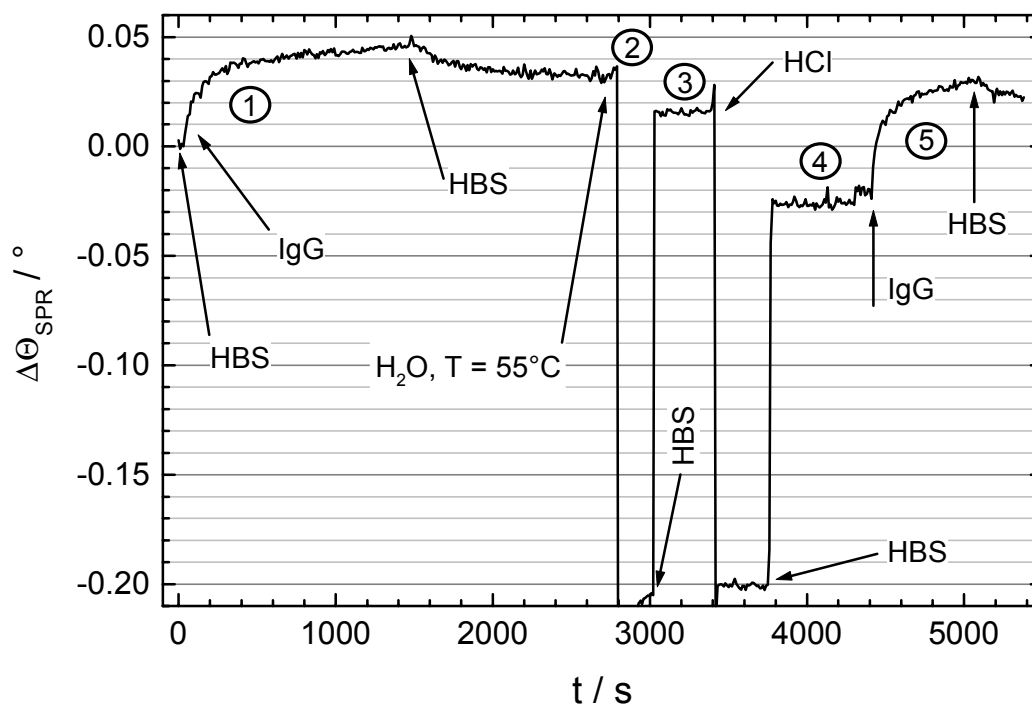


Figure 53. SPR measurements of the binding of IgG to protein A and regeneration experiments with water at $T = 55^{\circ}\text{C}$ and 0.05mol/l HCl . The encircled numbers are addressed in the text.

The kinetic of the first protein A – IgG interaction is marked with 1 in figure 53. A fit to the association part of the curve (according to equation 23) yields an observed rate constant of $k_{\text{obs}} = 0.009\text{s}^{-1}$ and an equilibrium SPR signal of $\Delta\Theta_{\text{SPR eq}} = 0.039^{\circ}$. The slight increase of the signal after $t = 1000\text{s}$ may be rather caused by drift than by actual binding of IgG. After the dissociation has reached equilibrium the injection of water at $T = 55^{\circ}\text{C}$ (2) gives rise to a large decrease of the SPR signal due to the lower refractive index of the heated water. Although the thermo-responsive collapse of surface-attached acetylated P-THMA occurs between $T \approx 26^{\circ}\text{C}$ and $T \approx 28.5^{\circ}\text{C}$ (see section 6.3.3), the water temperature chosen here was 55°C . The temperature should be high enough to induce a thermo-responsive collapse even if the LCST is shifted to higher values due to bound protein A. On the other hand, the water temperature of 55°C should be still low enough to ensure that the proteins do not denature and that the sulphur-gold bonds between the terminal group of the polymer and the gold surface does not break. Actually the HBS level after the injection of the warm water (3) is -0.017° lower than before injection (2). However, applying the well-known regeneration procedure of rinsing with 0.05mol/l HCl reveals that that offset was obviously not due to regeneration of the hydrogel. Full regeneration was only accomplished after application of 0.05mol/l HCl (offset between (3) and (4)) and amounted to -0.042° . However, the HBS base line after HCl regeneration is shifted below zero (4); the base line offset amounts to -0.026° . The reason for this offset is hard to identify, but it is definitely not caused by loss of functionality of the protein A-modified hydrogel. The second IgG incubation (5) proves the hydrogel to be even more efficient after the rinsing procedures. A fit to the association part of the curve yields an observed rate constant of $k_{\text{obs}} = 0.013\text{s}^{-1}$ and an equilibrium SPR signal of $\Delta\Theta_{\text{SPR eq}} = 0.044^{\circ}$. The

binding is faster and more IgG binds; apparently the application of harsh rinsing conditions (water at $T = 55^{\circ}\text{C}$, 0.05mol/l HCl of pH 1.3) has some conditioning effect on the functionalised hydrogel.

6.6.6 Conclusion

The bio-functionalisation of acetylated P-THMA with protein A was established. Some additional adsorption process occurred during immobilisation, but obviously the coupling of protein A to the hydrogel was not severely influenced. Biospecific interaction measurements with IgG were successfully performed.

The regeneration of the hydrogel by the thermo-responsive effect could not be evidenced. Either the specific bond between protein A and IgG could not be broken or the thermo-responsive collapse of the hydrogel did not occur at all. By immobilisation of protein A, a significant number of additional hydrophilic groups is introduced into the hydrogel. Probably, due to the additional hydrophilic groups a considerable shift of the HPL/HPB-balance is induced, obliterating the thermo-responsiveness of the functionalized hydrogel.

7 Binding Processes in Dextran Hydrogels

Today, dextran hydrogels are the most popular coating for SPR biosensor surfaces. However, as the SPR technique becomes more and more widespread and its applications become increasingly sophisticated and advanced (Rich 2000; Nedelkov 2001) there are still open questions concerning basic characteristics of the three dimensional dextran hydrogel matrix related to the distribution of immobilised receptor and bound analyte molecules inside the matrix and its swelling dynamics. These issues are subjects of theory and experimental based studies (for an overview see section 3.3.1), however, there is a lack of direct experimental evidence.

Here, a new experimental approach will be introduced to provide direct experimental evidence about hydrogel dynamics and the spatial distribution of biomolecules in a swollen three-dimensional structure. The new setup takes advantage of the real time measurement capability of SPR and of the different sensing depths of SPR waves being excited with different wavelengths: time-resolved SPR measurements performed simultaneously with two different wavelengths allow to resolve binding events spatially normal to the sensing surface and to gain information about the dynamics in biosensing polymer layers at interfaces.

The versatility of the SPR setup allows to follow all preparation and interaction steps during an experiment. Especially the integration of the immobilisation process into the analysis contributes to a deeper understanding of the processes taking place. Up to now, papers dealing with biomolecule distributions in dextran hydrogels neglect the immobilisation process.

7.1 Concept of the Investigation

The simultaneous real time data acquisition of two SPR signals from SP waves excited with different wavelengths allows direct identification of differences in the SPR responses evolving from different penetration depths during static and dynamic processes.

7.1.1 The Employed Wavelengths

In order to maximise the efficiency of the two-wavelengths concept, the employed wavelengths should fulfil two important conditions:

- 1) The wavelength difference between the employed wavelengths should be maximal.
Since the penetration depth of SP waves depends almost linearly on the excitation wavelength (see equation 10, figure 6) differences in SPR signals originating from the different penetration depths will be the more pronounced the larger the difference in excitation wavelengths is.
- 2) The evanescent field intensity of one SP wave should be concentrated inside the investigated hydrogel; the evanescent field of the other wavelength should also reach noticeable into the region above the hydrogel.

The shorter the exciting wavelength, the more concentrated is the electric field intensity inside the hydrogel (see equation 10). For that reason one wavelength should be as short as possible. Due to physical restrictions the lower limit is given with $\lambda = 570\text{nm}$ (see section 3.1.1). In order to achieve a distinct difference between the two SPR-signals, the electric field intensity of the second wavelength should rather be evenly distributed inside and outside of the hydrogel (or even have its emphasis outside the hydrogel).

Two wavelengths reasonably fulfilling these conditions are $\lambda = 784\text{nm}$ and $\lambda = 600\text{nm}$. Figure 54 shows the normalised electric field intensities of the respective SP waves as a function of the distance z from the gold surface. A dashed vertical line represents the extension of a dextran hydrogel with 120nm thickness. Table 11 shows the values of the normalised integrals of the electric field intensities for $z = 0 - 120\text{nm}$ and $120\text{nm} - \infty$. The integrals are a measure for the distribution of the sensitivity of the SP waves with respect to a 120nm thick hydrogel layer.

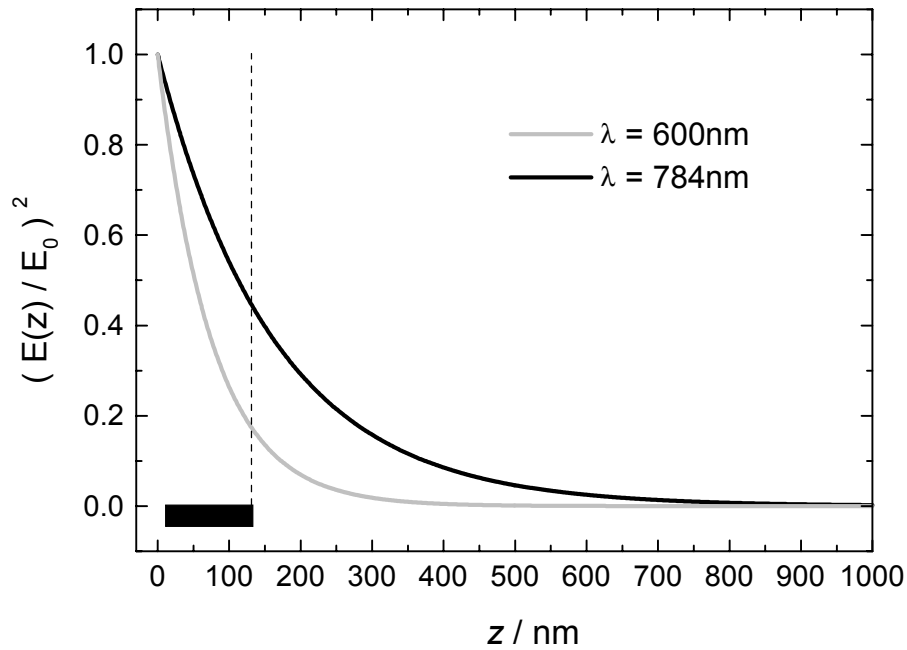


Figure 54. Squared normalised electric fields of surface plasmon waves being excited with light of wavelengths 600nm and 784nm in water, as a function of the distance from the gold surface. The corresponding SPR curves are shown in figure 8. The effective refractive index n_{eff} is probed by the intensity of the electric field, meaning squared electric field. The bar and the dashed vertical line represent the extension of a dextran layer with 120nm thickness.

λ / nm	d_{PD} / nm	$2/d_{PD} \int_0^{120} (E(z)/E_0)^2 dz$	$2/d_{PD} \int_{120}^{\infty} (E(z)/E_0)^2 dz$
600	150	0.80	0.20
784	324	0.52	0.48

Table 11. The penetration depths of the two wavelengths employed in this investigation and the normalised integrals of their electric field intensities for $z = 0 - 120\text{nm}$ and $120\text{nm} - \infty$. The integrals are a measure for the distribution of the sensitivity of the SP waves with respect to a 120nm thick hydrogel layer.

Light of $\lambda = 784\text{nm}$ was emitted by the GaAlAs laser diode of the SPR setup; light with $\lambda = 600\text{nm}$ was extracted from the spectrum of the halogen lamp by means of the monochromator.

In the following, quantities being different for employed wavelengths will be indexed with a respective subscript (e.g. refractive indices n_{784} and n_{600}).

7.1.2 Different Binding Regimes - Different Time-Dependence

When assuming that binding reactions and the corresponding increase of refractive index can take place in different z-coordinate positions inside the hydrogel, a distinction can be made between two extreme cases:

- 1) Binding events occur with the same probability for all binding sites with different z-coordinates. When measured with two different wavelengths, this gives rise to an equal time behaviour for both signals, because each wavelength interacts with the region of increasing refractive index with a fixed fraction of its electric field. Differences may only be observable in the relative amplitude for each wavelength corresponding to the ratio between the extension of the binding region and the integral electric field intensity of the SP wave.
- 2) Binding sites in certain zones of the hydrogel are preferably occupied by approaching molecules and the occurrence of binding events may shift to other regions when unoccupied binding sites in the preferred region become rarer. For instance, approaching molecules react first with their reaction partners in the upper zone of the hydrogel; when these sites are occupied, they also react more frequently in a zone closer to the substrate surface. Since the two surface plasmon waves employed in this experiment are differently sensitive in different zones, different time behaviour must be observable.

If the binding follows a pseudo-first-order kinetics of a Langmuir adsorption isotherm, the time dependence of the SPR signal can be described according to equation 23 (section 3.2.1).

To compare the two signals of SP waves of 784nm and 600nm, normalised SPR signals S_{norm} are suitable:

$$S_{\text{norm}}(t) = S(t)/S_{\text{eq}} \quad (42)$$

The slope of such a curve is

$$\frac{dS_{\text{norm}}(t)}{dt} = k_{\text{obs}} \cdot \exp(-k_{\text{obs}} \cdot t) \quad (43)$$

For $t \rightarrow 0$ the slope of the curve $S_{\text{norm}}(t)$ gives k_{obs} of the binding reaction.

However, for meaningful analysis of the time-dependent signals a model needs to be developed which facilitates extraction of the desired information from the data.

7.1.3 The Three-Zone Model

Here, a relatively simple model will be developed, which finally focuses the attention on only one parameter - the weighting factor for the upper hydrogel zone w_u . The analysis of the variation and behaviour of w_u and comparison with measurements will

provide deeper insight into processes taking place during incorporation of biomolecules into the hydrogel.

The half space over the gold surface from $z = 0$ to $z \rightarrow \infty$ can be subdivided into three zones: 1) a lower zone inside the hydrogel starting from $z = 0$ with a thickness d_l , 2) an upper zone inside the hydrogel with thickness d_u starting from $z = d_l$ and extended to the top of the hydrogel and 3) the region above the hydrogel extended to $z \rightarrow \infty$ (figure 55).

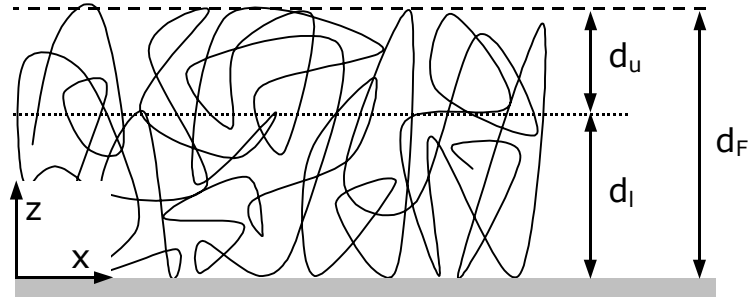


Figure 55. The subdivision of the half space over the gold surface in three zones with the dimensions d_l , d_u and $z = d_u - \infty$. The extensions d_l of the lower hydrogel zone and d_u of the upper hydrogel zone are variable but have to fulfil the condition $d_l + d_u = d_F$. d_F is the thickness of the hydrogel film.

The dimensions d_l and d_u are supposed to be variable but they have to fulfil the condition $d_l + d_u = d_F$ (d_F : thickness of hydrogel). Assuming spatially constant refractive indices n_l , n_u , n_M (M: medium) inside these zones, the effective refractive index n_{eff} can be written according to equation 9:

$$\begin{aligned} n_{eff} = & n_l \cdot (1 - \exp(-2(d_F - d_u)/d_{PD})) + \\ & n_u \cdot (\exp(-2(d_F - d_u)/d_{PD}) - \exp(-2d_F/d_{PD})) + \\ & n_M \cdot (\exp(-2d_F/d_{PD})) \end{aligned} \quad (44)$$

The expressions in brackets which are multiplied by the refractive indices can be conceived as weighting factors describing the contribution of each zone to the probed effective refractive index n_{eff} for each wavelength. If the weighting factors are denoted with w_l , w_u , w_M , equation 44 becomes

$$n_{eff} = n_l \cdot w_l + n_u \cdot w_u + n_M \cdot w_M \quad (45)$$

If the effective refractive index before binding n_{eff0} is given by

$$n_{eff0} = n_F \cdot w_l + n_F \cdot w_u + n_M \cdot w_M \quad (46)$$

a change of the effective refractive index Δn_{eff} at a certain time can be written as

$$\Delta n_{eff} = n_{eff} - n_{eff0} = w_l \cdot (n_l - n_F) + w_u \cdot (n_u - n_F) \quad (47)$$

provided a change of the refractive index n_M of the medium, e.g. due to exchange of buffer solution with a protein solution, is negligible.

Assuming the binding to start in the upper region of the hydrogel, the refractive index for the lower region n_l can be supposed to equal n_F . Then equation 47 becomes

$$\Delta n_{eff} = w_u \cdot (n_u - n_F) \quad (48)$$

The change of the resonance angle $\Delta\Theta_{SPR}$ depends linearly on the change of effective refractive index Δn_{eff} in a good approximation. Considering the linear dependence of $\Delta\Theta_{SPR}$ on the refractive index increment Δn (see section 6.3.1) means for an estimation of the SPR signal response it is sufficient to take into account the evolution of Δn_{eff} and thus to examine equation 48.

Equation 48 describes the probed effective refractive index at a certain time. When molecules bind to the hydrogel, the refractive index n_u will increase in time, but this increasing refractive index will be seen by both wavelengths. Hence, it can be concluded that different time behaviour of the signals can only arise from the particular time behaviour of the weighting factors $w_{u\ 600}$ and $w_{u\ 784}$. The weighting factors can be calculated according to equation 49 (see equations 44 and 45) considering the particular penetration depth d_{PD} for each wavelength:

$$w_u = \exp(-2(d_F - d_u) / d_{PD}) - \exp(-2d_F / d_{PD}) \quad (49)$$

Time dependence can be established in equation 49 by introducing a time dependence of d_u : $d_u = d_u(t)$. Since d_u is the extension of the upper hydrogel zone, $d_u(t)$ with $d_{u0}(t=0) = 0$ can be interpreted as a function which describes the diffusion of a refractive index frontier into the hydrogel caused by binding of molecules. However, for evaluating the relative evolution of $w_{u\ 600}$ and $w_{u\ 784}$ considering an increasing d_u is sufficient; the real time dependence $d_u(t)$ is not required. The relative evolution of $w_{u\ 600}$ and $w_{u\ 784}$ as a function of $d_u \in [0, d_F]$ will represent the time evolution of the two-wavelengths measurements.

In order to explore the case that the binding of biomolecules starts in the lower hydrogel zone, the functions $w_{l\ 600}(d_l)$ and $w_{l\ 784}(d_l)$ can be easily deduced from $w_{u\ 600}(d_u)$ and $w_{u\ 784}(d_u)$:

Following the same argumentation as outlined above, equation 48 turns into

$$\Delta n_{eff} = w_l \cdot (n_l - n_F) \quad (50)$$

From equation 44 follows

$$w_l = 1 - \exp(-2(d_F - d_u) / d_{PD}) = 1 - (w_u + \exp(-2d_F / d_{PD})) \quad (51)$$

meaning (by consideration of equation 49)

$$w_l(d_u) = w_u(d_F) - w_u(d_u) \quad (52)$$

or

$$w_l(d_l) = w_u(d_F) - w_u(d_F - d_l)$$

$$\frac{dw_l(d_l)}{dd_l} = \frac{dw_u(d_F - d_l)}{dd_l} \quad (53)$$

Equation 53 simply means that $w_{1600}(d_l)$ and $w_{1784}(d_l)$ are the mirror images of the curves $w_{u600}(d_u)$ and $w_{u784}(d_u)$ reflected on the straight connection line between the points $w_u(d_u = 0)$ and $w_u(d_u = d_F)$.

7.2 Surface Modification and Biorecognition Procedures

Here, the immobilisation of streptavidin and the subsequent biospecific interaction between streptavidin and biotinylated protein A will be investigated. In addition, a method will be introduced for the determination of both the thickness and the refractive index of a swollen dextran layer. Furthermore, in the course of the experiment, the fundamental prerequisite of the two-wavelength principle will be directly evidenced: the different penetration depths of the employed wavelengths by performing binding reactions on top of and inside the dextran matrix. Big objects like liposomes cannot penetrate into the hydrogel, therefore they can only bind at the periphery. Using low molar mass molecules and proteins, which are capable of penetrating into the 3D polymer matrix, allows to study binding processes inside the matrix.

After hydrogel preparation and subsequent immobilisation of streptavidin, the sample was incubated in a solution containing biotinylated liposomes. These were bound to the hydrogel through the specific streptavidin-biotin interaction and formed a layer on top of the hydrogel. Further successive incubation steps with streptavidin and biotinylated liposomes followed until a liposome stack was formed, having a large enough vertical extension that it appeared to be infinitely thick for both SP waves. After this part of the experiment, the liposome stack was removed by adding the detergent sodium dodecyl sulfate (SDS) in phosphate-buffered saline (PBS), breaking up the liposomes. Binding of liberated biotinylated lipids from the liposomes and of SDS molecules inside the hydrogel provided the second internal hydrogel binding event after the immobilisation of streptavidin; incubation with biotinylated protein A followed.

7.2.1 The Streptavidin - Biotin Complex

The protein streptavidin is produced by the bacterium *Streptomyces avidinii*. Streptavidin is a tetrameric protein (MW = 4 × 13kDa, each of the four identical chains consists of 159 amino acids) that has various biochemical applications, mostly because of its high affinity to biotin, a small (MW = 244Da) water-soluble vitamin: $K_A \sim 10^{14} \text{M}^{-1}$. Each monomer of streptavidin binds one molecule of biotin. The

complexes are also extremely stable over a wide range of temperature and pH. The structure of the streptavidin-biotin complex was determined by Weber *et al.* (Weber 1989).

Biotin is typically conjugated to proteins via primary amines (e.g. lysine). The streptavidin-biotin system can be employed for almost irreversible attachment of the biotinylated proteins. For instance, biotinylated antibodies were used for implementation of a biospecific biosensor surfaces (Morgan 1992) (see section 3.3). In this investigation the streptavidin-biotin system was also employed because of its high affinity. Since the binding of biotin to streptavidin is almost irreversible no undesired dissociation will occur during the single experimental steps. Furthermore, the ability of streptavidin to bind four biotins allowed to build up a liposome stack by successive incubations.

7.2.2 Chemicals

The chemicals 0,965mol/l hydrochloric acid (HCl) (Aldrich, Steinheim, Germany), 1-ethyl-3-(3-diethylaminopropyl) carbodiimide (EDC) (Sigma, St. Louis, MO, USA), 20%w/v sodium dodecyl sulfate (SDS) (Bio-Rad, Hercules, CA, USA), 30wt% hydrogen peroxide (H₂O₂) (Fluka, Buchs, Switzerland), 4-(2-Hydroxyethyl)piperazine-1-ethanesulfonic acid (HEPES) (Fluka), 40wt% poly(acrylic acid, sodium salt) MW~30,000 (PAA) (Aldrich), 95wt% sulphuric acid (H₂SO₄) (Prolabo, Fontenay, France), ammonium chloride (Fluka), bromoacetic acid (BrCH₂COOH) (Aldrich), cholesterol (Sigma), cysteamine hydrochloride (Riedel-de Haën, Seelze, Germany), dextran T500 (Pharmacia, Uppsala, Sweden), dimethylsulfoxide (Fluka), dipalmitoylphosphatidylcholine (DPPC) and dipalmitoylphosphatidylglycerol (DPPG) (a gift from Lipoid, Ludwigshafen, Germany), disodium hydrogenphosphate (Na₂HPO₄) (Merck, Darmstadt, Germany), ethanolamine hydrochloride (Sigma), ethylenediaminetetraacetic acid (EDTA) (Fluka), *N*-{[6-(biotinoyl)amino]hexanoyl}-1,2-dihexadecanoyl-*sn*-glycerophosphoethanolamine, triethylammonium salt (B-X-DHPE, where X represents a six-membered alkane chain) (Molecular Probes, Eugene, OR, USA), *N*-hydroxysuccinimide (NHS) (Sigma), potassium chloride (KCl) (Merck), potassium dihydrogen phosphate (KH₂PO₄) (Merck), potassium hydroxide (KOH) (Merck), protein A - biotin (Sigma-Aldrich, Steinheim, Germany), sodium (meta)periodate (Fluka), sodium acetate (NaAc) (Sigma), sodium chloride (NaCl) (Fluka), sodium cyanoborohydride (Fluka), sodium dihydrogenphosphate (Merck), sodium hydroxide (NaOH) (Sigma), streptavidin (Jackson ImmunoResearch, West Grove, PA, USA) were all used as received. Millipore-filtered water (18 MΩ) was used for the preparation of all aqueous solutions and rinsing.

7.2.2.1 Preparation of Buffers

Phosphate buffer (pH 7.4) was prepared by mixing 0.01mol/l aqueous solutions of disodium hydrogenphosphate and sodium dihydrogenphosphate.

Phosphate-buffered saline (PBS) was prepared by dissolving 0.14mol/l NaCl, 0.0027mol/l KCl, 0.01mol/l Na₂HPO₄ and 0.0018mol/l KH₂PO₄ in water.

NaAc-buffer was prepared as described in section 6.6.3.1.

HEPES-buffered saline (HBS) was prepared as described in section 6.5.3.4.

7.2.2.2 Preparation of Liposome Solution

The liposomes used for the binding experiments were prepared as described earlier by the film method (Wink 1998). In short, a chloroform solution of DPPC:DPPG:cholesterol:B-X-DHPE (molar ratio 10:1:4:0.001) is dried under reduced pressure in a rotavapor. The formed film is resuspended in phosphate buffer, followed by successive extrusions through 0.2, 0.1 and 0.05 μ m polycarbonate filters, respectively. The average size (133nm) and polydispersity (0.10) of the liposomes was determined by dynamic light scattering using the Malvern 4700 system (Malvern, UK). The liposomes were stored at +4°C in the refrigerator.

7.2.3 Surface Chemistry

The same gold coated glass slides as described in section 6.3.2.1 were employed. The cleaning procedure yielding a hydrophilic gold surface is also outlined there.

The hydrophilic gold surfaces were incubated in a 0.01mol/l cysteamine hydrochloride solution for 24h. After preparation of the cysteamine self assembled monolayer (SAM), the surface was incubated with a solution of 0.02mol/l polyacrylic acid (PAA) / 0.1mol/l EDC / 0.1mol/l NHS in H₂O/DMSO 40:60 by volume for 20min, resulting in a PAA layer chemically linked to the SAM via amid bonds. The remaining activated ester groups of the PAA derivative were used for the following coupling of aminodextran (AMD) supplied in a 10wt% aqueous solution (AMD was synthesised according to the procedure describe in section 6.5.3.2). After these preparation steps, the layer system was thoroughly rinsed with millipore water, NaAc-buffer and 0.05mol/l HCl in aqueous solution.

In order to provide carboxy groups within the dextran layer for the immobilisation of biomolecules, the assembly was incubated in 1mol/l BrCH₂COOH in 2mol/l NaOH for 14h followed by intensive rinsing with water and NaAc-buffer.

7.2.4 Interaction Experiments

In Figure 56 the immobilisation of streptavidin and the course of binding events is depicted. Step 1 represents the unmodified dextran hydrogel after binding to the PAA underlayer. Step 2 is the state after the immobilisation of streptavidin -mainly inside the hydrogel- according to a widely used protocol (Johnsson 1991): incubation with 0.05mol/l NHS / 0.2mol/l EDC in aqueous solution for 7min, followed by rinsing with NaAc-buffer and incubation of 167 μ g/ml streptavidin in NaAc-buffer for 20min. Residual activated ester groups were deactivated by incubating with 1mol/l ethanolamine hydrochloride pH 8.5. The assembly was rinsed with NaAc-buffer and finally this buffer was replaced by phosphate buffer. After these preparation steps, the biotinylated liposomes in phosphate buffer were injected into the flow chamber. The

liposomes containing biotinylated lipids bind specifically to streptavidin immobilised in the hydrogel (preferably to those molecules being immobilised in peripheral positions). The binding was monitored in real time by SPR at 600nm and 784nm. After about 90min, a stable equilibrium state was reached, which was assumed to indicate the completed formation of a liposome layer (step 3). After the formation of the first liposome layer, the sample was incubated with 50 μ g/ml streptavidin in phosphate buffer for about 40min. This procedure established new binding sites on top of the bound liposomes exploiting that each streptavidin molecule has four binding sites for biotin (step 4). The incubation steps 3 and 4 were repeated until no significant change in SPR signal through liposome binding was detectable any more for both wavelengths. This part of the experiment was terminated after the fifth incubation of liposomes (steps 5-8). Next, a 0.5wt% solution of SDS in PBS was rinsed through the flow cell. The SDS solution destroys the liposomes and single lipid molecules are flushed out of the flow chamber except those biotinylated lipids bound to streptavidin in the hydrogel. SDS molecules are believed to form some aggregates with the remaining biotinylated lipids (step 9). After step 9, the assembly was rinsed with phosphate buffer and then the phosphate buffer was replaced by HBS. Finally, the sample was incubated with biotinylated protein A 100 μ g/ml in HBS for 115min and the binding was monitored in real time.

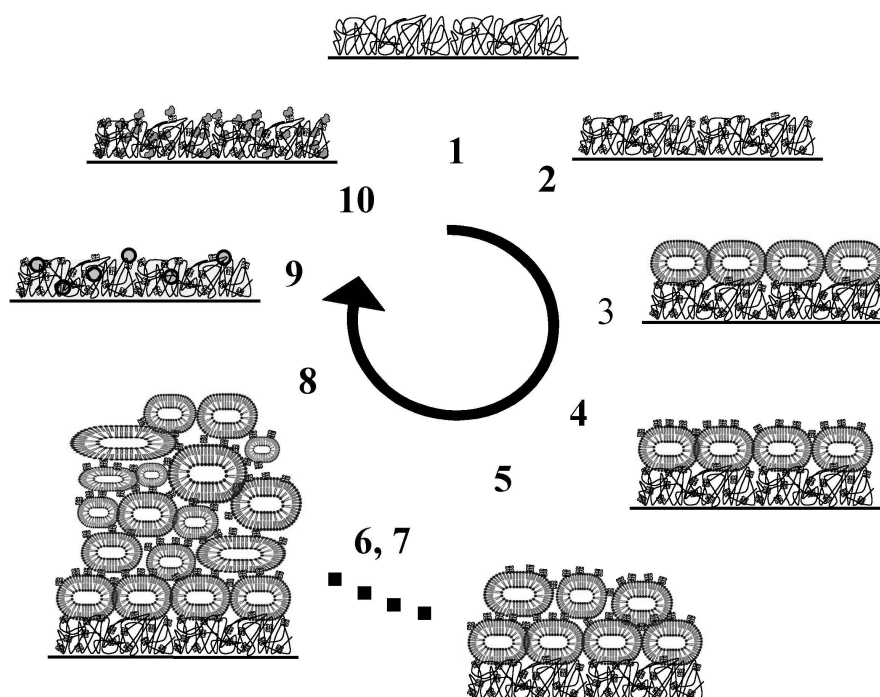


Figure 56. Experimental procedure designed to investigate binding events inside and on top of a hydrogel layer. Detailed information is provided in the text. 1: the dextran hydrogel, 2: dextran hydrogel with immobilised streptavidin, 3: binding of first liposome layer containing biotinylated lipids via streptavidin-biotin interaction, 4: binding of streptavidin on top of the liposome layer, 5-8: successive incubation with liposome solution / streptavidin results in a liposome stack appearing infinite thick for surface plasmon waves excited with 600nm and 784nm, 9: after rinsing with SDS in PBS, 10: binding of biotinylated protein A to streptavidin. The sketch does not reflect the actual size ratios of the structures. The liposomes employed here have a diameter of 133nm in average and their wall thickness is about 5nm.

7.3 Results and Discussion

7.3.1 Determination of the Optical Properties of the Initial Hydrogel Layer System and Employed Solutions

Starting from the values given in table 1 for the uncoated gold surface, the optical properties of the PAA layer, the dextran layer and different solutions (phosphate buffer, 0.5wt% of SDS in PBS, HBS) were determined by comparison of the SPR measurements with simulations.

The refractive indices of the solutions were measured with an uncoated gold surface covered with the solutions as bulk medium. The values are given in table 12.

The refractive indices of the surface attached polymers were determined for their swollen state when being immersed in water. A graphical solution was employed to find values which are consistent in terms of the measured angle shifts due to polymer attachment, the polymer layer thickness and refractive indices at both wavelengths. For this purpose an important empirical relation was exploited which results from the referenced refractive indices of BK7 glass and water (see values given in table 1):

$$\frac{n_{600}^{BK7}}{n_{784}^{BK7}} = \frac{n_{600}^{H_2O}}{n_{784}^{H_2O}} = 1.003 \quad (54)$$

For simulations which take additional layers or other liquid media like buffers into account the ratio of 1.003 was used to calculate the index of refraction n_{600} for $\lambda = 600\text{nm}$ from the index of refraction n_{784} for $\lambda = 784\text{nm}$.

The values found for the PAA layer are given in table 12. Figure 57 shows the graphical solution for the determination of the properties of the dextran hydrogel layer.

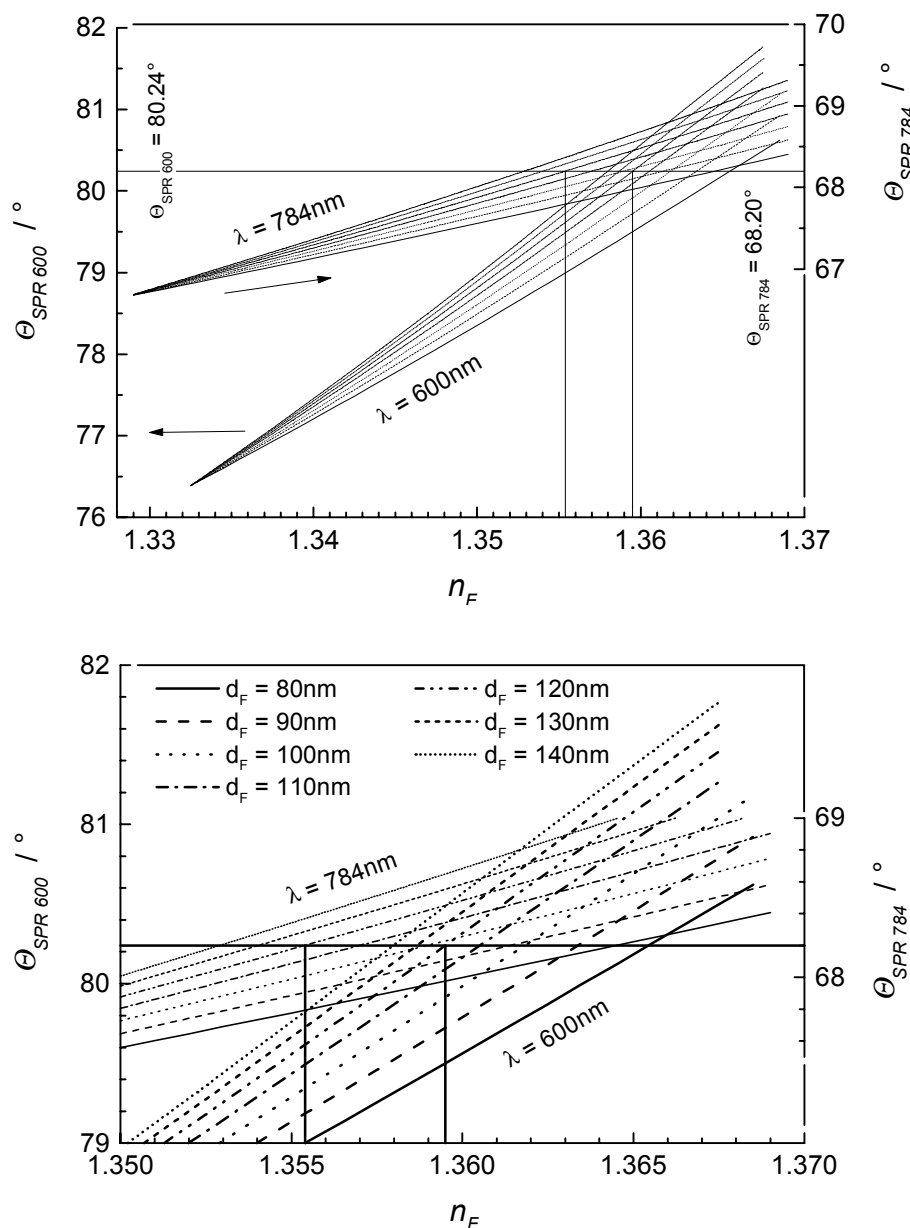


Figure 57. The graphical solution to find values for the thickness d_F and the refractive index $n_F(\lambda)$ of the dextran layer which correspond to the measurements and simultaneously satisfy $d_{F 784} = d_{F 600}$ and $n_{F 600} = 1.003 \cdot n_{F 784}$. The vertical lines mark points within the graph bundles of 784nm and 600nm which fulfil these conditions. The lower graph is an enlargement of the intersection region of the upper graph. Detailed information about the construction of the graph is given in the text.

In figure 57, each line graph $\Theta_{SPR}(d_F, n_F)$ represents the calculated dependence of the resonance angles for a swollen dextran layer with fixed thickness d_F as a function of mixed refractive index n_F of the polymer / water composition. An increasing mixed refractive index reflects an increasing volume fraction Φ of hydrogel polymer, a measure for the degree of swelling of the hydrogel caused by incorporation of water.

Two bundles of graphs, each bundle for one wavelength, are plotted against a shared abscissa but own ordinate; the measured resonance angles are marked in either coordinate systems with an horizontal line and the coordinate systems are shifted in order to match these lines.

The desired solution are points of intersection of the horizontal line with line graphs $\Theta_{\text{SPR}}(d_F, n_F)$ and simultaneously satisfying $d_{F\ 784} = d_{F\ 600}$ and $n_{F\ 600} = 1.003 \cdot n_{F\ 784}$.

A swollen dextran layer with $d_F=120\text{nm}$, $n_{F\ 784}=1.355$ and $\Phi=0.12$ fulfils these conditions. The volume fraction Φ is calculated according to the equation of Garnet (equation 34) with n_M the index of refraction of water $n_M = n_{\text{H}_2\text{O}\ 784} = 1.329$, n_0 the index of refraction of the dry hydrogel $n_0 = n_{\text{Dex}} = 1.56$ (Elender 1996).

Layer no. i	Designation of layer	d / nm	n
The initial layer sytem			
3	Swollen PAA, medium: water	10	1.373
4	Swollen dextran, medium: water	120	1.355
Dextran layer modifications by incorporation of molecules			
4	Swollen dextran with immobilised streptavidin, medium: phosphate buffer	120	1.391
4	Swollen dextran with incorporated SDS, medium: 0.5wt% SDS in PBS	120	1.392
4	Swollen dextran with bound biotinylated protein A, medium: HBS	120	1.401
Liposome stack			
5	Liposomes, medium: phosphate buffer	0 - ∞	1.339
Bulk solutions			
5 / 6	Phosphate buffer	∞	1.329
5	0.5wt% SDS in PBS	∞	1.331
5	HBS	∞	1.331

Table 12. The refractive indices and thicknesses that were found by comparison of measurements with simulations for 784nm. The index of refraction of the liposome stack is an average. The indices of refraction of the buffer solutions and of SDS in PBS were determined by SPR measurements with an uncoated gold surface. The refractive indices used in the simulations for 600nm can be calculated by multiplying the given values for 784nm with 1.003.

7.3.2 Equilibrium SPR Signals During Binding Experiments and Comparative Simulation

Figure 58 shows the results of the SPR measurements. Each step represents the measured equilibrium SPR signal for the annotated event. In order to represent the data in a format, which makes them comparable, both signals are normalised to their

amplitude for the exchange of phosphate buffer to HBS (a signal of 100% corresponds to change from phosphate buffer to HBS). The buffer exchange is assumed to be a spatially homogeneous change in refractive index and is thus suitable as standard for comparison.

In this context, using the terminology “SPR signal”, a special feature of the differential intensity measurements needs to be mentioned. The immobilisation of streptavidin leads to an angle shift of $\Delta\Theta_{\text{SPR } 784} = 2.34^\circ$ resp. $\Delta\Theta_{\text{SPR } 600} = 3.30^\circ$. This results in a resonance angle $\Theta_{\text{SPR } 600} = 83.54^\circ$ with extreme grazing incidence of the light beam. This can cause practical measurement problems like shadowing of the light beam by the edges of the glass slide coupled to the prism (see figure 4). In addition, for a reliable measurement of the SPR curve minimum even data points beyond the resonance angle must be acquired. Furthermore, the minimum is quite shallow and broad. This all together makes it more or less impossible to perform conventional Θ -2 Θ SPR measurements with 600nm on a dextran layer system with high immobilisation density. On the contrary, differential intensity measurements generate still a vital signal even if subsequent binding events result in SPR curves, which can no longer be analysed by determination of the shift in the resonance minimum, because of the extreme grazing incidence of the light. The calculated SPR curve of dextran + immobilised streptavidin + bound biotinylated protein A in figure 60 may serve as an example. But, of course, for cases like these, thorough data validation by comparison with simulations is mandatory to understand the evolution of the measured signal. Since the apparent intensity minimum of the 600nm SPR curve shifts to even smaller angles of incidence when binding biotinylated protein A, for 600nm the change in intensity is used as "SPR signal"; for 784nm $\Delta\Theta_{\text{SPR}}$ is used calculated according to equation 33.

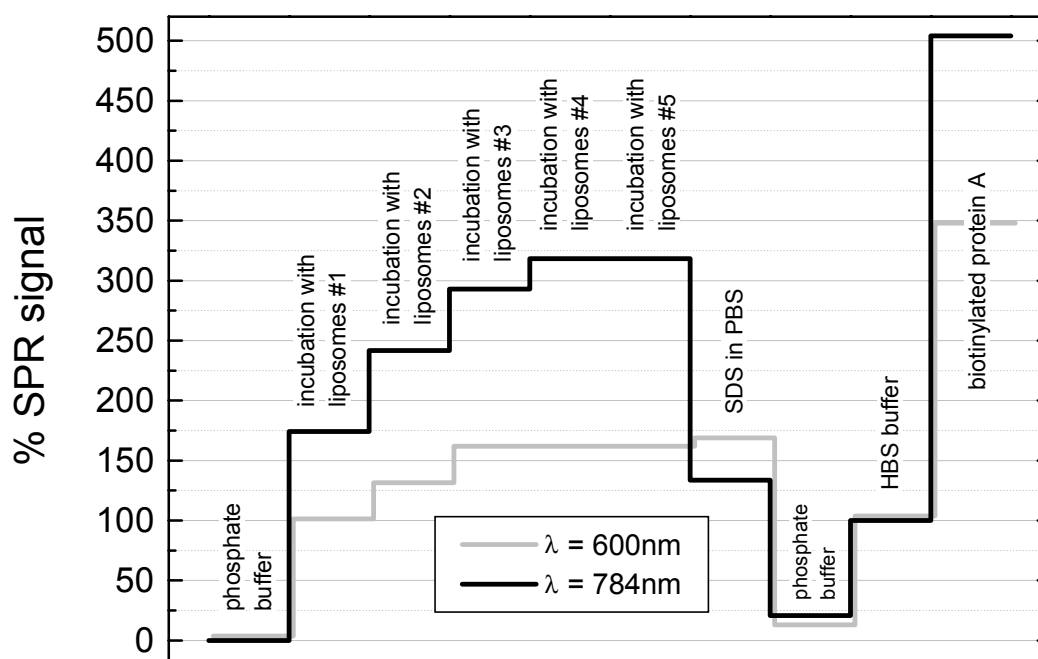


Figure 58. The measured SPR equilibrium signals during the course of experimental steps no. 3 - 10 (see figure 56) for 784nm and 600nm. Both signals are normalised to their amplitude for the replacement of phosphate buffer (starting point in the graph) by HBS (corresponds to 100% SPR signal).

The measurements plotted in figure 58 show clear and distinct differences between the long and the short wavelength. However, in order to provide a consistent explanation and to ensure a correct interpretation of the data extensive simulations were carried out and compared to the experimental results. Based on the hydrogel properties deduced from the graphical solution in figure 57 (see also table 12), a successive comparison between experimental results and simulations was performed. For the simulations it was assumed that the immobilisation of streptavidin causes an increase of the refractive index of the swollen hydrogel, but no change of its thickness. As stated later in chapter 7.3.3.1 at least during the immobilisation the hydrogel seems to expand under the pH conditions during immobilisation. Under milder pH conditions as considered here (phosphate buffer with pH 7.4), the hydrogel will reduce its extension, but, probably, steric requirements due to streptavidin incorporation demand an increased thickness of the hydrogel. Of course, data pairs can be found which also resemble the measurements while considering an increased thickness of the hydrogel caused by streptavidin incorporation combined with corresponding slightly lower refractive index of the expanded hydrogel. But this could only be considered as speculation and thus it was decided to base the simulations on the established original hydrogel properties. In this context it needs also to be mentioned that the increased refractive index caused by the incorporation of streptavidin was assumed to be homogeneously distributed over the hydrogel after completed immobilisation, although the time-resolved two wavelengths measurements of the immobilisation kinetics suggest a gradient in immobilisation density, at least in the beginning of the immobilisation (see chapter 7.3.3.1).

Based on these assumptions, the simulations were carried out for each experimental step for the wavelength of 784nm. Values which give rise to accordance between experiment and simulation (see table 12, figure 59 shows the corresponding calculated plasmon resonance curves) were transferred to 600nm by multiplying n_{784} by 1.003. The simulated resonance curves for 600nm nicely reproduce the experimentally found evolution of the SPR signal (figure 60).

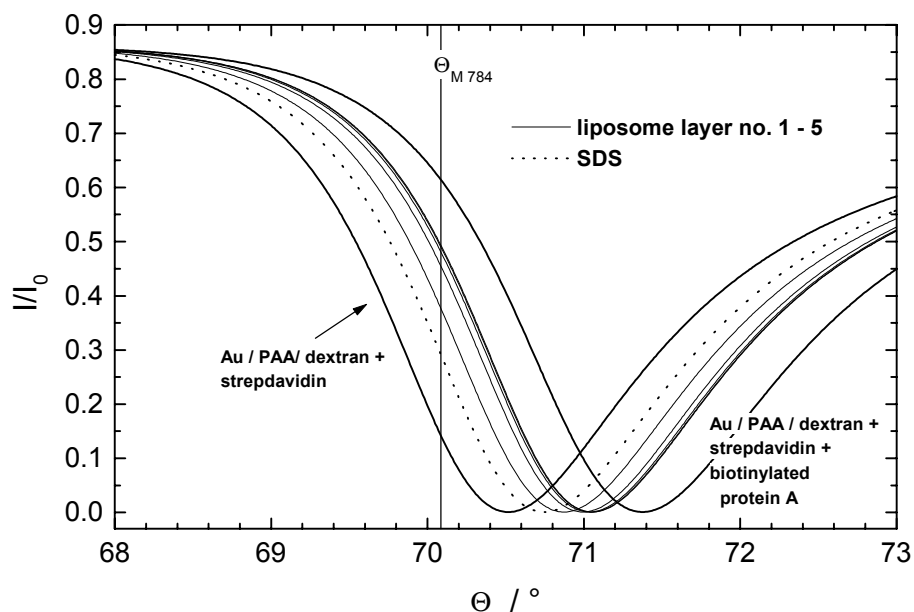


Figure 59. Simulated SPR curves for 784nm which resemble the differential intensity measurement results; the layer parameters can be borrowed from tables 1 and 12. The thin curves representing the binding of liposomes are simulated with thickness increment of 133nm. This corresponds to the average size of the liposomes in solution. After the third layer, the curves are hardly distinguishable. The dotted curve represents the status after flushing the flow chamber with 0.5wt% SDS in PBS; the minimum is located at a lower resonance angle Θ_{SPR} than for the first liposome layer. The vertical line marks the position for the differential intensity measurements.

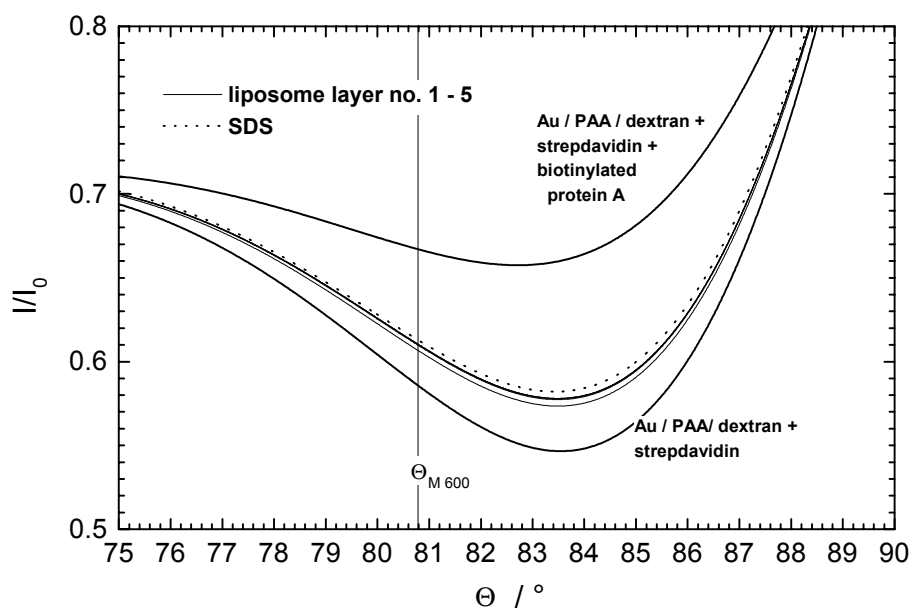


Figure 60. Simulated SPR curves for 600nm. These curves correspond to the curves in figure 59; the layer parameters employed here can be borrowed from table 1 and from table 12 by multiplying the refractive indices in table 12 by 1.003. Here the liposome curves appear indistinguishable after the first layer. The dotted SDS curve gives higher intensity than the last liposome curve, as experimentally observed. Binding of biotinylated protein A gives a significant increase of intensity. However, the minimum of the curve is practically almost not analysable. The vertical line marks the position for the differential intensity measurements.

The binding of liposomes successively increases the SPR signals; for 784nm the first liposome layer gives 55% of the total signal reached after five liposome injections; for 600nm it is 62%. After the third incubation with liposomes, an increase in the 600nm signal is no longer observable; for 784nm after the fourth injection no increase in signal is observable anymore. As expected, the increase in signal decreases with the number of liposome binding cycles.

Figure 61 shows the results from calculations. Since the real structure of the liposome stack is unknown, in the calculations, a layer with homogenous and constant mixed refractive index $n_{784} = 1.339$ is supposed to constantly increase in thickness. Although this is certainly a simplification, the calculations show that the signal for 784nm reaches saturation at a thickness of about 700nm; the signal for 600nm reaches saturation already at a thickness of about 350nm. The average refractive index $n_{784} = 1.339$ of the liposome stack ensures conformity between the measured and the simulated signal saturation level. When assuming a refractive index of 1.5 for lipid molecules and the medium is phosphate buffer, the volume fraction Φ of lipid molecules within the liposome stack amounts to about 0.06 according to equation 34. Assuming the liposomes were spheres with an outer diameter of 133nm and a wall thickness of 5nm ($2 \times$ the length of a lipid molecule) and assuming they were packed cubic densely, the lipid molecule fraction would amount to 0.15. This means the assembled layer stack is less densely packed in terms of volume fraction by a factor of 2.5 compared to ideally cubic densely packed spheres.

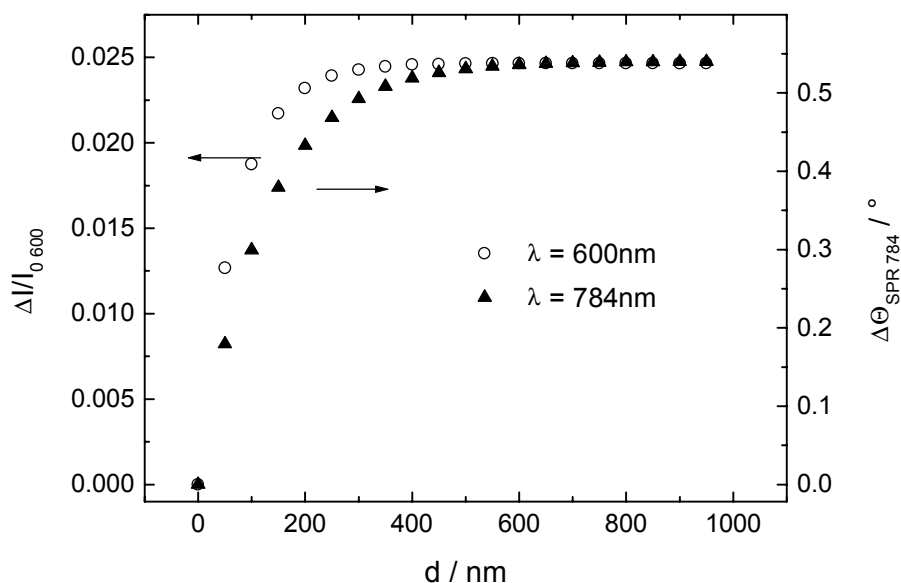


Figure 61. The simulated evolution of the SPR signals for 600nm and 784nm when a layer with fixed refractive index $n_{784}=1.339$ on top of the dextran layer starts to increase its thickness. This is assumed to resemble the successive deposition of liposomes. The point from which the slope of a curve approaches zero indicates the thickness from which the layer appears to be infinitely thick when probed with the respective wavelength.

The most distinct difference between the SPR signals from 600nm and 784nm arises when flushing 0.5% SDS in PBS through the flow cell. The detergent destroys the liposomes and the liposome / streptavidin layer structure is removed from top of the hydrogel. SDS molecules will either be bound to streptavidin within the hydrogel or will form micelles with the hydrophobic moieties of lipid molecules originating from the liposomes and being still bound to streptavidin by their biotin residues. The signal of the longer wavelength decreases drastically caused by the removal of the liposomes and dropped below the signal level of the first liposome layer. The signal of the short wavelength increases; the binding of SDS within the hydrogel overcompensates the loss of the liposomes. The simulations reproduce this picture if a slight increase in refractive index of the hydrogel layer is assumed due to SDS incorporation and 0.5wt% SDS in phosphate buffer is taken into consideration as medium above the hydrogel (for refractive indices see table 12). Thus, the response of the signals serves as a direct proof for the different sensitivities of these two wavelengths in z-direction: SPR waves excited by 600nm are mainly sensitive inside the hydrogel; SPR waves excited by 784nm are also strongly influenced by the medium above the hydrogel layer.

The SPR response on replacement of phosphate buffer by HBS in comparison to the SPR response on binding the first liposome layer also serves as an indicator for the pronounced difference in field penetration depth of the two wavelengths. In contrast to the binding of liposomes on top of the hydrogel, an exchange of buffer can be supposed to be a spatially homogenous change in refractive index. For the shorter wavelength the SPR signal increase due to buffer exchange (100% SPR signal in figure 58) is larger than due to binding of the first liposome layer (98%); for the longer wavelength vice versa (174%).

The presented experimental results clearly indicate that surface plasmon waves of 600nm are more sensitive to changes inside than to changes above the hydrogel. Surface plasmon waves of 784nm are almost equally sensitive in both zones. This can be clearly verified by comparison of the curves for 600nm and 784nm in figure 58 with respect to the SPR signals gained while assembling the liposome stack on top of the hydrogel and the SPR signals gained while binding of biotinylated protein A inside the hydrogel.

7.3.3 Time-Dependence of Binding Processes

In the section above it was proven that the amplitudes of the two SPR signals actually behave distinctly different for binding events occurring at different z-positions over the gold surface. In this section the evolution of the SPR signals in time will be investigated and compared. The time dependence for 600nm and 784nm is shown in figures 62, 64, 65 for three different experimental steps.

7.3.3.1 Immobilisation of Streptavidin

Figure 62 shows the kinetics of the immobilisation of streptavidin. The time behaviour of the two signals is markedly different. In the beginning of the immobilisation, the signal for 784nm increases over three times faster than that of 600nm. It is $k_{\text{obs } 784}=0.07\text{s}^{-1}$ and $k_{\text{obs } 600}=0.02\text{s}^{-1}$.

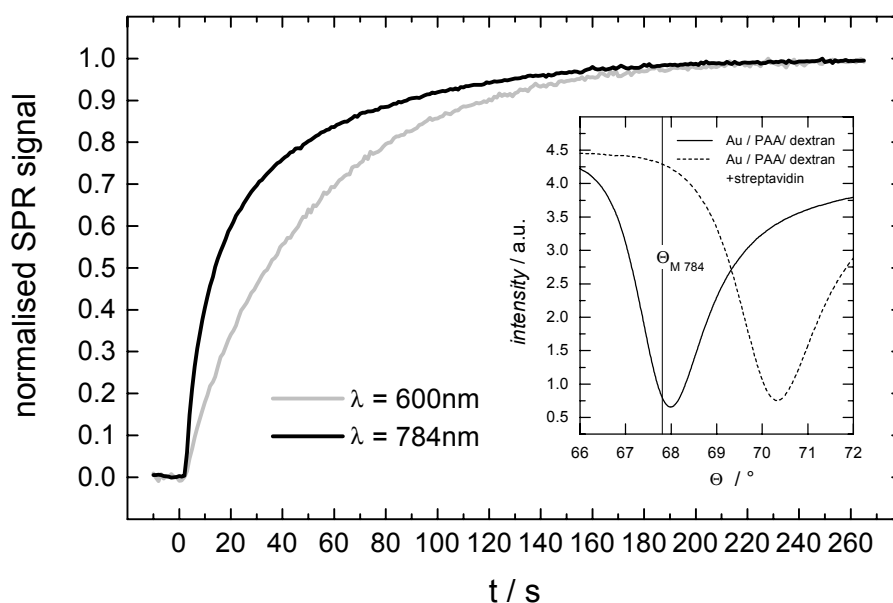


Figure 62. Kinetics of the immobilisation of streptavidin. Both signals are normalised to their equilibrium level. The immobilisation seems to appear faster when probed with 784nm than with 600nm: in the very beginning of the immobilisation the slope of the kinetic curve measured with 784nm is more than three times steeper than for 600nm.

The inset shows the measured plasmon resonance curves for 784nm before and after the immobilisation and the position for the differential intensity measurements $\Theta_{M\ 784}$. The angle shift $\Delta\Theta_{SPR\ 784}$ amounts to 2.34° . At the end of the measurement, the slope of the plasmon resonance curve decreases, therefore the slope of the kinetic curve appears slightly too small in the end. The shape of the plasmon resonance curve also changes slightly, however, this effect is small and can be neglected.

As stated in section 7.1.2, such a difference in time behaviour is most likely to explain by an inhomogeneous increase of refractive index in z-direction. By applying the three-zone model to this particular layer system, information about the binding mechanisms inside the hydrogel can be obtained.

The topmost graphs in figure 63 show the calculated weighting factors for 784nm and 600nm for a dextran film thickness of 120nm as determined earlier. The weighting factors are plotted against a growing thickness of the upper hydrogel region, which corresponds to streptavidin binding at first to the uppermost binding sites of the hydrogel and later streptavidin molecules diffusing deeper into the hydrogel. Independent from the real time behaviour the graph shows that at least for the first 30nm both signals should increase equally fast. Beyond about 30nm thickness the signal of 600nm should even increase faster. This is not observed. The lower graphs show curves calculated analogously, but the dextran film is supposed to be thicker. The curves separate from each other and the slope of the curve of 784nm increases more and more compared to the slope of 600nm. At $d_F = 300\text{nm}$ the weighting factor for 784nm increases initially 3.7 times faster than for 600nm. Obviously, an explanation for a significantly faster increase of 784nm-SPR signal additionally requires an expanding hydrogel besides the proposed mechanism of binding starting in the periphery of the hydrogel and then propagating into deeper hydrogel zones.

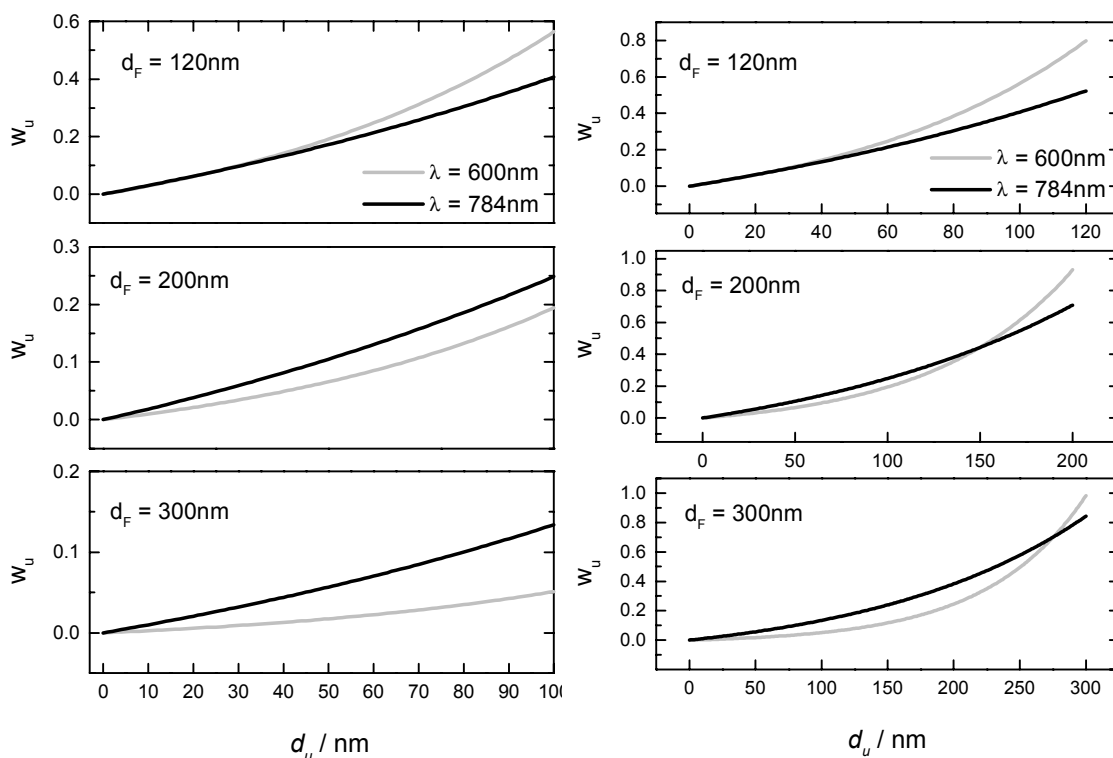


Figure 63. The dependence of the weighting factor w_u on the thickness of the upper region in the hydrogel calculated for different dextran film thicknesses d_F . The three graphs on the left show the data for the first 100nm of d_u . The three graphs on the right show the evolution of w_u over the entire dextran film thickness range. If d_u is approaching d_F , $w_{u,600}$ is exceeding $w_{u,784}$ in each case. Detailed information about the specific meaning of this circumstance is given in the text.

An expansion of the hydrogel during immobilisation of streptavidin as proposed here can be considered as quite likely because the immobilisation is performed in NaAc-buffer pH 4.7. At this pH value, some of the few remaining carboxy groups linked to dextran (after preparation of active esters with EDC/NHS-chemistry) are negatively charged and streptavidin is positively charged.¹ Consequently, before streptavidin immobilisation the hydrogel was probably already slightly expanded by electrostatic repulsive forces between the negatively charged carboxy-groups and expanded eminently with the beginning of streptavidin incorporation since the streptavidin molecules repelled each other. Furthermore, steric requirements are also likely to play a role for the expansion since the binding of streptavidin within the hydrogel means incorporation of relatively big macromolecules. Thus, the hydrogel expansion is supposed to be a complex and dynamic process which is driven by electrostatic repulsive forces taking effect together with steric influences. Due to this process, the hydrogel expands into regions where the surface plasmon wave of 784nm has still a substantial sensitivity whereas the sensitivity of the 600nm surface plasmon waves

¹ Measurements at different pH values concerning the efficiency of electrostatic pre-concentration of streptavidin at a negatively charged interface have revealed an isoelectric point of streptavidin of about 5.2.

dramatically decreases. This effect seems to be one necessary condition for an apparently faster increase in signal for 784nm than for 600nm in addition to the advancement of the reaction front from upper to deeper hydrogel zones. The binding mechanism proposed for streptavidin immobilisation is sketched in figure 66 a).

It must be mentioned that some simplifications were made for the interpretation of the measured immobilisation kinetics. Certainly the real immobilisation process can not be described by the simple three zones model employed here. Furthermore, for this rather qualitative discussion only the evolution of w_{u} respectively n_{eff} was considered. This can not be supposed to supply exact quantitative elucidation, for instance because surface plasmon waves of 600nm are principally more sensitive to refractive index changes than surface plasmon waves of 784nm (for 600nm and 784nm applies: $\Delta\Theta_{\text{SPR } 600}/\Delta n = 1.66 \cdot \Delta\Theta_{\text{SPR } 784}/\Delta n$). Apart from this limitations, this model is believed to have the potential to explain the findings without speculative and unreasonable assumptions and giving unquestionably qualitatively reasonable answers.

7.3.3.2 Binding of Biotinylated Protein A to Streptavidin

In contrast to the measurements during immobilisation of streptavidin to the reactive groups of the dextran, the time behaviour for biomolecule - biomolecule interaction in the hydrogel is significantly different. Figure 64 shows the signals for the binding of biotinylated protein A to streptavidin.

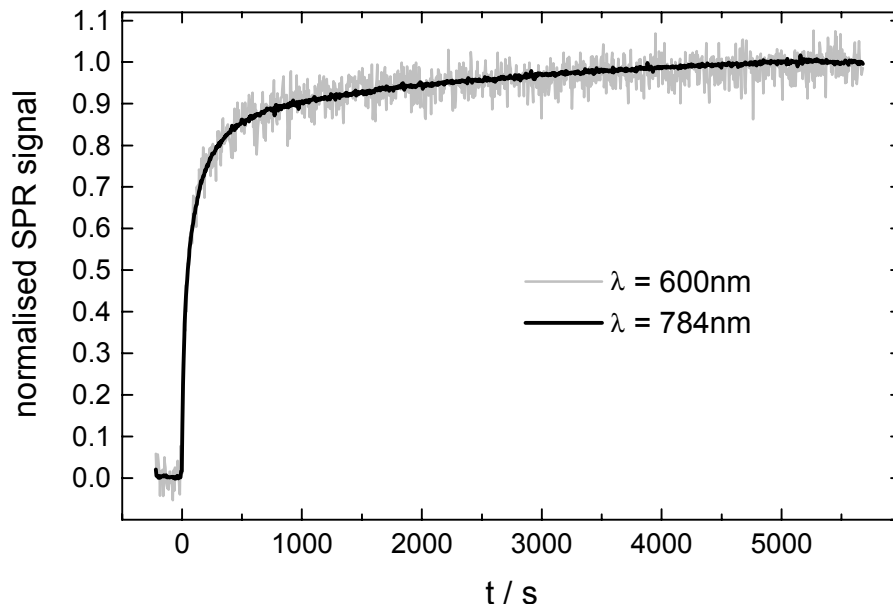


Figure 64. Kinetics of the binding of biotinylated protein A to streptavidin. Both signals are normalised to their equilibrium level. The evolution in time is identical for both signals.

The signals evolve absolutely identically in time. As stated earlier (see section 7.1.2), this seems to be only explainable when assuming binding either to occur inside the entire thickness range of the hydrogel with equal probability or, alternatively, inside a certain region (z-coordinate increment) with equal probability, while only a negligible

number of binding events take place in other regions. In terms of the preceded argumentation this would mean the weighting factors w_u are constant in time; only the refractive index n_u increases in time. In addition, a constant w_u means no expansion of the hydrogel during binding of biotinylated protein A.

The kinetic measurement of the binding of the first liposome layer can serve as a further example supporting this view and showing again an identical time behaviour of both signals (see figure 65). In this case of forming the liposome layer on top of the hydrogel, it seems to be most reasonable to assume a limited but constantly extended binding region (i.e. in this case the thickness of the first liposome layer) with increasing refractive index in time.

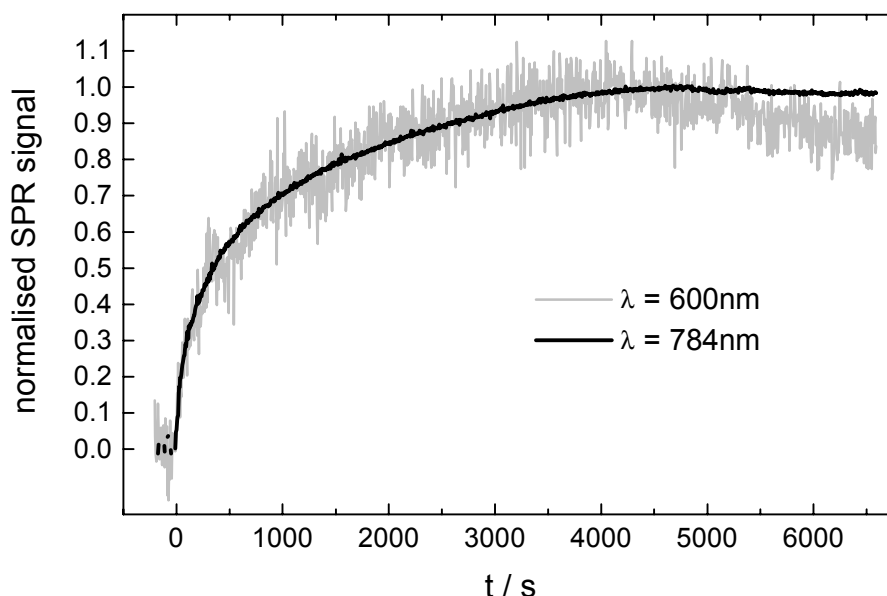


Figure 65. Kinetics of the binding of the first liposome layer. Both signals are normalised to their equilibrium level. The evolution in time is identical for both signals. At $t=5400s$ the sample was rinsed with phosphate buffer. After reaching the maximum value a slight decrease is observable which might indicate a reordering of the liposomes on the hydrogel.

Figure 58 shows that the amplitude for binding of biotinylated protein A is higher for 784nm than for 600nm. However, when consulting again figure 63, a dextran layer thickness of 120nm can hardly explain this finding, because for each upper layer thickness d_u the response of the 600nm signal should be at least equal. An increased dextran layer thickness gives a better explanation for the observed difference in amplitudes. This can suggest that the dextran layer thickness is actually larger than 120nm after immobilisation of streptavidin also for a neutral pH value. This may be a consequence of the altered steric requirements after immobilisation of the rather bulky biomolecules. On the other hand, all simulations in section 7.3.2 were performed with a dextran layer thickness of 120nm and resembled the experimental findings quite exact.

Apart from this, a more important issue seems to be that the weighting factor $w_{u,600}$ always exceeds $w_{u,784}$ from a certain d_u on (see graphs on right side in figure 63). Independent from the actual dextran layer thickness an occupation of binding sites over

the entire hydrogel thickness would give rise to a 600nm signal significantly higher than the 784nm signal, since $w_{u,600}$ exceeds $w_{u,784}$ notably, if d_u approaches d_f . From this it follows that it is unlikely that biotinylated protein A binds over the entire hydrogel thickness to streptavidin, because the observed signal of 600nm amounts only about 0.6 times of the signal of 784nm. It seems to be more likely that the binding to streptavidin only occurs in the upper hydrogel region, maybe because diffusion of biotinylated protein A into deeper regions of the hydrogel is hindered by already bound biotinylated protein A. However, a reliable estimation for the thickness of the upper occupied hydrogel region can be hardly given.

Summarised, the binding of protein A to streptavidin seems to occur in an upper hydrogel zone with limited extension, which remains constant in time. The hydrogel extension seems not to be influenced by the binding of protein A. The mechanism proposed for binding of biotinylated protein A to streptavidin is sketched in figure 66 b).

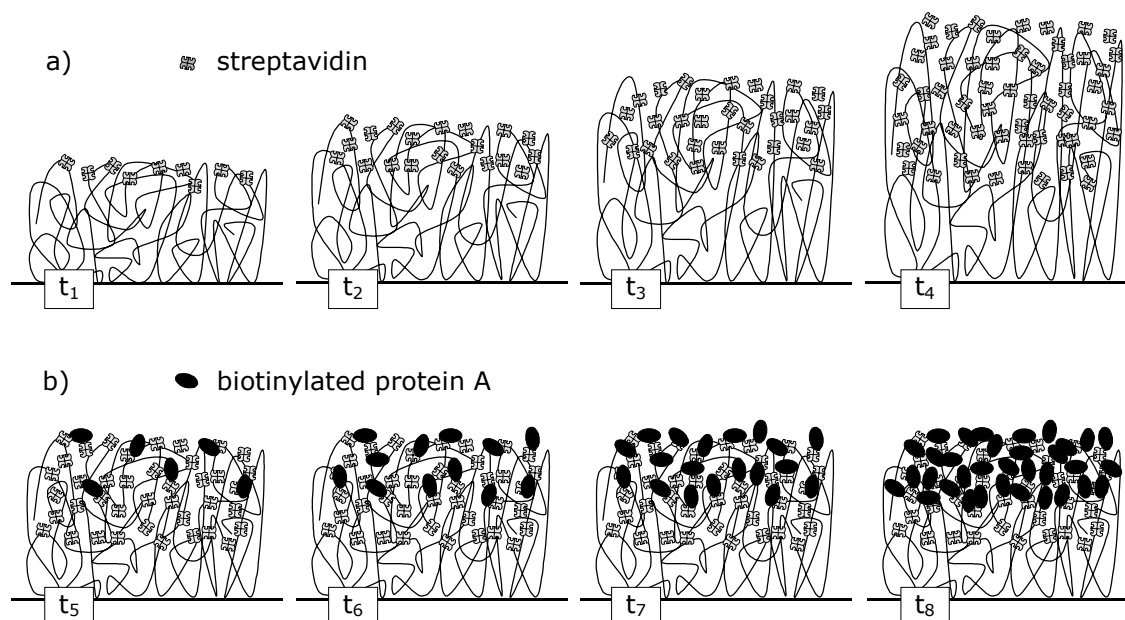


Figure 66. The proposed two different binding mechanisms inside the hydrogel. **a)** Immobilisation of streptavidin; $t_1 < t_2 < t_3 < t_4$. The hydrogel expands due to electrostatic repulsive forces and steric influences during immobilisation. Streptavidin molecules bind first in the upper hydrogel region, then the reaction front propagates into deeper hydrogel zones. **b)** Binding of biotinylated protein A to streptavidin; $t_5 < t_6 < t_7 < t_8$. The hydrogel may be slightly expanded due to steric requirements of streptavidin, but does not additionally expand due to binding of biotinylated protein A. Biotinylated protein A binds in an upper hydrogel zone with fixed extension, only the refractive index of this zone increases in time.

This sketch only illustrates the binding mechanisms and the assigned hydrogel zones; the dimensions of the interaction zones relative to the hydrogel dimension can not be reliably given.

7.4 Conclusion

The novel experimental setup which allows simultaneous real-time SPR measurements with two wavelengths is able to deliver valuable new information about the binding mechanisms in dextran hydrogels. Employing a dextran hydrogel and performing binding experiments on top of and inside the hydrogel it was possible to directly prove that the sensitivity of the short wavelength is primarily concentrated inside the polymer matrix in contrast to the long wavelength. With this the basis was created to gain supplementary information about interaction processes at biosensing interfaces in terms of spatial resolution normal to the surface. Especially the analysis of the time dependence of the SPR signals, combined with the newly developed three-zone model, led to some new insights into the dynamics of the binding behaviour of biomolecules to a dextran hydrogel.

References

- Alberts, B.; Bray, D.; Johnson, A.; Lewis, J.; Raff, M.; Roberts, K. and Walter, P. (1998), *Essential Cell Biology: An Introduction to the Molecular Biology of the Cell*, New York, Garland
- Andersson, K.; Gülich, S.; Hämäläinen, M.; Nygren, P.-A.; Hober, S. and Malmqvist, M. (1999), *Kinetic Characterization of the Interaction of the Z-Fragment of Protein A With Mouse-IgG3 in a Volume in Chemical Space*, *Proteins: Struct., Funct., Genet.* 37, 494-498
- Barthélemy, P.; Maurizis, J. C.; Lacombe, J. M. and Pucci, B. (1998), *Bioorg. Med. Chem. Lett.* 8, 1559-1562
- Boardman, A. D. (1982), *Hydrodynamic Theory of Plasmon-Polaritons on Plane Surfaces*, in *Electromagnetic Surface Modes*, A. D. Boardman Ed., New York, John Wiley & Sons
- Brockman, J. M.; Nelson, B. P. and Corn, R. M. (2000), *Surface plasmon resonance imaging measurements of ultrathin organic films*, *Annu. Rev. Phys. Chem.* 51, 41-63
- Chapman, R. G.; Ostuni, E.; Liang, M. N.; Meluleni, G.; Kim, E.; Yan, L.; Pier, G.; Warren, H. S. and Whitesides, G. M. (2001), *Polymeric Thin Films That Resist the Adsorption of Proteins and the Adhesion of Bacteria*, *Langmuir* 17, 1225-1233
- Chapman, R. G.; Ostuni, E.; Takayama, S.; Holmlin, R. E.; Yan, L. and Whitesides, G. M. (2000), *Surveying for Surfaces that Resist the Adsorption of Proteins*, *J. Am. Chem. Soc.* 122 (34), 8303-8304
- Chen, W. P. and Chen, J. M. (1981), *Use of surface plasma waves for determination of the thickness and optical constants of thin metallic films*, *J. Opt. Soc. Am.* 71 (2), 189-191
- Christensen, L. L. H. (1997), *Theoretical Analysis of Protein Concentration Determination Using Biosensor Technology under Conditions of Partial Mass Transport Limitation*, *Anal. Biochem.* 249, 153-164

- Coqueret, X. (1999), *Photoreactivity of polymers with dimerizable side-groups: Kinetic analysis for probing morphology and molecular organization*, *Mocromol. Chem. Phys.* 200 (7), 1567-1579
- Cuatrecasas, P. and Parikh, I. (1972), *Absorbents for Affinity Chromatography. Use of N-Hydroxysuccinimide Esterst of Agarose*, *Biochemistry* 11 (12), 2291-2299
- Earp, R. L. and Dessy, R. E. (1998), *Surface Plasmon Resonance*, in *Commercial Biosensors: Applications to Clinical, Bioprocess and Enviromental Samples*, G. Ramsay Ed., New York, John Wiley & Sons
- Edwards, P. R.; Gill, A.; Pollard-Knight, D. V.; Hoare, M.; Buckle, P. E.; Lowe, P. A. and Leatherbarrow, R. J. (1995), *Kinetic of Protein-Protein Interactions at the Surface of an Optical Biosensor*, *Anal. Biochem.* 231, 210-217
- Elam, J. H.; Nygren, H. and Stenberg, M. (1984), *Covalent coupling of polysaccharides to silicon and silicon rubber surfaces*, *J. Biomed. Mat. Res.* 18, 953 - 959
- Elender, G.; Kühner, M. and Sackmann, E. (1996), *Functionalisation of Si/SiO₂ and glass surfaces with ultrathin dextran films and deposition of lipid bilayers*, *Biosens. Bioelectron.* 11 (6/7), 565 - 577
- Fägerstam, L. G.; Frostell-Karlsson, Å.; Karlsson, R.; Persson, B. and Rönnberg, I. (1992), *Biospecific interaction analysis using surface plasmon resonance detection applied to kinetic, binding site and concentration analysis*, *J. Chromatogr.* 597, 397-410
- Fischer, T.; Beyermann, M. and Koch, K.-W. (2001), *Application of Different Surface Plasmon Resonance Biosensor Chips to Monitor the Interaction of the CaM-Binding Site of Nitric Oxide Synthase I and Calmodulin*, *Biochem. Biophys. Res. Commun.* 285, 463-469
- Fivash, M.; Towler, E. M. and Fisher, R. J. (1998), *BIAcore for macromolecular interaction*, *Curr. Opin. Biotechnol.* 9, 97-101
- Fong, C.-C.; Wong, M.-S.; Fong, W.-F. and Yang, M. (2002), *Effect of hydrogel matrix on binding kinetics of protein-protein interactions on sensor surface*, *Anal. Chim. Acta* 456, 201-208
- Frazier, R. A.; Matthijs, G.; Davies, M. C.; Roberts, C. J.; Schacht, E. and Tendler, S. J. B. (2000), *Characterization of protein-resistant dextran monolayers*, *Biomaterials* 21, 957-966
- Fujishige, S. (1987), *Intrinsic viscosity-molecular weight relationships for poly(N-isopropylacrylamide) solutions*, *Polym. J. (Tokyo)* 19 (3), 297-300

-
- Fujishige, S.; Kubota, K. and Ando, I. (1989), *Phase-Transition of aqueous-solutions of poly(N-isopropylacrylamide) and poly(N-isopropylmethacrylamide)*, J. Phys. Chem. 93 (8), 3311-3313
- Garland, P. B. (1996), *Optical evanescent wave methods for the study of biomolecular interactions*, Q. Rev. Biophys. 29, 91-117
- Garnet, M. (1904), *Colours in metal glasses and in metallic films*, Phil. Trans. A 203, 385-420
- Garrett, Q.; Chatelier, R. C.; Griesser, H. J. and Milthorpe, B. K. (1998), *Effect of charged groups on the adsorption and penetration of proteins onto and into carboxymethylated poly(HEMA) hydrogels*, Biomaterials 19, 2175-2186
- Geddes, N. J.; Martin, A. S.; Caruso, F.; Urquhart, R. S.; Furlong, D. N.; Sambles, J. R.; Than, K. A. and Edgar, J. A. (1994), *Immobilisation of IgG onto gold surfaces and its interaction with anti-IgG studied by surface plasmon resonance*, J. Immunol. Methods 175, 149 - 160
- Glaser, R. W. (1993), *Antigen-Antibody Binding and Mass Transport by Convection and Diffusion to a Surface: A Two-Dimensional Computer Model of Binding and Dissociation Kinetics*, Anal. Biochem. 213, 152-161
- Gombotz, W. R.; Guanghui, W.; Horbett, T. A. and Hoffman, A. S. (1991), *Protein adsorption to poly(ethylene oxide) surfaces*, J. Biomed. Mat. Res. 25, 1547 - 1562
- Granzow, R. and Reed, R. (1992), *Interactions in the Fourth Dimension*, Bio/Technology 10, 390 - 393
- Green, R. J.; Corneillie, S.; Davies, J.; Davies, M. C.; Roberts, C. J.; Schacht, E.; Tendler, S. J. B. and Williams, P. M. (2000a), *Investigation of the Hydration Kinetics of Novel Poly(ethylene oxide) Containing Polyurethanes*, Langmuir 16, 2744-2750
- Green, R. J.; Frazier, R. A.; Shakeshe!, K. M.; Davies, M. C.; Roberts, C. J. and Tendler, S. J. B. (2000b), *Surface plasmon resonance analysis of dynamic biological interactions with biomaterials*, Biomaterials 21, 1823-1835
- Hall, D. (2001), *Use of Optical Biosensors for the Study of Mechanistically Concerted Surface Adsorption Processes*, Anal. Biochem. 288, 109-125
- Häussling, L.; Ringsdorf, H.; Schmitt, F.-J. and Knoll, W. (1991), *Biotin-Functionalized Self-Assembled Monolayers on Gold: Surface Plasmon Optical Studies of Specific Recognition Reactions*, Langmuir 7, 1837-1840

- Heinz, B. S.; Laschewsky, A.; Rekaï, E. D.; Wischerhoff, E. and Zacher, T. (2001), *Grafting of Functionalized Water Soluble Polymers on Gold Surfaces: Stable Stimuli-Responsive Thin Hydrogel Films Exhibiting a LCST or UCST*, in Stimuli-Responsive Water Soluble and Amphiphilic Polymers, C. L. McCormick Ed., ACS Symposium Series vol. 780, Washington DC, The American Chemical Society: 162-180
- Hoffman, A. S.; Horbett, T. A. and Ratner, B. D. (1977), *Interactions of blood and blood components at hydrogel interfaces*, Ann. N. Y. Acad. Sci. 283, 372-382
- Holmberg, K.; Tiberg, F.; Malmsten, M. and Brink, C. (1997), *Grafting with hydrophilic polymer chains to prepare protein-resistant surfaces*, Colloids and Surfaces A: Physicochemical and Engineering Aspects 123-124, 297-306
- Homola, J.; Yee, S. S. and Gauglitz, G. (1999), *Surface plasmon resonance sensors: review*, Sens. Actuators, B 54, 3-15
- Humphery-Smith, I. and Blackstock, W. (1997), *Proteome Analysis: Genomics via the Output Rather Than the Input Code*, J. Protein Chem. 16 (5), 537-544
- Jackson, J. D. (1982), *Classical Electrodynamics*, New York, John Wiley & Sons
- Johansen, K.; Arwin, H.; Lundström, I. and Liedberg, B. (2000), *Imaging surface plasmon resonance sensor based on multiple wavelengths: Sensitivity considerations*, Rev. Sci. Instrum. 71, 3530-3538
- Johnsson, B.; Löfås, S. and Lindquist, G. (1991), *Immobilization of Proteins to a Carboxymethyl-dextran-Modified Gold Surface for Biospecific Interaction Analysis in Surface Plasmon Resonance Sensors*, Anal. Biochem. 198, 268-277
- Jung, L.; Campbell, C. T.; Chinowsky, T. M.; Mar, M. N. and Yee, S. S. (1998), *Quantitative Interpretation of the Response of Surface Plasmon Resonance Sensors to Adsorbed Films*, Langmuir 14, 5636-5648
- Kajenski, P. J. (1997), *Tunable optical filter using long-range surface plasmons*, Opt. Eng. 36 (5), 1537-1541
- Karlsson, R. and Fält, A. (1997), *Experimental design for kinetic analysis of protein-protein interactions with surface plasmon resonance biosensors*, J. Immunol. Methods 200, 121-133
- Kim, S. Y.; Cho, S. M.; Lee, Y. M. and Kim, S. J. (2000), *Thermo- and pH-Responsive Behaviors of Graft Copolymer and Blend Based on Chitosan and N-Isopropylacrylamide*, Journal of Applied Polymer Science 78, 1381-1391

-
- Kjellander, R. and Florin, E. (1981), *Water structure and changes in thermal stability of the system polyethylene oxide-water*, J. Chem. Soc., Faraday Trans. 1 77, 2053-2077
- Köberle, P.; Laschewsky, A. and van den Boogard, D. (1992), *Self-organization of hydrophobized polyzwitterions*, Polymer 33, 4029-4039
- Konak, C.; Rathi, R. C.; Kopeckova, P. and Kopecek, J. (1997), *Photoregulated association of water-soluble copolymers with spirobenzopyran-containing side chains*, Macromolecules 30, 5553-5556
- Kooyman, R. P. H.; Kolkman, H.; Van Gent, J. and Greve, J. (1988), *Surface plasmon immunosensors: sensitivity considerations*, Anal. Chim. Acta 213, 35-45
- Kretschmann, E. (1971), *The Determination of the Optical Constants of Metals by Excitation of Surface Plasmons*, Z. Physik 241, 313-324
- Kretschmann, E. and Raether, H. (1968), *Radiative Decay of Non Radiative Surface Plasmons Excited by Light*, Z. Naturforsch. 23 a, 2135-2136
- Krevelen, D. W. v. (1990), *Properties of Polymer*, Amsterdam, Elsevier
- Kyriakides, T. R.; Cheung, C. Y.; Murthy, N.; Bornstein, P.; Stayton, P. S. and Hoffman, A. S. (2002), *pH-Sensitive polymers that enhance intracellular drug delivery in vivo*, Journal of Controlled Release 78, 295-303
- Langmuir, I. (1916), *The Constitution and Fundamental Properties of Solids and Liquids: I. Solids*, J. Am. Chem. Soc. 38, 2221-2295
- Langone, J. J. (1982), *Protein A of Staphylococcus aureus and related immunoglobulin receptors produced by streptococci and pneumococci*, in Advances in Immunology, F. J. Dixon and H. G. Kuhnel Eds., New York, Academic Press: 157-252
- Laschewsky, A. and Rekaï, E. D. (2000), *Photochemical modification of the lower critical solution temperature of cinnamoylated poly(N-2-hydroxypropylmethacrylamide) in water*, Macromol. Rapid Commun. 21 (13), 937-940
- Laschewsky, A.; Rekaï, E. D. and Wischerhoff, E. (1999), *Stimuli-Responsive Water Soluble Polymers and Hydrogels: Tailoring of the Lower Critical Solution Temperature, and Efficient Grafting on Gold Surfaces*, Polym. Prepr. Am. Chem. Soc. Div. Polym. Chem. 40 (2), 189-190

- Laschewsky, A.; Rekaï, E. D. and Wischerhoff, E. (2001), *Tailoring of Stimuli-Responsive Water Soluble Acrylamide and Methacrylamide Polymers*, *Macromol. Chem. Phys.* 202 (2), 276-286
- Lee, J. H.; Lee, H. B. and Andrade, J. D. (1995), *Blood compatibility of polyethylene oxide surfaces*, *Prog. Polym. Sci.* 20, 1043-1079
- Lide, D. R. Ed. (1998), *CRC Handbook of Chemistry and Physics*, Boca Raton, CRC Press LLC
- Liedberg, B.; Lundström, I. and Stenberg, E. (1993), *Principles of biosensing with an extended coupling matrix and surface plasmon resonance*, *Sens. Actuators*, B 11, 63-72
- Liedberg, B.; Nylander, C. and Lundström, I. (1983), *Surface Plasmon Resonance for Gas Detection and Biosensing*, *Sens. Actuators* 4, 299-304
- Liedberg, B.; Nylander, C. and Lundström, I. (1995), *Biosensing with Surface Plasmon Resonance - how it all started*, *Biosens. Bioelectron.* 10, i-ix
- Lodish, H.; Baltimore, D.; Berk, A.; Zipursky, S. L.; Matsudaira, P. and Darnell, J. (1996), *Molekulare Zellbiologie*, Berlin, de Gruyter
- Löfås, S. and Johnsson, B. (1990), *A Novel Hydrogel Matrix on Gold Surfaces in Surface Plasmon Resonance Sensors for Fast and Efficient Covalent Immobilization of Ligands*, *J. Chem. Soc., Chem. Commun.*, 1526 - 1528
- Löfås, S.; Johnsson, B.; Edström, A.; Hansson, A.; Lindquist, G.; Hilgren, R.-M. and Stigh, L. (1995), *Methods for site controlled coupling to carboxymethyl dextran surfaces in surface plasmon resonance sensors.*, *Biosens. Bioelectron.* 10, 813-822
- MacBeath, G. and Schreiber, S. L. (2000), *Printing Proteins as Microarrays for High-Throughput Function Determination*, *Science* 289, 1760-1763
- Malmqvist, M. and Granzow, R. (1994), *Biomolecular Interaction Analysis - Introduction*, *Methods (San Diego)* 6 (2), 95-98
- Marsh, R. J.; Jones, R. A. L. and Sferrazza, M. (2001), *Adsorption and displacement of a globular protein on hydrophilic and hydrophobic surfaces*, *Colloids Surf.*, B 23 (1), 31-42
- Mayo, C. S. and Hallock, R. B. (1989), *Immunoassay based on surface plasmon oscillations*, *J. Immunol. Methods* 120, 105-114

-
- Morgan, H. and Taylor, D. M. (1992), *A surface plasmon resonance immunosensor based on the streptavidin-biotin complex*, *Biosens. Bioelectron.* 7, 405-410
- Morton, T. A.; Myszka, D. G. and Chaiken, I. M. (1995), *Interpreting Complex Binding Kinetics from Optical Biosensors: A Comparison of Analysis by Linearization, the Integrated Rate Equation, and Numerical Integration*, *Anal. Biochem.* 227, 176-185
- Myszka, D. G. and Morton, T. A. (1998), *Clamp - A Biosensor Kinetic Data-Analysis Program*, *Trends Biochem. Sci.* 23 (4), 149-150
- Myszka, D. G.; Morton, T. A.; Doyle, M. L. and Chaiken, I. M. (1997), *Kinetic analysis of a protein-antibody interaction limited by mass transport on an optical biosensor*, *Biophys. Chem.* 64, 127-137
- Nayak, D. P.; Davis, A. R.; McQueen, N. L.; Bos, T. J.; Jabbar, M. A.; Sivasubramanian, N. and Lionelli, G. (1985), *Biological and immunological properties of haemagglutinin and neuraminidase expressed from cloned cDNAs in prokaryotic and eukaryotic cells*, *Vaccine* 3, 165-171
- Nedelkov, D. and Nelson, R. W. (2001), *Analysis of native proteins from biological fluids by biomolecular interaction analysis mass spectrometry (BIA/MS): exploring the limit of detection, identification of non-specific binding and detection of multi-protein complexes*, *Biosens. Bioelectron.* 16, 1071-1078
- Neumaier, K. (1998), *Fresnel für WIN32*
- Nieba, L.; Krebber, A. and Plückthun, A. (1996), *Competition BIAcore for Measuring True Affinities: Large Differences from Values Determined from Binding Kinetics*, *Anal. Biochem.* 234, 155-165
- Nylander, C.; Liedberg, B. and Lind, T. (1982), *Gas detection by means of surface plasmon resonance*, *Sens. Actuators* 3, 79-88
- Omidian, H.; Hashemi, S. A.; Sammes, P. G. and Meldrum, I. (1999), *Modified acrylic-based superabsorbent polymers (dependence on particle size and salinity)*, *Polymer* 40, 1753-1761
- O'Shannessy, k. J. and Winzor, D. J. (1996), *Interpretation of Deviations from Pseudo-First-Order Kinetic Behavior in the Characterization of Ligand Binding by Biosensor Technology*, *Anal. Biochem.* 236, 275-283
- Ostuni, E.; Chapman, R. G.; Holmlin, R. E.; Takayama, S. and Whitesides, G. M. (2001), *A Survey of Structure-Property Relationships of Surfaces that Resist the Adsorption of Protein*, *Langmuir* 17 (18), 5605-5620

- Otto, A. (1968), *Excitation of Nonradiative Surface Plasma Waves in Silver by the Method of Frustrated Total Reflection*, *Zeitschrift für Physik* 216, 398-410
- Oya, T.; Enoki, T.; Grosberg, A. Y.; Masamune, S.; Sakiyama, T.; Takeoka, Y.; Tanaka, K.; Wang, G.; Yilmaz, a.; Feld, M. S.; Dasari, R. and Tanaka, T. (1999), *Reversible Molecular Adsorption Based on Multiple-Point Interaction by Shrinkable Gels*, *Science* 286, 1543-1545
- Parsons, I. D. and Stockley, P. G. (1997), *Quantitation of the Escherichia coli methionine repressor-operator interaction by surface plasmon resonance is not affected by the presence of a dextran matrix*, *Anal. Biochem.* 254, 82-87
- Patel, N.; Davies, M. C.; Hartshorne, M.; Heaton, R. J.; Roberts, C. J.; Tendler, S. J. B. and Williams, P. M. (1997), *Immobilization of Protein Molecules onto Homogeneous and Mixed Carboxylate-Terminated Self-Assembled Monolayers*, *Langmuir* 13, 6485-6490
- Peng, B.; Johannsmann, D. and Rühle, J. (1999), *Polymer Brushes with Liquid Crystalline Side Chains*, *Macromolecules* 32 (20), 6759-6766
- Peppas, N. A. and Langer, R. (1994), *New Challenges in Biomaterials*, *Science* 263, 1715
- Piehler, J.; Brecht, A.; Geckeler, K. E. and Gauglitz, G. (1996), *Surface modification for direct immunoprobes*, *Biosens. Bioelectron.* 11 (6/7), 579-590
- Piehler, J.; Brecht, A.; Hehl, K. and Gauglitz, G. (1999), *Protein interactions in covalently attached dextran layers*, *Colloids Surf., B* 13, 325-336
- Piehler, J.; Brecht, A.; Valiokas, R.; Liedberg, B. and Gauglitz, G. (2000), *A high-density poly(ethylene glycol) polymer brush for immobilization on glass-type surfaces*, *Biosens. Bioelectron.* 15, 473-481
- Putnam, F. W. (1975), *The Plasma Proteins: Structure, Function and Genetic Control*, Vol. 1, New York, Academic Press
- Raether, H. (1988), *Surface Plasmons on Smooth and Rough Surfaces and on Gratings*, 136, Hamburg, Springer-Verlag
- Rich, R. L. and Myszka, D. G. (2000), *Advances in surface plasmon resonance biosensor analysis*, *Curr. Opin. Biotechnol.* 11, 54-61
- Ringsdorf, H.; Simon, J. and Winnik, F. (1992), *Hydrophobically modified poly(N-isopropylacrylamides) in water: a look by fluorescence techniques at the heat-induced phase transition*, *Macromolecules* 25, 7306-7312

-
- Ritchie, R. H. (1957), *Plasma Losses by Fast Electrons in Thin Films*, Phys. Rev. 106 (5), 874-881
- Salamon, Z.; Macleod, H. A. and Tollin, G. (1997), *Surface plasmon resonance spectroscopy as a tool for investigating the biochemical and biophysical properties of membrane protein systems. II: Applications to biological systems*, Biochim. Biophys. Acta 1331, 117-152
- Schiebener, P.; Straub, J.; Sengers, J. M. H. L. and Gallagher, J. S. (1990), *Refractive Index of Water and Steam as Function of Wavelength, Temperature and Density*, J. Phys. Chem. Ref. Data 19 (3), 677-715
- Schott (2000), *Optisches Glas - Katalog 2000*, Version 1.0D 2000, http://www.schott.com/optik/german/applications/optical_glass/index.html
- Schuck, P. (1996), *Kinetics of Ligand Binding to Receptor Immobilized in a Polymer Matrix, as Detected with an Evanescent Wave Biosensor. I. A Computer Simulation of the Influence of Mass Transport*, Biophys. J. 70, 1230-1249
- Schuck, P. (1997a), *Reliable determination of binding affinity and kinetics using surface plasmon resonance biosensors*, Curr. Opin. Biotechnol. 8, 498-502
- Schuck, P. (1997b), *Use of surface Plasmon Resonance to probe the equilibrium and dynamik aspects of interactions between biological macromolecules*, Annu. Rev. Biopmol. Struct. 26, 541-566
- Sommerfeld, A. (1909), *Über die Ausbreitung der Wellen in der drahtlosen Telegraphie*, Annal. Phys. 28, 665-736
- Stamler, J. S.; Singel, D. J. and Loscalzo, J. (1992), *Biochemistry of Nitric Oxide and its Redox-Activated Forms*, Science 258, 1898-1902
- Stayton, P. S.; Hoffman, A. S.; Murthy, N.; Lackey, C.; Cheung, C.; Tan, P.; Klumb, L. A.; Chilkoti, A.; Wilbur, F. S. and Press, O. W. (2000), *Molecular engineering of proteins and polymers for targeting and intracellular delivery of therapeutics*, Journal of Controlled Release 65, 203-220
- Stayton, P. S.; Shimoboji, T.; Long, C.; Chilkoti, A.; Chen, G.; J, M. H. and Hoffman, A. S. (1995), *Control of Protein-Ligand recognition using a stimuli-responsive polymer*, Nature 378, 472-474
- Steiner, G.; Sablinskas, V.; Hübner; Kuhne, C. and Salzer, R. (1999), *Surface plasmon resonance imaging of microstructured monolayers*, J. Mol. Struct. 509, 265-273

- Stenberg, E.; Persson, B.; Roos, H. and Urbaniczky, C. (1991), *Quantitative Determination of Surface Concentration of Protein with Surface Plasmon Resonance Using Radiolabeled Proteins*, J. Colloid Interface Sci. 143 (2), 513-526
- Stern, E. A. and Ferrell, R. A. (1960), *Surface Plasma Oscillations of a Degenerate Electron Gas*, Phys. Rev. 120 (1), 130-136
- Szabo, A.; Stolz, L. and Granzow, R. (1995), *Surface plasmon resonance and its use in biomolecular interaction analysis (BIA)*, Curr. Opin. Struct. Biol. 5, 699-705
- Taylor, L. D. and Cerankowski, L. D. (1975), *Preparation of films exhibiting a balanced temperature dependence to permeation by aqueous solution. Lower consolute behavior*, J. Polym. Sci., Polym. Chem. Ed. 13 (11), 2551-2570
- Wadu-Mesthrige, K.; Amro, N. A. and Liu, G.-Y. (2000), *Immobilization of Proteins on Self-Assembled Monolayers*, Scanning 22, 380-388
- Weber, P. C.; Ohlendorf, D. H.; Wendoloski, J. J. and Salemme, F. R. (1989), *Structural Origins of High-Affinity Biotin Binding to Streptavidin*, Science 243, 85-88
- Wink, T.; Zuilen, S. J. v.; Bult, A. and Benekom, W. P. v. (1997), *Self-assembled Monolayers for Biosensors*, The Analyst 122, 43R-50R
- Wink, T.; Zuilen, S. J. v.; Bult, A. and Bennekom, W. P. v. (1998), *Liposome-Mediated Enhancement of the Sensitivity in Immunoassays of Proteins and Peptides in Surface Plasmon Resonance Spectrometry.*, Anal. Chem. 70 (5), 827-832
- Wischerhoff, E. (2000), *Products with Biofunctional Coating*, European Patent Application 00203767.9
- Wischerhoff, E. (in press), *Functionalized Surfaces for Protein Microarrays - State of the Art and Perspectives*, in Proteomics: The Next Phase of Genomic Discovery, J. S. Albala and I. Humphrey-Smith Eds., New York, Marcel Dekker
- Witz, J. (1999), *Kinetic Analysis of Analyte Binding by Optical Biosensors: Hydrodynamic Penetration of the Analyte Flow into the Polymer Matrix Reduces the Influence of Mass Transport*, Anal. Biochem. 270, 201-206
- Wofsy, C. and Goldstein, B. (2002), *Effective Rate Models for Receptors Distributed in a Layer above a Surface: Application to Cells and Biacore*, Biophys. J. 82, 1743-1755

- Yamada, N.; Okano, T.; Sakai, H.; Karikusa, F.; Sawasaki, Y. and Sakurai, Y. (1990), *Thermo-responsive polymeric surfaces; control of attachment and detachment of cultured cells*, *Macromol. Chem., Rapid Commun.* 11, 571-576
- Yeh, P. (1988), *Optical waves in layered media*, New York, John Wiley & Sons
- Zhizhin, G. N.; Moskalova, M. A.; Shomina, E. V. and Yakovlev, V. A. (1982), *Surface Electromagnetic Wave Propagation on Metal Surfaces*, in *Surface Polaritons - Electromagnetic Waves at Surfaces and Interfaces*, V. M. Agranovich and D. L. Mills Eds., *Modern Problems in Condensed Matter Sciences* Amsterdam, North-Holland Publishing Company: 93-143
- Zhu, P. W. and Napper, D. H. (1999), *The effect of molecular weight on the dynamics of adsorbed poly(N-isopropylacrylamide) at particle surfaces in water*, *Macromol. Chem. Phys.* 200, 698-705

Parts of this thesis are published in

- Heinz, B. S.; Laschewsky, A.; Rekaï, E. D.; Wischerhoff, E. and Zacher, T. (2001), *Grafting of Functionalized Water Soluble Polymers on Gold Surfaces: Stable Stimuli-Responsive Thin Hydrogel Films Exhibiting a LCST or UCST*, in *Stimuli-Responsive Water Soluble and Amphiphilic Polymers*, C. L. McCormick Ed., *ACS Symposium Series* vol. 780, Washington DC, The American Chemical Society: 162-180
- Wischerhoff, E.; Zacher, T.; Laschewsky, A. and Rekaï, E. D. (2000), *Direct Observation of the Lower Critical Solution Temperature of Surface-Attached Thermo-Responsive Hydrogels by Surface Plasmon Resonance*, *Angew. Chem. Int. Ed.*, 39, (24), 4602-4604
- Zacher, T. and Wischerhoff, E. (2002), *Real-Time Two-Wavelength Surface Plasmon Resonance as a Tool for the Vertical Resolution of Binding Processes in Biosensing Hydrogels*, *Langmuir*, 18, 1748-1759

Acknowledgement

The work presented here was started with BioTuL AG, Germany and was completed with Glaucus Proteomics B.V., The Netherlands under the supervision of Dr. Erik Wischerhoff.

First and foremost I would like to thank Dr. Erik Wischerhoff for supporting my work in every possible way and for his guidance in completing this thesis. His scientific expertise, his care in research and his advice have proven invaluable.

I want to thank Prof. Erich Sackmann for supporting my thesis and allowing me to graduate in his department.

I am grateful to Prof. Ian Humphery-Smith for giving me the opportunity to join Glaucus and to continue and complete my research.

A big thank you goes to all my colleagues at Glaucus, especially to the members of the Surface Chemistry Group Dr. Michel Arotçarena, Menno Deij, Hykal Mughal and Soesila Ganeshie for many helpful discussions. Apart from the scientific part, maybe most important is the enjoyable atmosphere.

I thank Dr. Ronald Oosting from the University of Utrecht for being helpful and patient in trying to explain all these biological procedures and facts. I thank Martin Bart from the University of Utrecht for helpful discussions and his support.

A big thank you to Dr. Bernhard Steinbauer for interesting and nice discussions about everything and for continuous sourcing of scientific literature.

Moreover, I like to thank all my former colleagues at BioTuL for a fantastic spirit and a really pleasant time.

I owe special thanks to my parents who, when times got tough, offered plentiful support both morally and materially. I am grateful to my brother for his continuous support, especially in terms of all this computer stuff.